ESL-TR-89-14

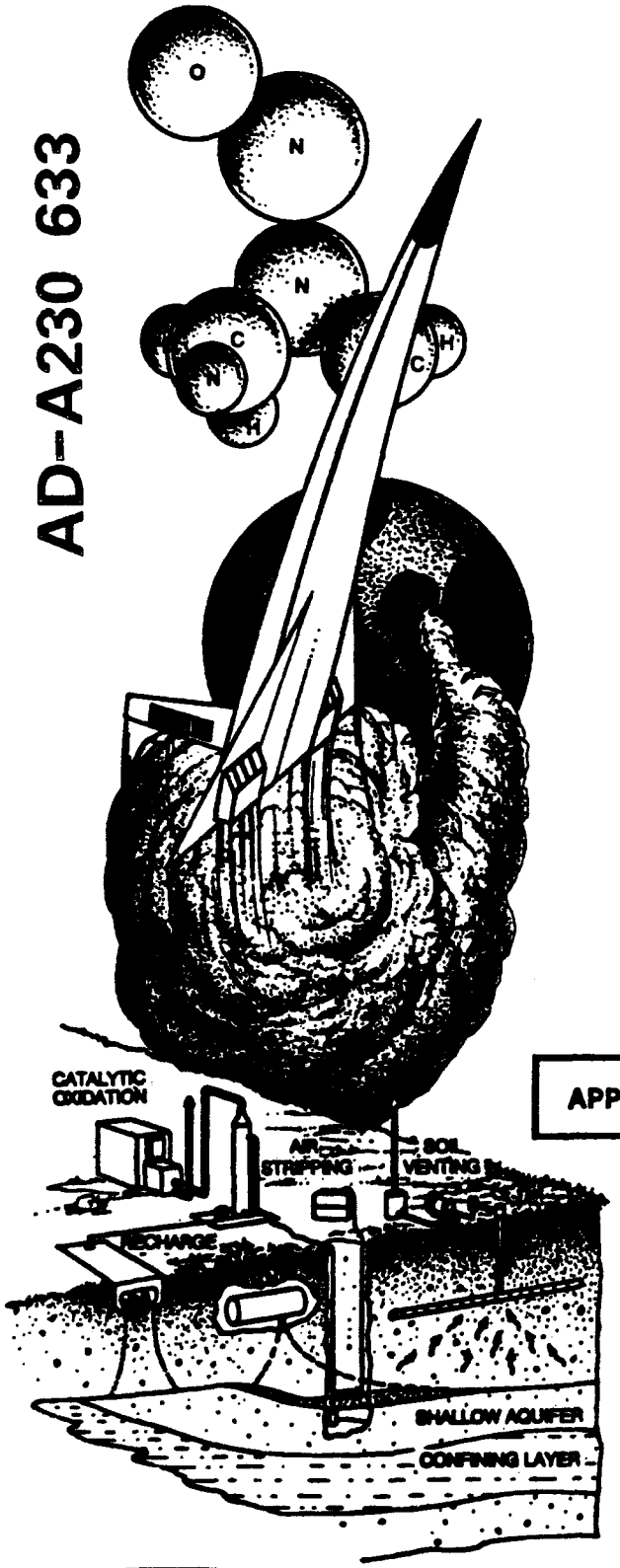

THE EFFECT OF FUEL ADDITIVES ON SOOT FORMATION

A.M. STERLING, G.B. ARBOUR, N.P. ADAMS III

DEPT. CHEMICAL ENGINEERING
LOUISIANA STATE UNIVERSITY
BATON ROUGE LA 70803

MARCH 1990

FINAL REPORT

FEBRUARY 1986 — NOVEMBER 1988

ENVIRONICS DIVISION
Air Force Engineering & Services Center
ENGINEERING & SERVICES LABORATORY
Tyndall Air Force Base, Florida 32403

NOTICE

PLEASE DO NOT REQUEST COPIES OF THIS REPORT FROM HQ AFESC/RD (ENGINEERING AND SERVICES LABORATORY). ADDITIONAL COPIES MAY BE PURCHASED FROM:

NATIONAL TECHNICAL INFORMATION SERVICE
5285 PORT ROYAL ROAD
SPRINGFIELD, VIRGINIA 22161

FEDERAL GOVERNMENT AGENCIES AND THEIR CONTRACTORS REGISTERED WITH DEFENSE TECHNICAL INFORMATION CENTER SHOULD DIRECT REQUESTS FOR COPIES OF THIS REPORT TO:

DEFENSE TECHNICAL INFORMATION CENTER
CAMERON STATION
ALEXANDRIA, VIRGINIA 22314

UNCLASSIFIED

SECURITY CLASSIFICATION OF THIS PAGE

REPORT DOCUMENTATION PAGE

Form Approved OMB No. 0704-0188

1a. REPORT SECURITY CLASSIFICATION: UNCLASSIFIED	1b. RESTRICTIVE MARKINGS
2a. SECURITY CLASSIFICATION AUTHORITY	3. DISTRIBUTION/AVAILABILITY OF REPORT: Approved for public release. Distribution unlimited.
2b. DECLASSIFICATION/DOWNGRADING SCHEDULE	
4. PERFORMING ORGANIZATION REPORT NUMBER(S)	5. MONITORING ORGANIZATION REPORT NUMBER(S): ESL-TR-89-14
6a. NAME OF PERFORMING ORGANIZATION: Dept. Chemical Engineering, Louisiana State University; 6b. OFFICE SYMBOL (If applicable)	7a. NAME OF MONITORING ORGANIZATION
6c. ADDRESS (City, State, and ZIP Code): Baton Rouge, LA 70803	7b. ADDRESS (City, State, and ZIP Code)
8a. NAME OF FUNDING/SPONSORING ORGANIZATION: Air Force Engineering and Services Center; 8b. OFFICE SYMBOL (If applicable): RDVS	9. PROCUREMENT INSTRUMENT IDENTIFICATION NUMBER: F08635-86-K-0042, P00003
8c. ADDRESS (City, State, and ZIP Code): Air Force Engineering and Services Center, Tyndall AFB FL 32403	10. SOURCE OF FUNDING NUMBERS

PROGRAM ELEMENT NO.	PROJECT NO.	TASK NO	WORK UNIT ACCESSION NO.
6.2	1900	20	86

11. TITLE (Include Security Classification): The Effect of Fuel Additives on Soot Formation

12. PERSONAL AUTHOR(S): Sterling, Arthur MacLean; Arbour, Gregory Bahlinger; Adams, Nathan Pankey III

13a. TYPE OF REPORT	13b. TIME COVERED	14. DATE OF REPORT (Year, Month, Day)	15. PAGE COUNT
Final	FROM 86/2/1 TO 88/11/4	March 1990	112

16. SUPPLEMENTARY NOTATION: Availability of this report is specified on reverse of front cover.

17. COSATI CODES		
FIELD	GROUP	SUB-GROUP
21	05	
21	02	

18. SUBJECT TERMS (Continue on reverse if necessary and identify by block number)

Soot Formation, Pyrolysis, Optical Probe, Benzene, Oxidation, Additives, Fuel, Shock Tube, Iron

19. ABSTRACT (Continue on reverse if necessary and identify by block number)

The effect of an iron additive on soot formation during the pyrolysis and oxidation of benzene was studied in a conventional, 7.6-cm i.d. shock tube. Iron pentacarbonyl, $Fe(CO)_5$, as a surrogate for ferrocene, was used as the additive. As a control, carbon monoxide (CO) was also considered an additive. Measurements were carried out at two pressure levels (2-3 atm. and 5-7 atm.) over a temperature range from 1600-2400 K.

No direct influence of iron could be demonstrated, although a weak effect would have been obscured by a surprisingly strong enhancement of sooting by CO during low-pressure pyrolysis and high-pressure oxidation. An indirect effect of iron was to reduce or eliminate the enhancement of soot yield by CO.

The experimental evidence strongly suggests that the effect of $Fe(CO)_5$ and CO are chemical in nature. It is suggested that these additives may serve as useful chemical probes in the study of soot formation chemistry.

20. DISTRIBUTION/AVAILABILITY OF ABSTRACT	21. ABSTRACT SECURITY CLASSIFICATION
☒ UNCLASSIFIED/UNLIMITED ☐ SAME AS RPT ☐ DTIC USERS	Unclassified

22a. NAME OF RESPONSIBLE INDIVIDUAL	22b. TELEPHONE (Include Area Code)	22c. OFFICE SYMBOL
MARK D. SMITH, Capt, USAF, BSC	(904) 283-4234	HQ AFESC/RDVS

DD Form 1473, JUN 86 — Previous editions are obsolete.

SECURITY CLASSIFICATION OF THIS PAGE

UNCLASSIFIED

(The reverse of this page is blank.)

PREFACE

This program was conducted in the Combustion Research Laboratories of the Department of Chemical Engineering, Louisiana State University, Baton Rouge, Louisiana 70803, under Contract No. FO863-86-K-0042 with the Headquarters Air Force Engineering and Services Center, Directorate of Engineering and Services Laboratory (HQ AFESC/RD), Tyndall AFB FL 32403-6001.

Work on this program was performed between 1 February 1986 and 4 November 1988. The AFESC project officers were Major Paul E. Kerch and Captain Mark D. Smith.

The individuals who participated in and provided major contributions to the program include graduate students Gregory B. Arbour and Nathan P. Adams III, and undergraduate student James E. Dautenhahn.

This report has been reviewed by the Public Affairs Office (PA) and is releasable to the National Technical Information Service (NTIS). At NTIS it will be available to the general public, including foreign nationals.

This report has been reviewed and is approved for distribution.

MARK D. SMITH, Capt, USAF, BSC
Project Officer

F. THOMAS LUBOZYNSKI, Maj, USAF, BSC
Chief, Environics Division

WAYNE P. CHEPREN, Capt, USAF
Chief, Environmental Sciences Branch

RICHARD M. HANES, Col, USAF
Director, Engineering and Services Laboratory

(The reverse of this page is blank)

TABLE OF CONTENTS

Section	Title	Page
I	INTRODUCTION	1
	A. OBJECTIVE	1
	B. BACKGROUND	1
	C. APPROACH	3
	D. SCOPE	4
II	BACKGROUND	5
	A. SOOT FORMATION MECHANISMS	5
	1. Soot Formation by Pyrolysis	7
	a. Soot Precursors and Nucleation	7
	b. Surface Growth and Coagulation	11
	c. Agglomeration	11
	2. Soot Formation by Oxidation	12
	B. FUEL ADDITIVE EFFECTS	
	1. Gaseous Additives	13
	2. Alkali and Alkaline Earth Additives	14
	3. Iron Additives	15
III	EXPERIMENTAL METHODS	17
	A. SHOCK TUBE FACILITY	18
	1. Shock Tube	18
	2. Vacuum System	18

TABLE OF CONTENTS

(Continued)

Section	Title	Page
	3. Pressure Transducers	20
	4. Gas Handling System	21
	5. Optical Probe	22
	a. Soot Yield Measurements by Light Extinction	22
	b. Linearity and Frequency Response of Optical Probe	23
	6. Data Acquisition and Processing	26
	B. TEST MIXTURE PREPARATION	26
	C. SHOCK TUBE OPERATION	28
IV	PRESENTATION AND DISCUSSION OF RESULTS	30
	A. OVERVIEW	30
	B. PYROLYSIS MEASUREMENTS	33
	1. Effect of Benzene Concentration	34
	2. Effect of Reaction Pressure on Benzene Pyrolysis	40
	3. Effect of Additives at 2-3 Atmosphere Reaction Pressures	43
	4. Effect of Additives at 5-7 Atmosphere Reaction Pressures	52

TABLE OF CONTENTS

(Concluded)

Section	Title	Page
	C. OXIDATION MEASUREMENTS	56
	1. Effect of Additives at 2-3 Atmosphere Reaction Pressures	57
	2. Effect of Additives at 5-7 Atmosphere Reaction Pressures	57
	D. SUMMARY OF EXPERIMENTAL RESULTS	68
V	CONCLUSIONS	71
	REFERENCES	73
APPENDIX		
A	DETAILS OF THE EXPERIMENTAL DATA	81

LIST OF FIGURES

Figure	Title	Page
1	A Schematic Overview of the Series and Parallel Pathways Involved in the Process of Soot Formation	6
2	Chain Mechanism for Benzene Pyrolysis Proposed by Bauer (Reference 12)	8
3	Mechanism for Benzene Pyrolysis Proposed by Asaba and Fujii (Reference 13)	8
4	The Conventional Shock Tube Facility Used in this Study	19
5	Linearity of the PMT Responce to Incident Intensity	25
6	Typical Digital Oscilliscope Trace of the Pressure and PMT Output	27
7	Graphical Depiction of Soot Formation Rate and Induction time	27
8	Effect of Benzene Concentration of Soot Yield During Pyrolysis at 2-3 Atmospheres Reaction Pressure	35
9	Comparison of Soot Yields at 1-ms Reaction Time Showing Effect of Benzene Concentration	37
10	Effect of Benzene Concentration on Induction Times and Rates of Soot Formation During Pyrolysis at 2-3 Atmosphere Pressures	39
11	Effect of Pressure on Soot Yield Holding Initial Carbon Atom Concentration at Reaction Pressures Constant	41
12	Effect of Pressure on Induction Times and Rates with Initial Carbon Atom Concentration Held Constant	42

LIST OF FIGURES

(Continued)

Figure	Title	Page
13	Effect of Carbon Monoxide, Iron Pentacarbonyl, and Oxygen as Additives During Benzene Pyrolysis at 2-3 Atmosphere Pressures .	44
14	Comparison of Soot Yields at 1-ms Reaction Time Showing Effect of Additives During Benzene Pyrolysis at 2-3 Atmosphere Pressures	46
15	Effect of Additives on Induction Times and Rates of Soot Formation During Benzene Pyrolysis at 2-3 Atmosphere Pressures	47
16	Effect of Additives on Soot Yield for the Pyrolysis of Benzene at Higher Benzene Concentrations	49
17	Comparison of Soot Yields at 1-ms Reaction Time Showing Effect of Additives at Higher Concentrations of Benzene	50
18	Effect of Additives on Induction Times and Rates of Soot Formation at Higer Concentration Levels of Benzene	51
19	Effect of Carbon Monoxide and Iron Pentacarbonyl on Soot Yield During Benzene Pyrolysis at 5-7 Atmosphere Pressure	53
20	Comparison of Soot Yields at 1-ms Reaction Time Showing Effect of Additives at Pyrolysis Pressures from 5-7 Atmospheres	54
21	Effect of Additives on Induction Times and Rates for Benzene Pyrolysis at 5-7 Atmosphere Reaction Pressures	55
22	Effect of Carbon Monoxide and Iron Pentacarbonyl Additives of Soot Yield During Benzene Oxidation at 2-3 Atmosphere Pressures	58

LIST OF FIGURES

(Concluded)

Figure	Title	Page
23	Comparison of Soot Yields at 1-ms Reaction Time Showing Effect of Additives During Benzene Oxidation at 2-3 Atmosphere Pressures	59
24	Effect of Additives on Induction Times and Rates of Soot Formation for Benzene Oxidation at 2-3 Atmosphere Pressures	60
25	Effect of Increased Additive Concentrations on Soot Yield During Benzene Oxidation at 2-3 Atmosphere Pressures	61
26	Comparison of Soot Yields at 1-ms Reaction Time Showing Effect of Additives at Higher Concentration Levels	62
27	Effect of Higher Additive Concentations on Induction Times and Rates During Benzene Oxidation at 2-3 Atmosphere Pressures	63
28	Effect of Carbon Monoxide and Iron Pentacarbonyl Additives on Soot Yield During Benzene Oxidation at 5-7 Atmosphere Pressures	65
29	Comparison of Soot Yields at 1-ms Reaction Time Showing Effect of Additives During Benzene Oxidation at 5-7 Atmosphere Pressures	66
30	Effect of Additives on Induction Times and Rates During Benzene Oxidation at 5-7 Atmosphere Reaction Pressures	67
31	Summary of Effects of Carbon Monoxide on Soot Yield During Benzene Pyrolysis and Oxidation	69

LIST OF TABLES

Table	Title	Page
1	SUMMARY OF EXPERIMENTAL SERIES	31
A-1	DETAILS OF EXPERIMENTAL DATA	82

(The reverse of this page is blank)

SECTION I

INTRODUCTION

A. OBJECTIVE

This study was initiated to investigate the effect of an iron additive on soot production during pyrolysis and oxidation of an aromatic fuel. A shock tube was used to initiate combustion reactions, and soot production was monitored by light-scattering techniques.

The pyrolysis measurements were designed to show clearly if an iron additive affects soot formation chemistry, and the oxidation measurements were intended to complement flame measurements being carried out elsewhere. In addition, pyrolysis and oxidation measurements at elevated pressures were included to assist in the extrapolation of data from flames, obtained at 1 atmosphere pressure, to the current and anticipated operating pressures of gas turbine combustors.

B. BACKGROUND

The emission of soot from gas turbine combustors is of increasing concern to the U.S. Air force. From a tactical viewpoint, the effectiveness of combat aircraft is substantially reduced by the large radar cross-section of a sooty plume. The formation of soot also reduces engine lifetime caused by the increased radiative heat transfer to and deposition of soot on the combustor internals. The relaxation of fuel standards to allow higher aromatic content, and the development of a new generation of gas turbine combustors designed to operate at pressures exceeding 10 atmospheres, will exacerbate these sooting problems.

The environmental issues, however, are of immediate concern; the inability to control soot emissions from gas turbines is currently hindering Air Force operations. Although the exhaust from gas turbine engines generally meets

environmental standards for particulate emissions from moving sources, standards for stationary sources are often exceeded. When an engine is removed from an aircraft and placed in a test cell, it becomes a stationary source. As a result, routine maintenance procedures have been curtailed in regions where stationary-source particulate-emission standards are exceeded.

The control of soot formation must ultimately lie in improved combustor design. The expense of retrofitting current engines to utilize improved designs, however, is prohibitive. Thus the use of smoke-suppressant fuel additives is an attractive alternative. In particular, ferrocene (dicyclopentadienyl iron) has been used by the Air Force for both tactical and test-cell soot emission control.

The mechanisms by which fuel additives affect soot production in gas turbine combustors, however, are poorly understood. As a result, additive effects are unpredictable. Although it is known that ferrocene, for example, can reduce the plume opacity for some gas turbine combustors under certain operating conditions, it is not yet clear whether the reduction owes to the generation of less soot, to the alteration of soot particle size, or to the enhanced burnout of the soot particles. An improved understanding of these mechanisms would provide guidance for the effective use of fuel additives and for new combustor design.

C. APPROACH

There have been no previous measurements of the effect of an iron additive on soot formation during fuel pyrolysis. Unlike measurements in premixed or diffusion flames, shock-tube measurements can be carried out in the absence of oxygen. Thus if iron-additive effects on soot formation are observed during fuel pyrolysis, the effects can be clearly identified as chemical. This would imply that the iron additive affects soot production. In contrast, if no effects are observed, the role of iron in the chemistry of soot formation can be discounted. This would imply that the additive may affect soot particle size but not the total soot mass produced. This principal result will provide a significant step in unraveling the role of metal additives on soot production.

Additional measurements will be carried out in the presence of oxygen. The effects of fuel, oxygen, and metal-additive concentrations over a range of reaction temperatures will compliment measurements in flames being carried out elsewhere.

Finally, pyrolysis and oxidations measurements will be repeated at an elevated pressure. Data on soot production in flames at elevated pressures is, at best, limited. Thus the high-pressure measurements carried out here will lead to an improved understanding of the effects of pressure on fuel pyrolysis and oxidation (both with and without additives) and provide a data base to help relate flame data to the sooting behavior of fuels at the elevated reaction pressures of full-scale, gas turbine combustors.

The standard fuel to be used in this study is benzene, diluted to 0.3 mole percent in argon. This mixture has been studied previously in our laboratory over a wide range of temperatures, pressures, and oxygen concentrations. Thus an established data base is available to confirm measurement reproducibility. Furthermore, benzene will provide the basic chemical characteristics of aromatic fuels without introducing possible complications of a complex aromatic fuel mixture.

The iron additive will be introduced into the fuel mixture in the form of iron pentacarbonyl, $Fe(CO)_5$. Although it would be preferable to use ferrocene, its low vapor pressure precludes its use in an unheated shock tube. Since it is accepted that it is the iron, rather than the cyclopentadienly ligands of ferrocene, that affects sooting, iron pentacarbonyl will be a suitable surrogate. It will provide an essentially instantaneous source of iron over the 0.5 - 3 ms observation times of the experiments.

Soot production will be monitored by the attenuation of a He-Ne laser beam passing through the observation section of the shock tube. The reduction in beam intensity will be converted, through conventional scattering calculations, to soot yield, i.e. the fraction of initial fuel carbon atoms converted to soot. Soot yield, at a given reaction pressure, will be presented as a function of

temperature, with observation times as parameters. In addition, two other parameters will be measured from the beam attenuation data; the induction delay time and the maximum rate of soot formation. These parameters will be correlated in terms of the reaction temperature. Fuel additive effects will be evidenced as an alteration of the so-called "soot-yield bells," the induction time, and the rate of soot formation, all in comparison to the benzene base case.

D. SCOPE

A review of the current concepts of soot formation is presented in the following section. Included is a discussion of the effects of fuel additives. This review focusses on the pyrolysis and oxidation of benzene and closely related aromatic compounds.

A detailed description of the experimental equipment and operating procedures is given in Section III, followed by the presentation and discussion of experimental results in Section IV. Data obtained for the pyrolysis of benzene, including the effects of the additive, are presented first. An increase in soot yield with the addition of trace amounts of carbon monoxide is a striking, and unexpected, feature of these data. The related oxidation measurements follow.

The observed effects of fuel and additive concentrations, and reaction pressure provide the basis the conclusions of this study. These conclusion are given in Section V.

SECTION II

BACKGROUND

A. SOOT FORMATION MECHANISMS

The mechanisms of soot formation are deeply imbedded in the complex process of combustion, a process that involves very rapid chemical reactions and physical transport, electrical interactions, and high temperatures. The process proceeds through several sequential steps to form the chainlike structures of soot, which can then be oxidized or emitted. The prevailing concept of the process is summarized by a pathway of series and parallel rate processes in Figure 1.

Fuel pyrolysis is the first and most important step in the process of soot formation. The overall rate of soot formation, as well as the total soot mass yield, appears to be determined by the chemical events in the very early stages of fuel pyrolysis. These early stages include initial fragmentation of the fuel molecules to acetylene, vinyl and phenyl radicals, and hydrogen ions. These fuel fragments then proceed along various routes (depending primarily on the reaction temperature) to form the first aromatic ring products (the soot precursors).

Nucleation (condensation and coagulation) occurs when molecular soot precursors combine to form young soot particles. The process is partially governed by chemical reactions and by physical and electrical interactions between the precursors. The particles increase in size through surface growth and aggregation. During the growth phase, the tiny particles can grow from 1-2 nm up to 10-50 nm spherules. These spherules then agglomerate to form soot chains, which can be as long as 1 μm (Reference 1).

Although this scheme is simple in concept, the details along the pathways are extremely complex. Each of the rate processes are strongly coupled to the local temperature, pressure, and species concentration, which, in turn, are coupled to the local rates of mass and heat transport, e.g., aerodynamics and radiation.

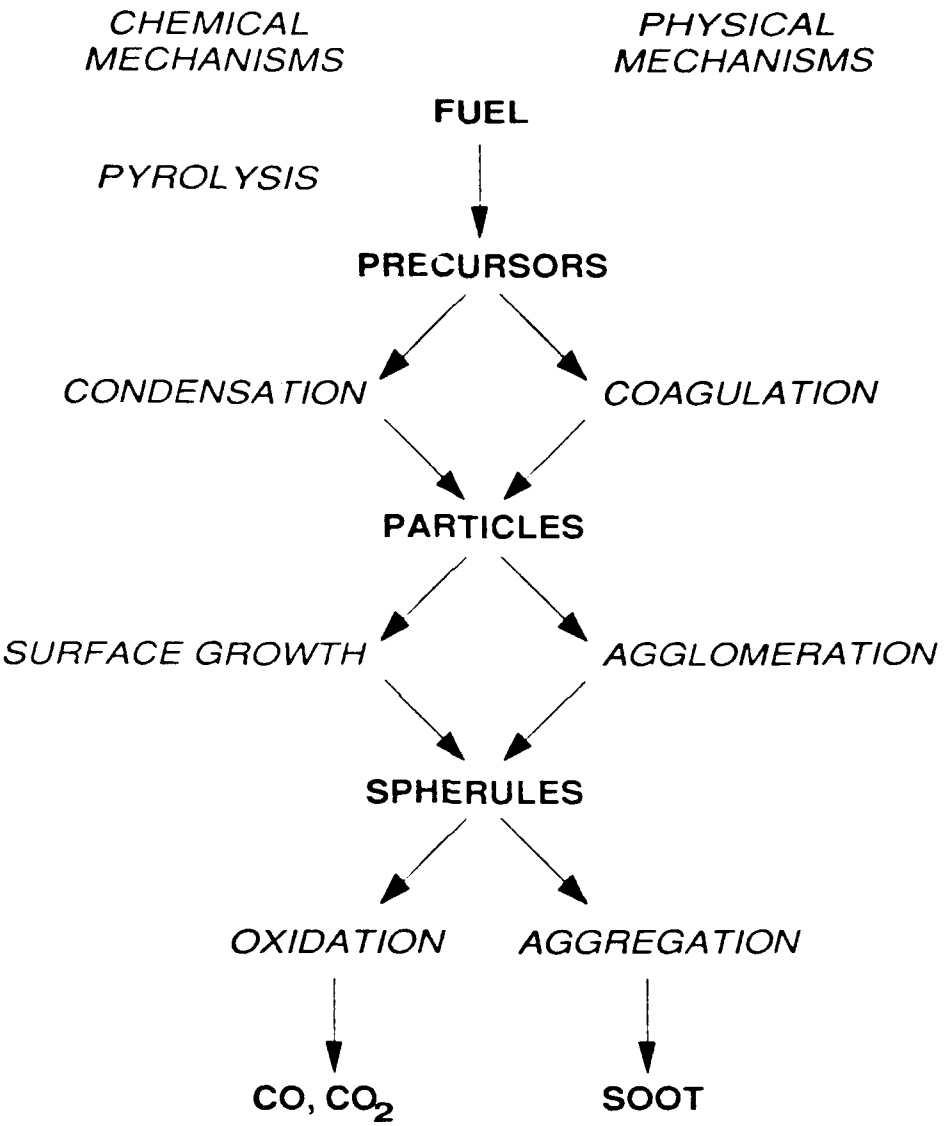

Figure 1. A Schematic Overview of the Series and Parallel Pathways Involved in the Process of Soot Formation.

The process is further complicated by the very large number of chemical species that take part in the reactions and the even larger number of chemical reactions involved.

Several excellent reviews provide details of the various mechanisms (References 2-7). Only the highlights of these reviews and other recent work, that closely relate to soot formation from aromatic fuels, are discussed below.

1. Soot Formation by Pyrolysis

a. Soot Precursors and Nucleation

The first step in the soot formation process is the pyrolysis of the fuel, leading to the reactive species that form soot precursors. Many studies have been made to track the development of these precursors. Kern (Reference 8) studied low-pressure pyrolysis of both benzene and toluene at temperatures ranging from 1400-2300 K. He observed that the major products formed were acetylene and polyacetylenes. No species with molecular weights higher than the parent compound were observed, leading Kern to conclude that fragmentation of the aromatic ring was the most important initial step at the conditions studied. Smith (Reference 9) performed a similar study with toluene in a high temperature, low pressure Knudsen cell and observed similar products. Mar'yasin (References 10 and 11), in an earlier shock tube study, considered benzene pyrolysis. It was observed that methane, ethylene, vinylacetylene, and diacetylene were produced. Significantly, all of the above authors proposed the ring fragmentation mechanism to explain their experimental results.

Bauer (Reference 12) suggested a chain mechanism for benzene pyrolysis. His mechanism (Figure 2) proceeds with benzene fragmenting into acetylenic groups, followed by recombination into unsaturated hydrocarbons. Asaba and Fujii (Reference 13) studied the pyrolysis of benzene using light absorption and a single pulse shock tube. They observed that the pyrolysis process was accelerated by the addition of methane and inhibited by adding

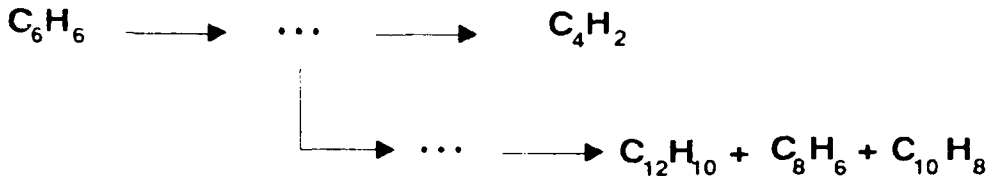

Figure 2. Chain Mechanism for Benzene Pyrolysis Proposed by Bauer (Reference 12).

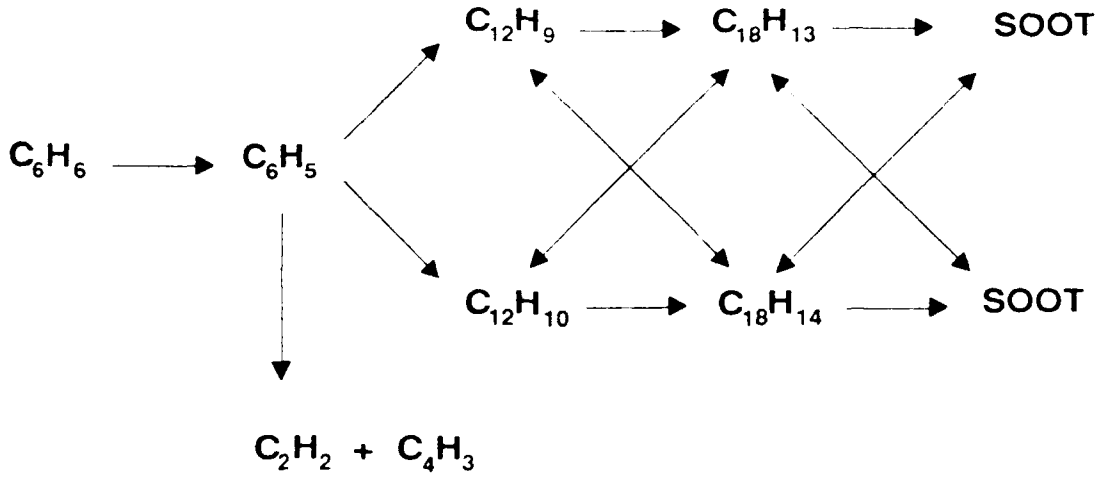

Figure 3. Mechanism for Benzene Pyrolysis Proposed by Asaba and Fujii (Reference 13).

hydrogen. They proposed the mechanism shown in Figure 3 to explain their experimental results.

In another study of benzene pyrolysis, Graham (Reference 14) noted a rapid decrease in the soot yield as temperatures exceeded 1800 K. The author accounted for an observed maximum in the soot yield at 1800 K by suggesting a mechanism involving two competing pathways. In one pathway, the aromatic character of the ring is never lost as it undergoes direct condensation to larger compounds. The second is the more familiar fragmentation followed by recombination. In a separate study, Clary (Reference 15) and Wang (Reference 16) confirmed this double-pathway hypothesis. Clary explained the process by suggesting that at high temperatures the fragmentation pathway dominates, whereas at low temperatures the condensation reaction is more prevalent. Frenklach (Reference 17) offered a conceptual model for the sooting process. He also saw the pyrolysis reaction as two competing pathways:

$$A \Longrightarrow X \qquad [1]$$

$$A + X \Longrightarrow S \qquad [2]$$

where A is the aromatic ring, X is an intermediate, and S is some final product. Reaction [1] is unimolecular; thus its activation energy is high, causing it to be the slow step. Reaction [2] is essentially a polymerization reaction and is the basic model for the soot formation process. This empirical model was shown to fit Clary's data.

Efforts to further define the nucleation process have led to the identification of possible soot precursors. Frenklach et al. (Reference 18) proposed that fused polycyclic aromatic hydrocarbons (PCAH) are the key to sooting in acetylene flames. Homann (Reference 19) found about 100 times the concentration of PCAH in aromatic soot as in aliphatic soot. This helps explain the observation that aromatics and polycyclic aromatics soot much more readily than nonaromatic compounds (Reference 5). Indeed, Davies (Reference 20) reports that the yield of soot seems closely related to the stability of the aromatic rings in the precursors.

Wang (Reference 21) attempted to find the point at which the particle inception takes place. The author found a polycyclic aromatic hydrocarbon (PCAH), $C_{96}H_{24}$, to be an important soot precursor. Equilibrium calculations were made which show $C_{96}H_{24}$ to be thermodynamically favored over acetylene below 2500 K (Reference 22).

The gap between the initial chain activation reaction and the particle formation remains a mystery. Several authors (References 23-25) have studied the electrical properties of flames and concluded that ions may play an important role in soot formation. Ball (Reference 26) noted that almost all of the carbonaceous particles were positively charged . Howard (Reference 27) proposed a mechanism for the formation of carbon particles which used positive ions as nuclei. He observed positively charged crystallites 20-30 Angstrom in size and spherules as large as 100-500 Angstrom. Bowser and Weinberg (Reference 23) found that as ions are formed, they force condensation reactions which in turn form PCAH.

Agreement has not been universal though. Abrahamson (Reference 28) observed that acetylene appears to be just as important in the soot formation process as ions. He also found that nonflame sources of pyrolysis could be electrically neutral and still produce soot. Ball (Reference 26) noted that charging continues through the agglomeration phase and may actually halt the process through electrostatic repulsions.

Detailed kinetic modeling (References 18,29-30) is now yielding significant insights into the early stages of the soot formation process and is providing a skeletal scheme by which experimental studies can be designed and experimental results can be interpreted. The modeling results emphasize the importance of pyrolysis fragments, especially H atoms, vinyl radicals, and acetylene in the formation of soot precursors. The utility of a general mechanism, derived through detailed kinetic modelling, in the interpretation of experimental results from shock tubes, premixed flames, and diffusion flames has been persuasively stated in the recent review Glassman (Reference 7).

The results of detailed modeling must, at the present, be used with caution. Westmorland (Reference 31), points out that it is important to verify that the reactions included in the kinetic modelling are indeed elementary. By considering how reactions occur on a molecular scale, Westmorland has shown that most of the important combustion reactions are association reactions disguised as abstraction reactions by chemical activation mechanisms. A failure to recognize the elementary character of the reactions can lead to large errors in the estimated rate constants, and thus a distorted picture of the reaction pathways.

b. Surface Growth and Coagulation

The process following particle inception has often been observed to be a mixture of chemical reactions and physical interactions. The chemical processes are referred to as surface growth and are largely comprised of the further addition of ring fragments to the spherules. Coagulation is the physical process by which young soot particles stick to each other, forming larger spherules and eventually chains. Together these processes account for a large part of the initial soot formation with the spherules growing to diameters up to 100 nm (Reference 32). It has been shown that the growth by chemical reaction is more consistent with surface reactions than further condensation reactions (Reference 33).

Also important is the role of ions. It has been observed that most of the ionic species in flames are heavy hydrocarbons and young soot particles, compounds ranging from 300 to several thousand atomic mass units. Enough of these species have been found to account for the amount of soot formed (Reference 34). Thus, clearly the ionic nature of the spherules must be an important factor in the surface growth and coagulation.

c. Agglomeration

The division between surface growth, coagulation, and agglomeration is not sharply drawn. In its earliest stages, agglomeration can be obscured by surface growth as the gaps between particles are filled in. Later, particle collisions predominate, forming twisted chains up to 1 μm in length (Reference

1). Also, some chains become heavily positively charged, leading to fragmentation by electrostatic repulsion (Reference 26).

2. Soot Formation by Oxidation

Complete combustion of a hydrocarbon is generally defined as the burning to carbon dioxide and water. Clearly, when this is the case, no soot is formed. It is only when the level of oxygen in a flame drops to a certain point that soot can be produced; this point is known as the critical carbon-to-oxygen (C/O) ratio. For benzene the critical C/O ratio has been shown to be 0.65 (Reference 4). As the C/O ratio is increased, the soot yield also increases, but the gain in soot is not always well correlated with the C/O ratio. Wang (Reference 16) studied the combustion of toluene in a shock tube. By increasing the mole fraction of oxygen approximately four-fold, he observed a corresponding four-fold decrease in the soot yield.

Most of the oxidation studies of aromatic hydrocarbons have been done at temperatures below 1000 K. Great caution should be exercised in extrapolating the results to higher temperatures (Reference 35). Fag and Asaba (Reference 36) studied the combustion of benzene at temperatures ranging from 1300 K to 1700 K. They observed little water formed in experiments on rich mixtures. Carbon monoxide and acetylene were observed and thought to be produced through a reaction of the phenyl radical with oxygen. Significantly, biphenyl and higher polymers were formed in ways similar to pyrolysis. Venkat (Reference 37) also studied the high temperature oxidation of aromatic hydrocarbons. Again, great similarities were noted as to the pyrolysis process, and the overall rate seemed dominated by the rate of oxidation of the phenyl radical.

Other authors have tried to explain the combustion process in slightly different terms. Glassman and Yaccarino (Reference 38) suggested that combustion is really a competition between the rate of pyrolysis to soot precursors (growth along pyrolysis routes) and the rate of oxidative attack on them. Frenklach (Reference 39) went further, observing that the addition of oxygen to toluene seemed to enhance soot production at lower temperatures and inhibited sooting at higher temperatures. He explained that oxygen does not alter the mechanism

of pyrolysis; instead it competes with it. At low temperatures the oxygen enhances fuel pyrolysis, while at high temperatures it destroys the soot precursors through oxidation (Reference 40).

B. FUEL ADDITIVE EFFECTS

In recent years, researchers have sought many ways to reduce the amount of soot formed during combustion. The most practical methods to date involve additives to the fuel. In theory, there are two ways to reduce sooting. First, one can reduce nucleation, thereby stopping the soot formation process before the soot particles are actually formed. Second, one can accelerate the oxidation of soot particles once they are formed, a process known as burnout (Reference 41). The real question, of course, is how does an additive affect the soot formation process.

Since relatively little is known about the mechanisms involved in additive effectiveness, only rough theories are available. The most popular is that additives affect the ionization of the young soot particles. Antisoot effects may be due to a permanent reduction in the number of ions available. Unfortunately, some additives promote soot formation by delaying ionization instead of preventing it (Reference 42). This reduces the time available for oxidation of the soot particles. Also, certain additives are known to both promote and reduce sooting depending on flame conditions.

1. Gaseous Additives

Studies have been made on the effects of gaseous additives. Gases such as NH_3, H_2, N_2, H_2S, SO_2, NO, and NO_2 have been added to flames (Reference 43). It was found that inert gases have little effect and that the soot reduction properties of the others are roughly proportional to their molar specific heat capacities. The most effective were the sulphur-containing species.

Other workers have studied the effects of adding CO to flames. CO was found to reduce the amount of oxygen necessary to eliminate soot formation. Also, CO has been observed to cause a yellow streak in flames, characteristic

of soot formation (Reference 44). It has long been known that small concentrations of CO in the hydrocarbon mixtures of hydrogenators can cause a comparatively large build-up of carbon on the reactor walls (Reference 45).

Schug (Reference 46) added small amounts of N_2O, an oxidizer, to ethane and butane diffusion flames. The soot height (that distance above the burner at which soot is first observed) was decreased dramatically, indicating increased soot production.

Du et al. (Reference 47) have studied the effects of He, Ar, N_2, CO_2, O_2, H_2, and CO on the sooting limits of strained diffusion flames. Propane and butane were used as fuels. In contrast to experimental method used by Schug, which was global in the sense that the additive effect on the overall process (inception, growth, and burnout) was measured, the measurement of the sooting limit in strained diffusion flames focusses on the additive effect on the inception process. Du et al. found that all additives, except CO, decreased the inception limit as the amount of additive was increased. In contrast, the inception limit increased linearly with the addition of CO up to a concentration of 0.4 mole percent. Further addition of CO decreased the inception limit. They accounted for the observed effect of CO partially by an increase in flame temperature and partially by an (unspecified) chemical effect.

2. Alkali and Alkaline Earth Metal Additives

A far more common choice has been to add metallic compounds to flames. These tend to increase the ionization level and concentratior of free electrons in the flame. The main mechanism appears to involve an electron-ion recombination, halting the growth process. This seems especially true for the alkali and alkaline earth metals (Reference 48). Several studies have been made using these metals. Haynes (Reference 49) studied alkali and alkaline earth metals added to a premixed flat flame. Na, K, and Cs were found to be only weak soot suppressors. They do, however, produce a greater number of smaller particles. Haynes suggested that both electrical and chemical mechanisms might be important.

Ndubizu (Reference 50) tried similar experiments on a polyethylene flame. Barium was found to be the most effective metal for suppressing soot formation. It reduced the total amount of smoke (soot) produced without affecting the size of the particles. It has been suggested that barium limits the nucleation step by producing hydroxyl radicals which oxidize soot precursors and young soot particles.

3. Iron Additives

Metals other than the alkali and alkaline earth metals have also been studied, particularly the transition metals. These metals have only proved effective at high equivalency ratios, indicating that a different mechanism is involved (41). Various iron compounds were added to a polyvinyl chloride flame. Using Mossbauer spectroscopy the iron was found to be converted to Fe_2O_3. Interestingly, there was an initial increase in the quantity of soot followed by a rapid decrease. The concentrations of carbon monoxide and carbon dioxide were found to grow simultaneously with the decrease in soot (Reference 51). Other authors have suggested that the function of a transition metal would be intervention in the agglomeration phase (Reference 52). Also, the metal could be occluded by the soot particles, thus speeding the burnout (Reference 53). Both processes are consistent with the data described above.

Dicyclopentadienyl iron, also known as ferrocene, has been extensively studied as a soot reduction additive. Loveland (Reference 54) added ferrocene to fuel in jet turbine engines. It was shown to reduce the opacity of the exhaust plume. Klarman (Reference 55) has reported that soot suppression by ferrocene in J52, J57, and TF-30 gas turbines is most effective when ferrocene is added at 0.05 - 0.06 weight percent of fuel. With J79 and TF-41 combustors, however, ferrocene increased emissions when they were operated at greater than 85 percent normal rated conditions.

Bonczyk (Reference 56) used ferrocene in diffusion flames and reported that it was an effective additive in a liquid-fueled wick flame. Strangely, it was not effective in a gas-fueled Wolfhard-Parker burner. Importantly, he found solid metal oxides in the plumes, indicating that although the soot content might

be reduced or even eliminated, the iron would still be present. Samuelsen (Reference 57) tested ferrocene in a swirl combustor with JP-8 jet fuel, reporting some reduction in the soot produced.

A thorough study of ferrocene in an premixed ethylene flame at atmospheric pressure was conducted by Ritrievi et al. (Reference 58). Ferrocene was added at 0.015 - 0.46 weight percent fuel, and the C/O ration of the flame was varied between 0.71 and 0.83. Light scattering, emission, and absorption were used to characterize the size, volume fraction, and number density of the soot particles. Transmission electron microscopy was used to size the particles collected during agglomeration. Unfortunately, the probe through which the particles were extracted interfered with the formation process. Hence the author concluded that only optical methods were suitable for size measurements.

Ferrocene was found to increase the final soot yield in lean flames (C/O=0.71) by a factor of 13.5. This enhancement factor decreased with an increasing C/O ratio, reaching a minimum value of 1.2 for the richest flame (C/O=0.83).

Iron was found concentrated at the core of the soot particles. Surrounding the core were layers of carbon-rich coatings. Ritrievi hypothesized that the iron nucleated well before the soot itself. Hence, the ferrocene underwent oxidation before the fuel and the iron oxide then acted as a surface for carbon deposition, shortening the inception phase.

The particle growth in the ferrocene-doped flames was controlled by the activity of the surfaces. The iron in the core was found to be iron metal, not iron oxide. The reduction of the iron took place by oxidizing the surrounding carbon. This liberated CO and CO_2, contributing to the burnout of the soot.

SECTION III

EXPERIMENTAL METHODS

All experimental work was conducted in the Department of Chemical Engineering Shock Tube Laboratory at Louisiana State University. The laboratory facilities, consisting of a conventional shock tube, an optical probe, and associated electronic and gas handling equipment, have been used extensively in the past to study incipient soot formation (References 15-16,59,60-61).

A shock tube is ideally suited for research in combustion. Two regions of the tube, a high-pressure "driver" section and a low-pressure "driven" section, are initially separated by two Mylar diaphragms secured at the ends of an intermediate spacer section. When the diaphragms burst, a shock wave is produced by expansion of the high-pressure driver gas into the low-pressure driven gas. The shock wave rapidly heats the test gas mixture by adiabatic compression to a high temperature and a predetermined pressure.

The shock tube provides several advantages not present in other laboratory combustion systems. First, the test gas mixture is heated homogeneously and nearly instantaneously (about 1 ns) to the desired temperature and pressure; consequently, no preheating delay is encountered. Second, because the duration of each experiment is so short, heat transfer to the walls is negligible. For the same reason, catalytic effects at the walls are also negligible. Finally, it is possible to shock-heat any gaseous compound; thus pyrolysis and oxidation experiments are easily studied.

The details of the shock tube and the ancillary equipment are given below. This is followed by a brief description of the procedures used in preparing and operating the shock tube and in collecting and reducing the experimental data.

A. SHOCK TUBE FACILITY

1. Shock Tube

The 7.6-cm i.d. stainless steel shock tube, shown in Figure 4, consists of a 3-m driver section and a 7.3-m driven section, separated by a 0.063-m spacer. The double diaphragm bursting technique, using Mylar diaphragms of 1.0- and 1.5-mil thicknesses, was employed in all the experiments of this study. In this method, an intermediate pressure is maintained in the spacer section between the two diaphragms until the initial driver and driven pressures are established. Rapid evacuation of the spacer section results in the rupture of the diaphragm on the driver side, followed immediately by rupture of the driven-side diaphragm. A normal shock wave then propagates into the driven (experimental) section. When the shock wave reaches the end of the driven section, it reflects off the end wall and propagates back toward the driver section. The test gas mixture then undergoes a second adiabatic compression with a concomitant increase in temperature and pressure. All measurements in this study were made behind the reflected shock wave.

As the compression wave is propagating into the driven section, a corresponding rarefaction wave propagates into the driver section, reflects off the end wall, and returns toward the driven section to interact with the reflected compression wave. Eventually, the effects of the rarefaction wave are evidenced at the end of the driven section by a rapid decrease in pressure. This event signals the end of the experiment. The time interval between the passage of the reflected compression wave 0.2 meters from the end of the driven section and the drop in pressure owing to the effects of the rarefaction wave at this same location determines the duration of an experiment. In this work a typical duration was about 3-4 ms.

2. Vacuum System

Before each experiment, the driven section of the shock tube and the gas handling manifold are evacuated by an Edwards ED-500 mechanical vacuum pump. After a sufficient vacuum (= 0.01 torr) is achieved, the system is further

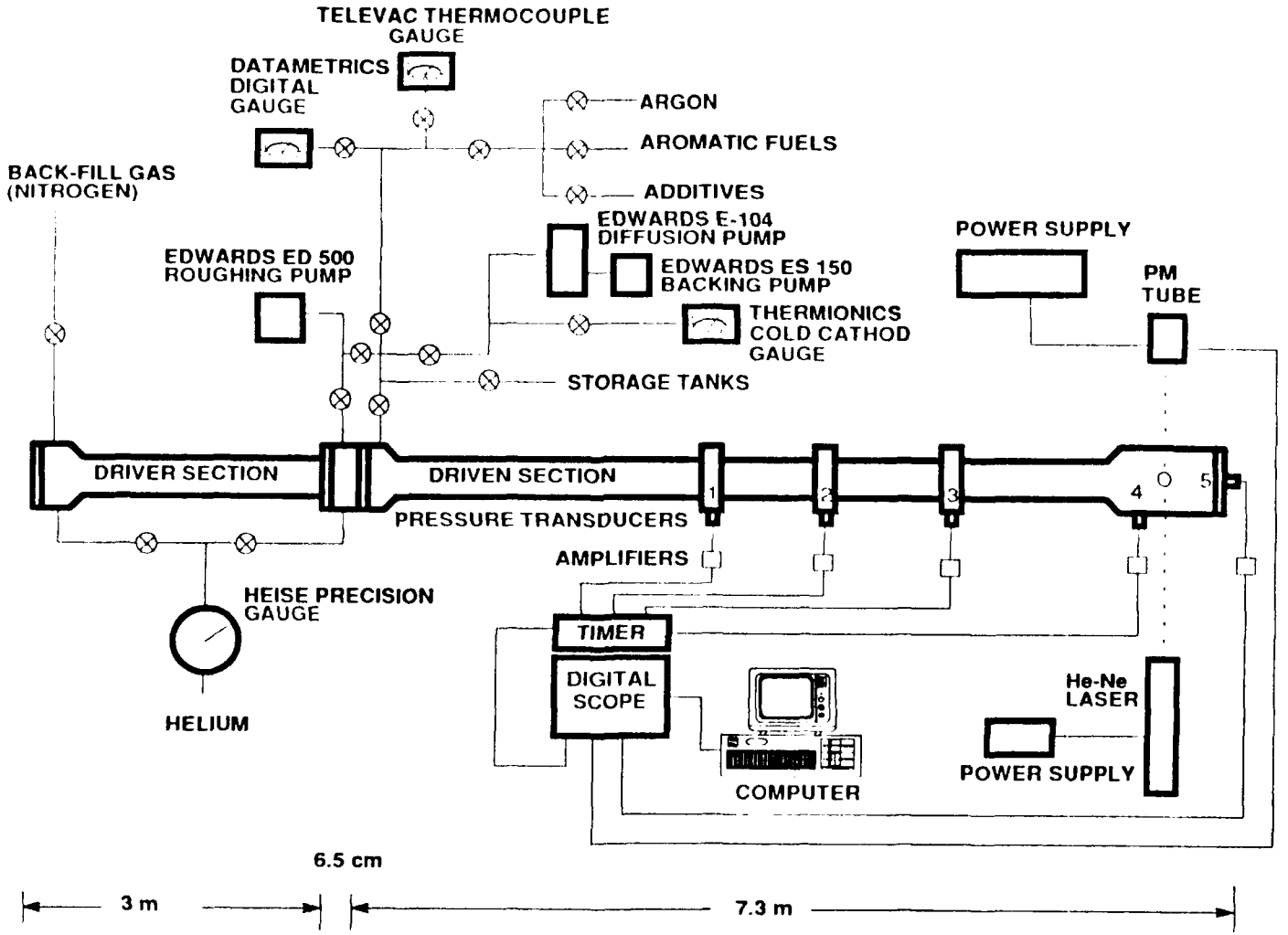

Figure 4. The Conventional Shock Tube Facility Used in this Study.

evacuated, using an Edwards Speedivac E-04 oil diffusion pump, to a pressure of 1.0×10^{-5} torr. The oil diffusion pump, fitted with a liquid nitrogen trap and continuously water cooled, is backed by an Edwards ES-150 mechanical pump.

3. Pressure Transducers

Intermediate pressures during the evacuation of the shock tube and gas-handling manifold are monitored with a Televac model 2A thermocouple gauge, which measures in the range of 0.001 to 1.0 torr. Higher vacua are monitored with a Thermionics PG7 cold cathode gauge, which measures between 1.0×10^{-3} and 1.0×10^{-6} torr. The sensor of the thermocouple gauge is located in the gas handling manifold; the cold cathode gauge sensor is attached to the foreline of the diffusion pump.

The pressure in the driven section during loading of the test gas mixture is measured by a Datametrics model 1174 capacitance manometer, with a pressure range of 0-100 psia. The sensor (Datmetrics model 570A) for the capacitance manometer is located in the gas handling manifold. The pressure of the driver gas is monitored with Heise models C and CM bourdon tube gauges.

The condition of the shock-heated gas is determined by calculations that require experimentally measured incident shock wave velocities as input. Incident shock speeds are measured using four Atlantic Research LD-25 pressure transducers located sequentially along the shock tube. To minimize shock nonuniformities, all pressure transducers are mounted flush with the tube. The transducers trigger start and stop channels of an interval timer, obtained from the Department of Chemistry, University of Texas, Austin. The transducer voltages are preprocessed by an amplifier and a comparitor latch circuit, also obtained from the University of Texas. The first transducer crossed by the incident shock wave defines zero time and distance; as the shock wave passes subsequent transducer stations, interval times, measured from the first transducer, are stored in the memory of the timer. The timer, driven by a 10-MHz crystal oscillator, has a storage delay of less than 300 ns, which results in a net accuracy of within 1 μs for all time intervals (which ranged from 700-2500 μs). Because the incident shock wave decelerates owing to boundary

layer growth and frictional drag between the shock wave and the tube wall, the measured velocity is extrapolated to the end wall of the tube using a linear equation (Reference 43). The observed shock wave attenuation is typically 2 percent/meter.

To monitor the progress of the reaction, the transient pressures are measured using a PCB model 113A24 piezoelectric pressure transducer with an in-line amplifier. The transducer, which has a rise time of less than 1.0 μs, is located on the tube surface above the optical station, 8 mm from the end wall. A PCB model 482A power supply is used to power the transducer and to couple it to a digital oscilloscope.

4. Gas-Handling System

The gas-handling system consists of a gas manifold and a gas vent. The manifold, constructed from lengths of stainless steel tubing sections and needle valves, provides gas transfer pathways between the shock tube, mixture tanks, driver gas, dilution gas, vacuum pumps, and the venting system. For proper operation, the gas manifold must hold a vacuum of 10^{-5} torr.

The original connections for the tubing and needle valves were Swagelock fittings. Persistent leaks in these fittings delayed the collection of experimental data during the early stages of the project. The manifold was completely rebuilt with new tubing and new fittings. Although the manifold could hold the required vacuum while on the bench, when it was installed in the control panel, leaks would again occur. The problem was finally solved by using welded connections wherever possible and replacing the Swagelock fittings with Cajon VCO fittings at critical connections (including valves).

A new gas-evacuation system was designed, constructed, and installed to assure safe operation with the highly-toxic iron pentacarbonyl additive. Originally, exhaust gases from the shock tube facility were vented to the building's hood ventilation system. Previous measurements on the ventilation system has shown that gases released into hoods recirculated back into the buildings air intake. Thus an independent exhaust system was required.

The exhaust system was constructed from PVC pipe with a 2-meter intermediate section constructed of stainless steel. An exhaust fan at the downstream end of the pipe vents the gas through the wall of the laboratory to the outside of the building. The stainless steel section contains a reactor packed with alumina. The reactor is wrapped with heating tape and a thermocouple inserted into the middle of the packed alumina allows the bed temperature to be monitored. The bed is maintained at 675 K during operation to ensure that all iron pentacarbonyl is disassociated before the gas is vented. Tests with sulfur hexaflouride showed that gases vented through the exhaust system were not recirculated to the building.

5. Optical Probe

The absorption of the beam from a 15 mW continuous wave Spectra-Physics model 124B He-Ne laser at a wavelength of 632.8 nm is used to detect the presence of soot particles. The laser is powered by a Spectra-Physics model 255 power supply, and its beam crosses the shock tube at an optical station 8 mm from the end wall. The attenuated laser light beam is monitored by an RCA model 1P28 photomultiplier tube supplied with a bias voltage of -500 Volts by a Power Design Pacific model HV-1547 power supply. To reduce detection of the continuous emission from the glowing shock heated gas, the laser is operated at maximum power, and a narrow-band interference filter (at 632.8 nm) together with various optical stops are placed between the shock tube and the photomultiplier tube. The output signal from the PM tube is displayed on the same digital oscilloscope used to record the pressure trace.

a. Soot Yield Measurements by Light Extinction

With the short reaction times used in these experiments, the soot particles can be considered young and, according to Graham et al. (Reference 14), are spherical, with diameters small (< 300 Å) compared to the wavelength of the incident laser radiation. In this regime, the small particle limit (Rayleigh limit) of the Mie theory applies. Below this limit, the ratio of scattering efficiency to extinction efficiency is so small that the soot particles are

considered to be emitters and absorbers only (Reference 62). Furthermore, it has been shown that the emission signal of soot is so small in comparison to the absorption signal that it can be neglected (Reference 63). Given these restrictions, the soot yield, Y, defined as the fraction of carbon atoms initially present which have been converted to soot is given as:

$$Y = N_o \rho_s \lambda [\ln(I_0/I(t)] / 72 \pi L E(m) [C_o] \quad (1)$$

where

Y is the fractional soot yield,
N_o is Avogadro's number,
ρ_s is the density of the hot soot particle,
λ is the wavelength of the incident light,
I_o is the initial beam intensity,
$I(t)$ is the beam intensity ant time t,
$I_o/I(t)$ is the absorbance,
L is the optical path length,
$[C_c]$ is the initial carbon concentration,
m is the complex refractive index of a soot particle,

and

$$E(m) = -Im\{(m^2 - 1)/(m^2 + 2)\}.$$

Since so little is known about the complex index of refraction, the soot yields presented in this work are in the form Y * E(m), to emphasize the uncertainty in the value of m.

b. Linearity and Frequency Response of the Optical Probe

An RCA Model IP28 photomultiplier tube (PMT) is used to monitor the attenuation of a He-Ne laser by soot particles formed in the test section, i.e. to measure I_o and I(t) used in Equation (1). For accurate measurements of I(t), it is imperative that the time constant of the PMT be small in comparison to the 2-3 ms reaction time involved in the experiments. Initial observations, however, indicated that the PMT, as configured by previous users of the shock-tube facility, had a relatively large time constant. This observation necessitated

investigation of the PMT response. In addition, the linearity of the PMT output with respect to incident intensity was verified.

A Stroboscope Model TS-805 strobe light was used to test the frequency response of the PMT. The time characteristics of the strobe output was first measured with the help of Dr. Louis DiMuro, Department of Physics. These measurements showed that, for a digital scope sweep rate of 2 μs/point (the sweep rate used in our experiments), the strobe output should appear as a sharp pulse followed by a barely perceptible decay back to the original zero voltage. When the strobe light was directed onto the PMT, however, the output was a sawtoothed shaped signal with a time constant of 166 μs, far too large for accurate measurements of beam intensity over the duration of our experiments. An inspection of the PMT configuration revealed that the output of the PMT was connected directly to the input of the oscilloscope, which has an input impedance of 1 MΩ. This resulted in a high output voltage but an excessive RC time constant.

The problem was corrected by installing a load resistor across the PMT output; the voltage across the resistor provided the input to the oscilloscope. With a load resistance of 10 kΩ, the time constant of the strobe response was reduced to 11 μs. To increase the PMT supply voltage to recommended values without driving the tube to saturation, however, it was necessary to introduce a neutral density filter into the path of the incident beam. A filter with 13 percent transmittance allowed the PMT supply voltage to be raised to 500 Volts, nearly twice the recommended minimum.

Once the circuitry was improved, the linearity of the PMT with incident intensity was measured by introducing neutral density filters with successively lower transmittances into the optical path. The results, shown in Figure 5 indicate excellent linearity over the range of incident intensities used in the experiment.

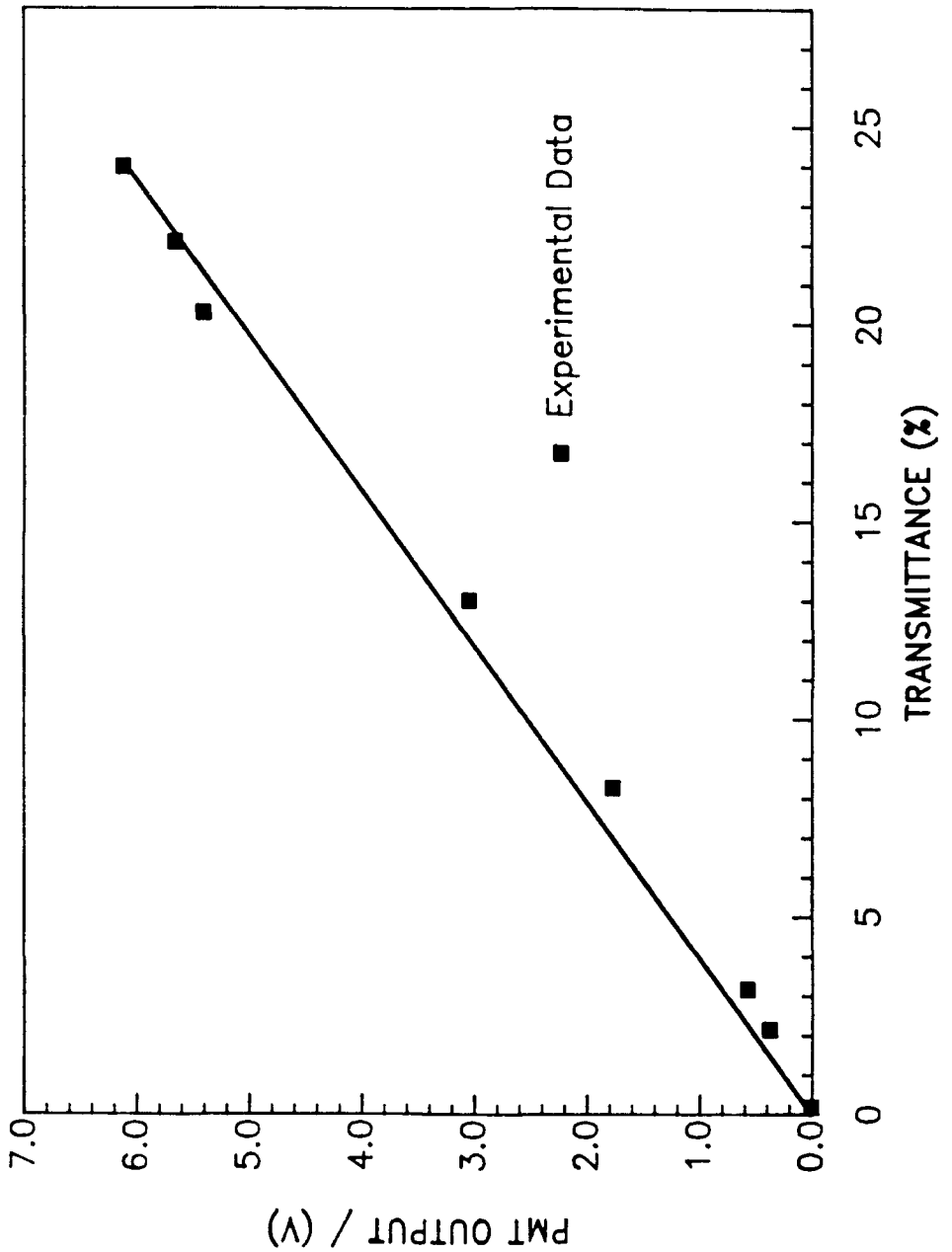

Figure 5. Linearity of the PMT Response to Incident Intensity.

6. Data Acquisition and Processing

The oscilloscope used to digitize, display, and record the output signals from the PCB transducer and PM tube was a Nicolet model 2090-III digital oscilloscope. This oscilloscope can sample voltages from two channels, each of which can store 2048 data points. The displayed oscilloscope traces can be stored permanently on magnetic diskettes for future analysis.

An example trace is displayed in Figure 6. The pressure rises from the initial driven-gas pressure, P1, to the incident shock pressure, P2, and then to the reflected shock pressure, P5, after which it falls off with the arrival of the expansion wave. The reflected shock arrival is seen on the laser-extinction trace as a Schlieren spike, which owes to the rapid change in density experienced by the test gas. The maximum test time is determined by the time between reflected shock arrival and expansion wave arrival at the transducer station, with experiment time varying from 3-4 ms at low temperatures to 2-3 ms at higher temperatures. Note that time is measured from the arrival of the reflected shock.

The fundamental data in these traces are the ratios $I_o/I(t)$, obtained by measuring the initial intensity I_o (proportional to the output voltage from the PMT) and the intensity I(t) at any time, t. These ratios are used in Equation (1) to determine the soot yield. The ratios are arbitrarily, but conveniently, taken at 0.25 ms intervals from 0 to 2 ms. Other parameters obtained from the traces are the inception time, τ_{soot}, and the soot production rate, R_{soot}, defined as the slope of the laser-extinction trace at its inflection point, as shown in Figure 7. The inflection point is not always easy to determine from the extinction trace, especially at high reaction temperatures. This leads to scatter in the values of both the soot production rate and the inception time.

B. TEST MIXTURE PREPARATION

The test gas mixtures are prepared manometrically in stainless steel tanks having volumes of 37 liter. Before a gas mixture is prepared, the tank in which

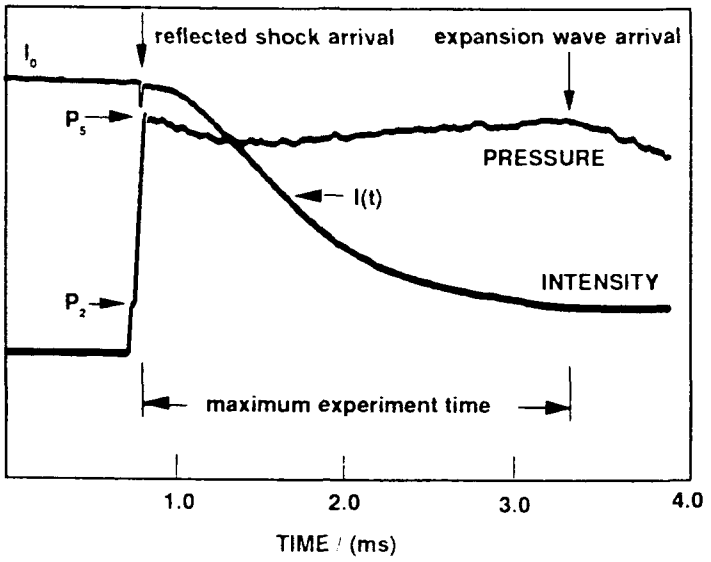

Figure 6. Typical Digital Oscilloscope Trace of the Pressure and PMT Output.

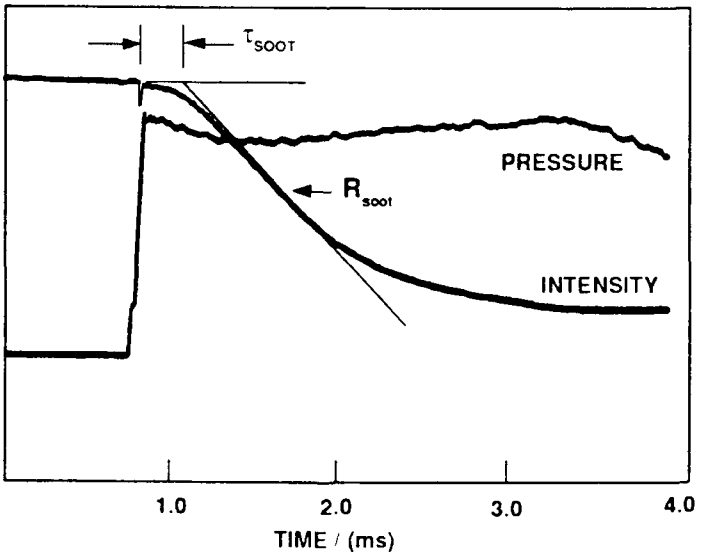

Figure 7. Graphical Depiction of Soot Formation Rate and Induction Time.

it is to be stored is heated for at least twelve hours at a temperature near 480 K while being continuously evacuated by the mechanical pump. After cooling to room temperature, the tank is pumped down to less than 1.0×10^{-5} torr by the diffusion pump. Gas phase components are injected directly into the mixture tanks through the gas handling manifold. Throughout the mixture preparation, gas pressures are measured using the Datametrics digital manometer. To ensure that there is no condensation of any vapor phase components, the total mixture pressure is kept to less than one half of the liquid vapor pressure of the fuel.

For liquid phase compounds, the vapor above the purified liquid is used. To purify the liquid, it is poured into a steel vessel and repeatedly frozen and thawed under vacuum. The frozen solid is evacuated to a pressure of $< 1.0 \times 10^{-5}$ torr to remove moisture and any dissolved impurities.

The composition of each test mixture used in the experiments of this study was verified by analysis with a Hewlett Packard model 9630 Gas Chromatograph. The concentration of benzene was measured to within ± 0.02 percent. The amount of iron in the $Fe(CO)_5$ mixtures was determined by atomic absorption. A known volume of the gaseous mixture was bubbled through a mixture of I_2-KI in a 3 percent HCl solution. The iron was absorbed in the solution, which was the analyzed with a Varian model AA-1475 Atomic Absorption Spectrophotometer. The iron concentration was accurately measured to within ± 0.2 ppm as $Fe(CO)_5$.

C. SHOCK TUBE OPERATION

The diaphragms are installed before each experiment and the driver and driven sections are evacuated with the mechanical pump. Once the pressure in the driven section is low enough, the section is further evacuated by the diffusion pump to a pressure of 1.0×10^{-5} torr. The laser beam aperture is opened, and the proper gain and sweep speed on the oscilloscope are set.

After it has been isolated from the diffusion pump, the driven section is filled with the test mixture to the prescribed pressure. Subsequently, the driver section and spacer are isolated from the mechanical pump and filled with helium. When the driver/spacer system pressure reaches one half the required

driver pressure, the spacer is isolated and the driver is filled to the appropriate driver pressure, P4, necessary to produce the chosen experimental conditions behind the reflected shock wave.

To initiate the shock, the valve connecting the spacer to the vacuum system is opened. As the spacer empties, the pressure differential across the diaphragms becomes sufficiently large to rupture them, and the expansion of the helium gas generates a normal shock wave which travels down the experimental section and reflects off the end wall, producing the high temperatures and pressures at which the reactions take place.

After the experiment, the product gases are vented into the laboratory exhaust system, and the timer readings and oscilloscope traces are recorded. After the tube had been thoroughly vented, nitrogen is used to backfill the system to atmospheric pressure, and the tube is opened. The shock tube is then cleaned out with laboratory wipes fitted over a pig, the diaphragms are replaced, and the entire procedure is repeated at a different experimental conditions.

The conditions behind the incident and reflected shock waves are calculated by measuring the velocity of the incident shock wave and iteratively solving the conservation equations of mass, momentum, and energy, along with the equation of state across a shock wave (Reference 64). The laser-extinction traces are transferred from the oscilloscope to an Apple II microcomputer via a GPIB/IEEE-488 interface, where it they are reduced using PASCAL language programs, which generate incident and reflected conditions, as well as soot yields. The soot yield data are then transferred to an IBM 370-3081 computer for plotting (Reference 65).

SECTION IV

PRESENTATION AND DISCUSSION OF EXPERIMENTAL RESULTS

A. OVERVIEW

The objective of the experimental measurements was to determine if iron has an effect on soot formation chemistry during the pyrolysis and oxidation of benzene over a range of reaction temperatures and pressures. A series of base-case measurements was obtained for the pyrolysis and oxidation of benzene-argon mixtures. Any effect induced by the addition of iron to the gas mixture could then be identified by deviations from the base-case measurements.

In addition, a series of measurements was made to determine the effect of variations in benzene concentration. All test mixtures used in this study were prepared manometrically and concentrations verified by gas chromatographic analysis. The GC analyses showed that, despite care in the preparation of test mixtures, benzene concentration could be replicated only to within about 10 percent. Thus any deviation of the measurements with additives from the base-case measurements must be interpreted with respect to any deviations caused by changes in benzene concentration.

The test mixtures used in this study, together with the relevant experimental conditions, are summarized in Table 1. Complete tables of experimental conditions and results for each mixture are provided in Appendix A. A map showing how the test conditions for individual experimental series were varied according to benzene and additive concentrations, pyrolysis and oxidation, and pressure is given in Figure 7. The range of initial carbon atom concentrations at the reaction pressures was from 1.07×10^{-17} atoms/cm^3 to 4.22×10^{-17} atoms/cm^3. Within each individual series, however, the initial carbon atom concentration was held to within $\pm$ 3 percent. Note that for measurements at the elevated pressure, we attempted to maintain the initial fuel and additive concentration (at the reaction pressure) approximately equal to the corresponding concentration used for measurements at the lower reaction pressure.

TABLE 1. SUMMARY OF EXPERIMENTAL SERIES

Series	C_6H_5 (volume %)	Additive	T_5 (K)	P_5 (atm)	$[C_o]x10^{-17}$ (atom/cm^3)
		Base Pressure -- Pyrolysis			
D	0.208	0	1685 - 2231	2.10 - 2.70	1.07 - 1.25
Q	0.270	0	1602 - 2213	2.13 - 2.85	1.52 - 1.58
C	0.293	0	1566 - 2231	1.88 - 2.68	1.53 - 1.62
K	0.373	0	1612 - 2249	2.09 - 2.8[illegible]	[illegible].04 - 2.13
G	0.278	3.0 ppm CO	1517 - 2127	1.82 - 3.02	1.47 - 1.61
F	0.380	3.5 ppm CO	1585 - 2257	2.03 - 2.86	1.50 - 1.57
P	0.361	63.8 ppm CO	1624 - 2203	2.16 - 2.92	2.5 - 3.00
H	0.275	0.56 ppm $Fe(CO)_5$	1539 - 2312	1.91 - 2.30	2.11 - 2.19
J	0.382	13.5 ppm $Fe(CO)_5$	1642 - 2286	2.03 - 2.93	2.13 - 2.19
CC	0.293	3.0 ppm O_2	1626 - 2240	2.00 - 2.67	1.51 - 1.59
		Elevated Pressure -- Pyrolysis			
M	0.114	0	1576 - 2189	4.90 - 6.82	1.49 - 1.56
L	0.373	0	1670 - 2259	4.22 - 5.64	4.05 - 4.22
O	0.114	0.755 ppm CO	1582 - 2155	4.82 - 6.47	1.51 - 1.53
N	0.123	0.151 ppm $Fe(CO)_5$	1650 - 2246	4.78 - 6.39	1.52 - 1.57
		Base Pressure -- Oxidation (0.28 % Oxygen)			
V	0.273	0	1549 - 2192	2.02 - 2.80	1.53 - 1.58
S	0.286	3 ppm CO	1600 - 2214	1.98 - 2.67	1.51 - 1.56
Y	0.295	62.5 ppm CO	1631 - 2193	2.10 - 2.79	1.56 - 1.66
T	0.289	0.5 ppm $Fe(CO)_5$	1561 - 2202	1.98 - 2.78	1.53 - 1.58
X	0.259	11.5 ppm $Fe(CO)_5$	1585 - 2175	2.18 - 2.90	1.53 - 1.57
		Elevated Pressure -- Oxidation (0.12% Oxygen)			
Z	0.111	0	1602 - 2152	4.98 - 6.76	1.52 - 1.58
BB	0.119	1.60 ppm CO	1626 - 2136	4.89 - 6.21	1.52 - 1.58
AA	0.123	0.318 ppm $Fe(CO)_5$	1644 - 2139	4.81 - 6.13	1.54 - 1.58

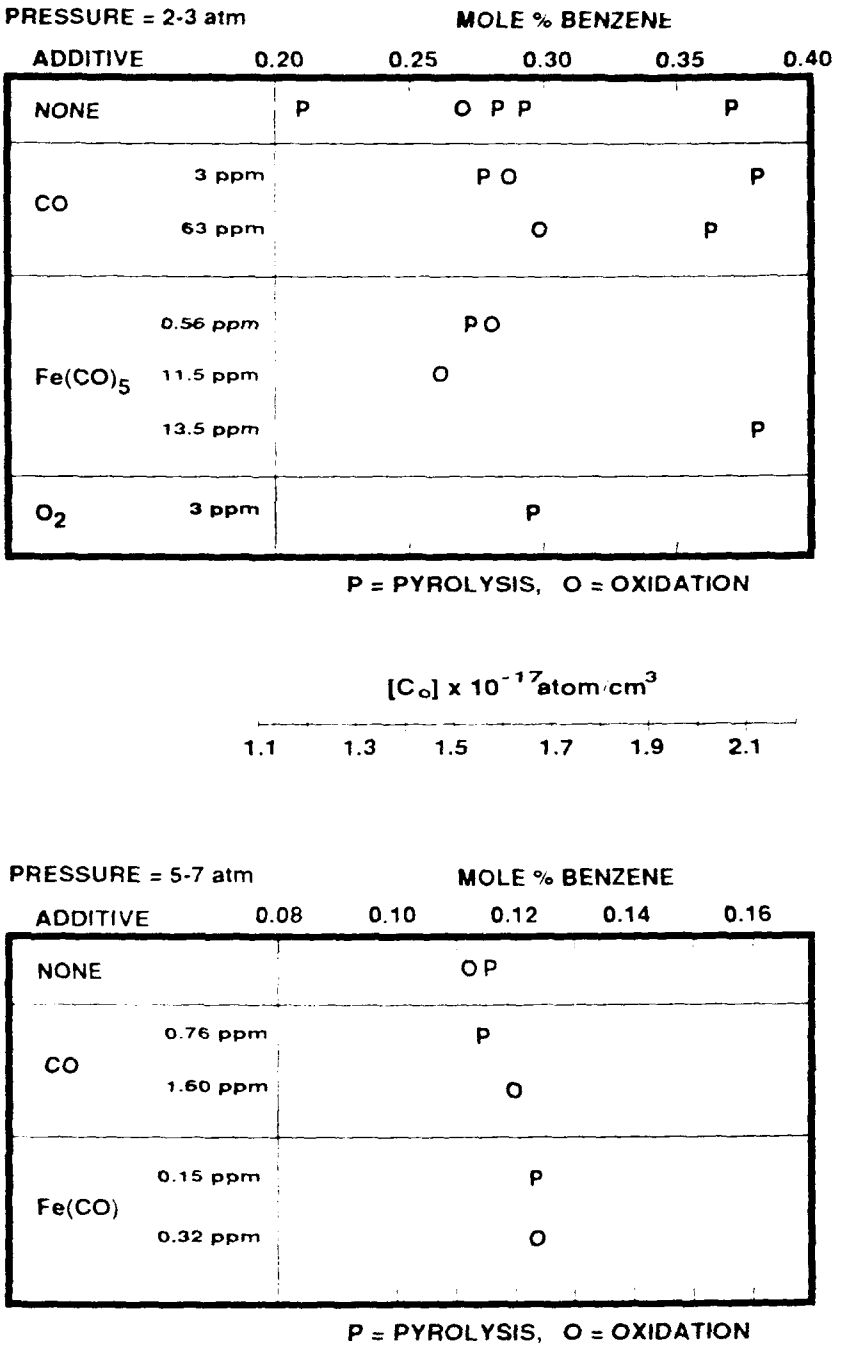

Figure 7. Map of Experimental Conditions

In the material that follows, we begin with the results for pyrolysis of the base benzene-argon mixtures, first at reaction pressures of 2-3 atmospheres and then at reaction pressures of 5-7 atmospheres. The effects of additives are then shown by comparing the experimental results obtained when iron pentacarbonyl (and as a control, carbon monoxide) was added to the corresponding results for the base mixtures. The large, unexpected increase in soot yield with the addition of small amounts of carbon monoxide is a striking feature of these data. A similar presentation of the results for oxidation then follows.

B. PYROLYSIS MEASUREMENTS

The series C, Q, D, and K were used to establish baseline cases for soot production during benzene pyrolysis. To study the effect of iron on soot production, iron pentacarbonyl was added in quantities to obtain 0.05 weight percent Fe and 0.89 weight percent Fe. Experiments were also performed with mixtures containing carbon monoxide at five times the molar concentration of $Fe(CO)_5$. Since the $Fe(CO)_5$ molecules dissociate into one Fe and five CO molecules before soot formation begins, the comparison of the data from these two mixtures ($Fe(CO)_5$ vs. CO) revealed the effect of elemental iron during benzene pyrolysis.

The map given in Figure 7 shows that, for the low pressure (2-3 atmosphere) measurements, there were two main groups of benzene concentrations studied. The concentrations of these groups were centered about 0.28 percent and 0.38 percent. At the reaction conditions, these concentrations resulted in an initial carbon atom concentrations centered about 1.5×10^{-17} atoms/cm^3 and 2.1×10^{-17} atoms/cm^3, respectively. Iron pentacarbonyl, at 0.05 weight percent Fe (0.557 ppm $Fe(CO)_5$), and carbon monoxide, at 3.0 ppm, were added to the mixtures in the lower concentration group. For the group at higher fuel concentrations, iron pentacarbonyl, at 0.89 weight percent of fuel Fe (13.50 ppm $Fe(CO)_5$), and CO, at 3.5 ppm and 63.8 ppm, were added.

For the elevated pressure (5-7 atmosphere) measurements, a single benzene concentration group centered about 0.14 percent was studied. At the reaction conditions, this concentration resulted in initial carbon atom concentrations

centered about 1.5×10^{-17} atoms/cm^3, and provided a basis for evaluating the effect of pressure. Iron pentacarbonyl and carbon monoxide were added, also at proportionately reduced concentrations, to maintain essentially the same mole ratio with benzene as was used the series at reduced pressures.

1. Effect of Benzene Concentration

Soot yields obtained for the four base-case benzene mixtures studied are plotted versus reaction temperature, at four reaction times, in Figures 8. To avoid excessive clutter, only the results for reaction times of 0.5, 1.0, 1.5, and 2.0 ms are shown. The symbols represent actual data, while the solid lines, which are least-squares fits to a Maxwell distribution, are added merely to guide the eye. The Maxwell distribution is a convenient fitting function because of its shape properties, but no representation of any kinetic model is implied.

The shape of the curves is bell-like, with the maximum soot yield occurring at 1800-1900 K. These soot yield "bells" are similar to those reported by Clary (Reference 15) and Frenklach (Reference 17), and the Series C measurements match the data obtained by Clary for a similar concentration of benzene in argon. The curves exhibit, as reaction time increases, a similar shift of the temperature at which the soot yield is a maximum. Note that the shift in temperature asymptotically approaches a limiting value of about 1900 K for long reaction times.

The soot yield dependence cn time, temperature, and concentration follows the general trends predicted by Frenklach's conceptual model mentioned in Section II (see page 9). In this model, the first reaction (R1) represents ring fragmentation, such as benzene forming acetylene, and the second reaction (R2) represents polymeric additions of intact aromatic rings. At low temperatures the addition of aromatic rings is the main pathway to soot formation. As the temperature increases, so does the conversion to soot via these polymeric additions. As the temperature is further increased, the fragmentation reaction begins to dominate, reducing the number of intact aromatic rings, and therefore slowing the polymerization reaction. At high temperatures, the fragmentation reaction becomes predominant, and the final soot yield is low because the amount

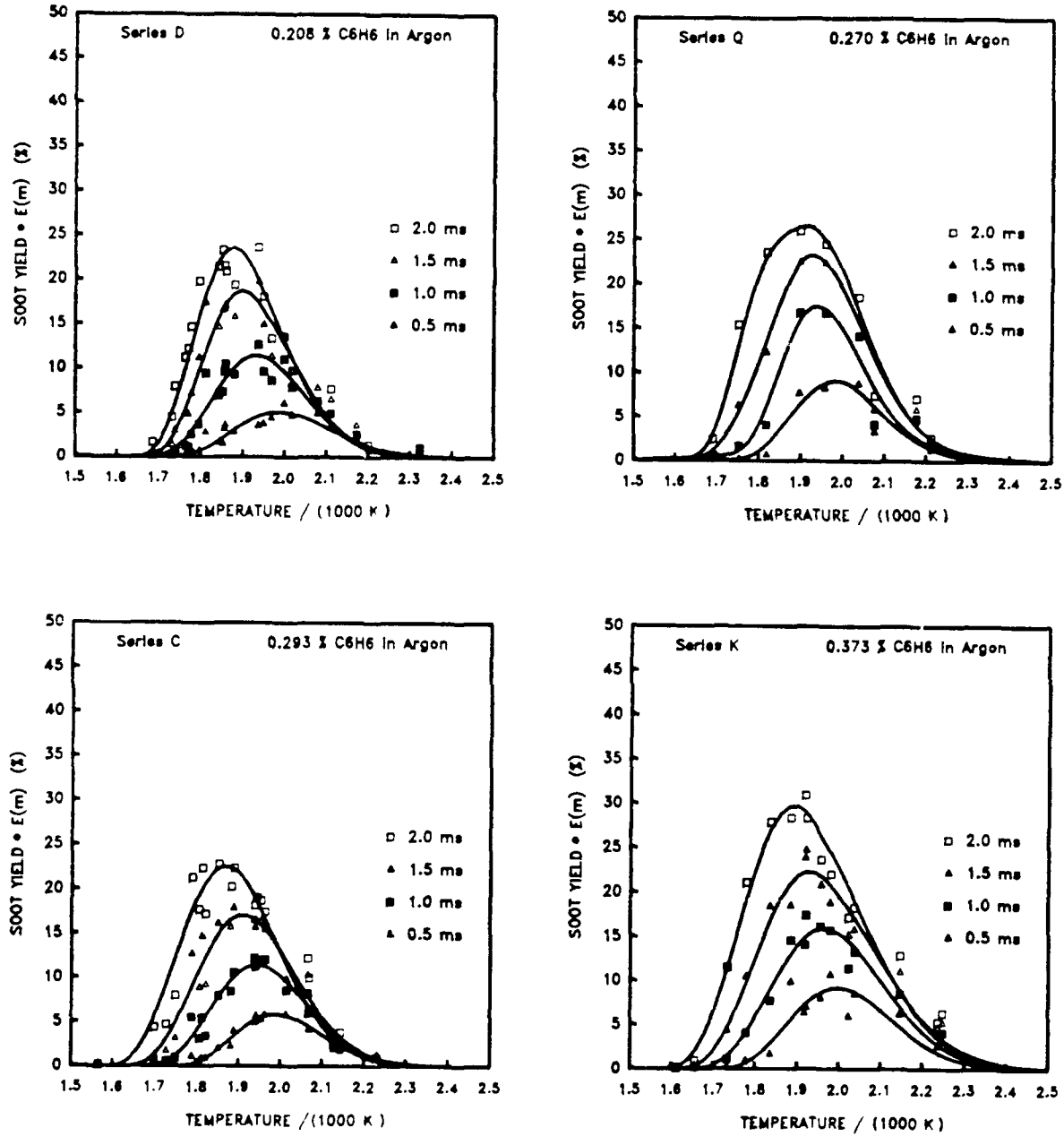

Figure 8. Effect of Benzene Concentration of Soot Yield During Pyrolysis at 2-3 Atmospheres Reaction Pressure.

of aromatic fuel available for polymerization is rapidly consumed. Soot formation from benzene fragments may still take place, but the reaction is much slower.

Note that the curves are steeper on the low temperature side, but tend to "tail off" at higher temperatures. This characteristic is a reflection of the temperature dependence of the laser-extinction traces. At lower temperatures, there is a relatively long induction period before soot particles began to appear. After this initial delay, however, the steepness of the laser-extinction trace indicates that the rate of soot formation is sufficiently high to form considerable amounts of soot before the experiment was over. At higher temperatures the induction time is much shorter, i.e., soot is formed much sooner. The laser-extinction trace is very steep at the shock wave arrival, but flattens out quickly.

The data for Series C (0.293 percent benzene, shown at the lower left in Figure 8) matched the data obtained by Clary (Reference 15) for a concentration of 0.311 percent benzene; the slight difference in concentration seemed to have little effect on the soot yield. The effect of increasing the benzene concentration from 0.208 percent (Series D, upper left) to 0.293 percent was negligible; the soot yield bells for these two mixtures were quite similar. As is seen in the lower right of Figure 8, the base-case mixture with 0.373 percent benzene (Series K) resulted in higher soot yields. At 2.0 ms, the maximum soot yield for this mixture was 34 percent, compared to 24 percent for series C and D. Series Q (upper right in Figure 8) is discussed below.

Soot yields for the base-case mixtures at a reaction time of 1 ms are compared in Figure 9. Note that Series D and C (0.208 and 0.293 percent benzene) are, within the scatter of the data, identical. The soot yields for series K (0.373 percent benzene) are approximately 50 percent greater. The soot yields for Series Q (0.270 percent benzene) follow those for Series D and C in the low and high temperature regions, but the fitted curve is narrower and higher in the central region between 1850 K and 2050 K. This behavior must be viewed with caution, however, since only three data points define the shape of the curve in the central region. Note also in Figure 8 that for longer reaction times, the

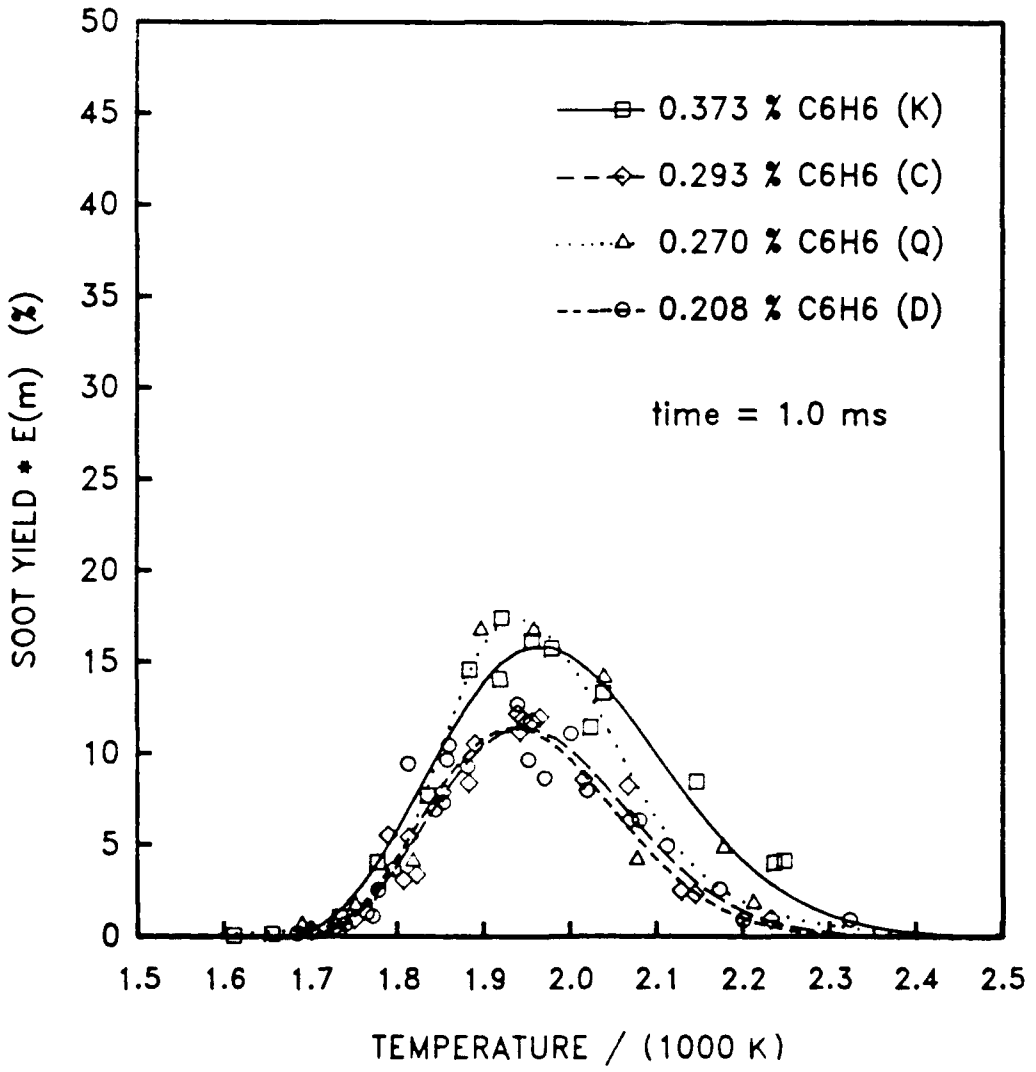

Figure 4. Comparison of Soot Yields at 1-ms Reaction Time Showing Effect of Benzene Concentration.

soot yields for Series Q follows more closely those for Series D and C than those for Series K.

The induction times and rates for these four series are shown in Figure 10. In this figure, as is the case for all induction time and rate data presented in this paper, the straight lines through the data points are least-square regressions of the natural logarithm of induction time (or rate) on absolute temperature (or inverse temperature). The induction time is seen to decrease as the reaction temperature is increased. There is, however, no apparent systematic variation of induction time with benzene concentration for the four base-case series. An analysis of variance revealed no statistically significant difference in either the slope or the magnitude of the regression lines at the 90 percent confidence level.

The trends of the regression lines for the soot formation rate are consistent with an Arrhenius rate expression of the form

$$R_{soot} = A\ [C_6H_6]^{\alpha}\ \exp(-E_a/RT) \qquad (2)$$

where A is the Arrhenius premultiplier, $[C_6H_6]$ is the benzene concentration, α is the reaction order, E_a is the activation energy, R is the gas constant, and T is the absolute temperature. The rate of soot formation is proportional to the slope of the laser-extinction trace at the inflection point. The slope was determined graphically, and it was often difficult to determine with precision the location of the inflection point, especially at high reaction temperatures. Since a small error in locating the inflection point can lead to a relatively large error in the slope, the measured rates of soot formation show considerable scatter. Nevertheless, the measured rates exhibit the expected Arrhenius behavior, i.e., the rate increases with both concentration and temperature. Although the slopes of the regression lines are not significantly different, indicating no statistically significant difference in the activation energies, the increase in rate with concentration is significant at the 90 percent confidence level.

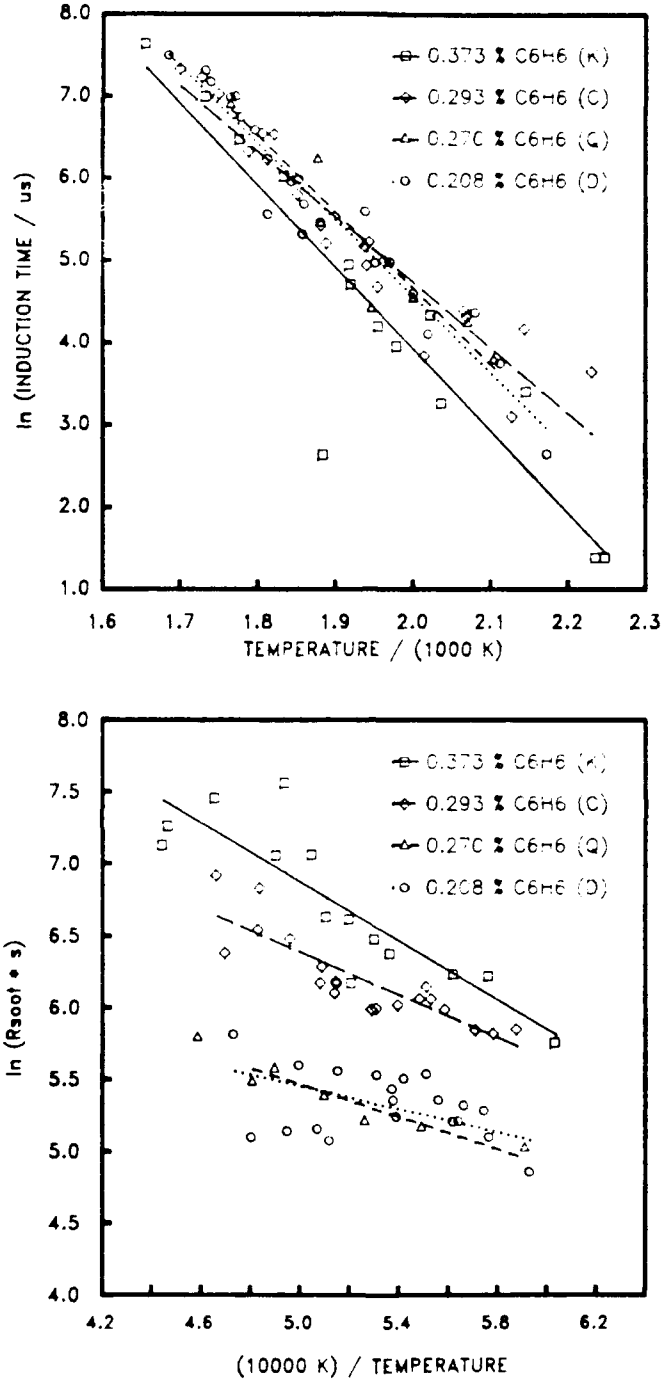

Figure 10. Effect of Benzene Concentration on Induction Times and Rates of Soot Formation During Pyrolysis at 2-3 Atmosphere Pressures.

2. Effect of Reaction Pressure on Benzene Pyrolysis

To test the effect of pressure on benzene pyrolysis, a mixture of 0.144 mole percent benzene was shocked at 5-7 atmosphere pressures (Series M). At the elevated reaction pressure, the initial carbon atom concentration ranged from (1.52 - 1.62) x 10^{-17} atoms/cm^3, closely matching the concentration range for Series Q. The soot yield curves for Series M and Q are shown in Figure 11; the 1-ms curves are compared in Figure 11. As can be seen, the magnitudes of the soot yields for the two series are scarcely different. The slight decrease in soot yield with increasing pressure is believed to be the result of scatter in the data and not to be a significant effect. Recall also that series Q exhibited a larger soot yield at a 1-ms reaction time than series C and Series D which had higher and lower benzene concentrations, respectively. One can note, however, that the maximum soot yield shifts to a lower temperature by about 50 degrees. This same temperature shift was characteristic of all of the elevated pressure measurements carried out in this study.

The induction times and rates for Series M and Q are shown in Figure 12. As shown in the figure, the rates at high reaction temperatures were excluded from the regression analysis because of the high uncertainty in the measured values. Within experimental error, the induction times and rates obtained for Series M and Q are identical. The small difference in the rate curves, although not statistically significant, supports the observed shift of the soot yield bell at the elevated pressure to temperatures about 50 K lower that the bell at the lower pressure.

Over the 2-7 atmosphere reaction-pressure range used in this study, there is little evidence of any significant effect of pressure on soot yield during benzene pyrolysis, when the initial carbon atom concentration is held constant. Although there is no apparent difference in the magnitude of the soot yield as reaction pressure is increased, the temperature at which the maximum soot yield occurs appears to decrease by about 50 K as the reaction pressure is increased from 2-3 atmospheres to 5-7 atmospheres.

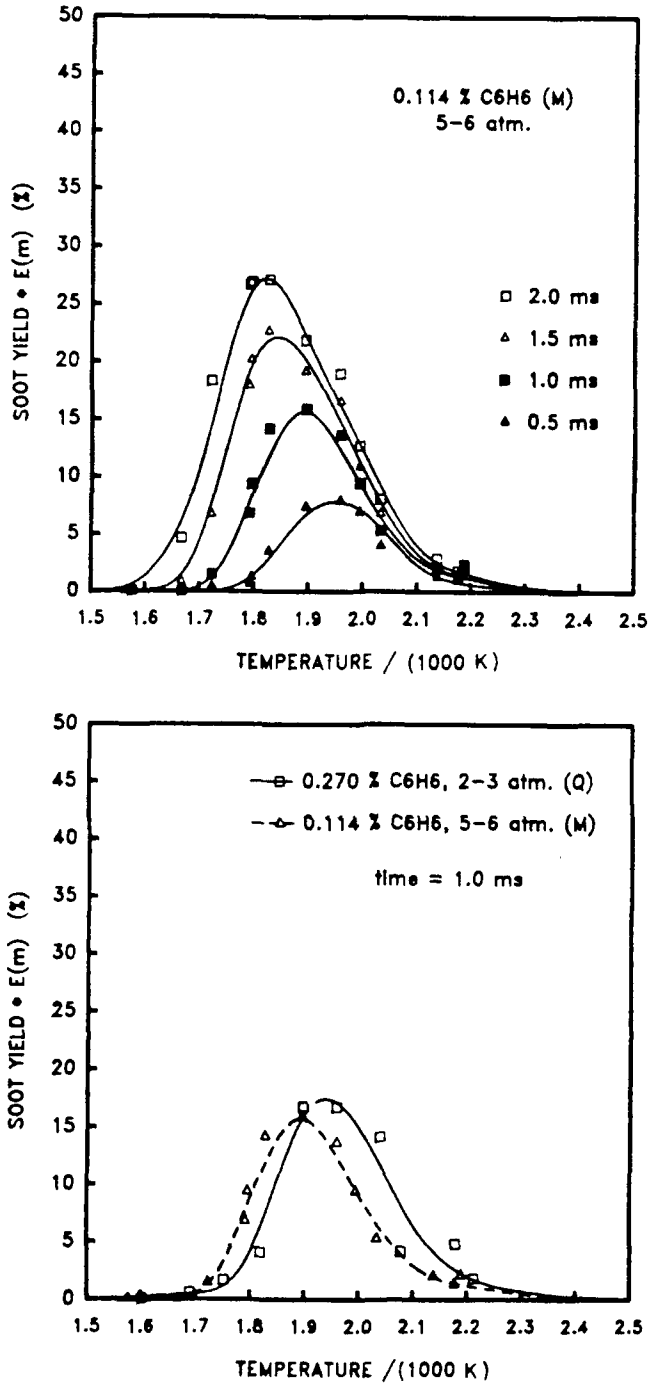

Figure 11. Effect of Pressure on Soot Yield Holding Initial Carbon Atom Concentration at Reaction Pressures Constant.

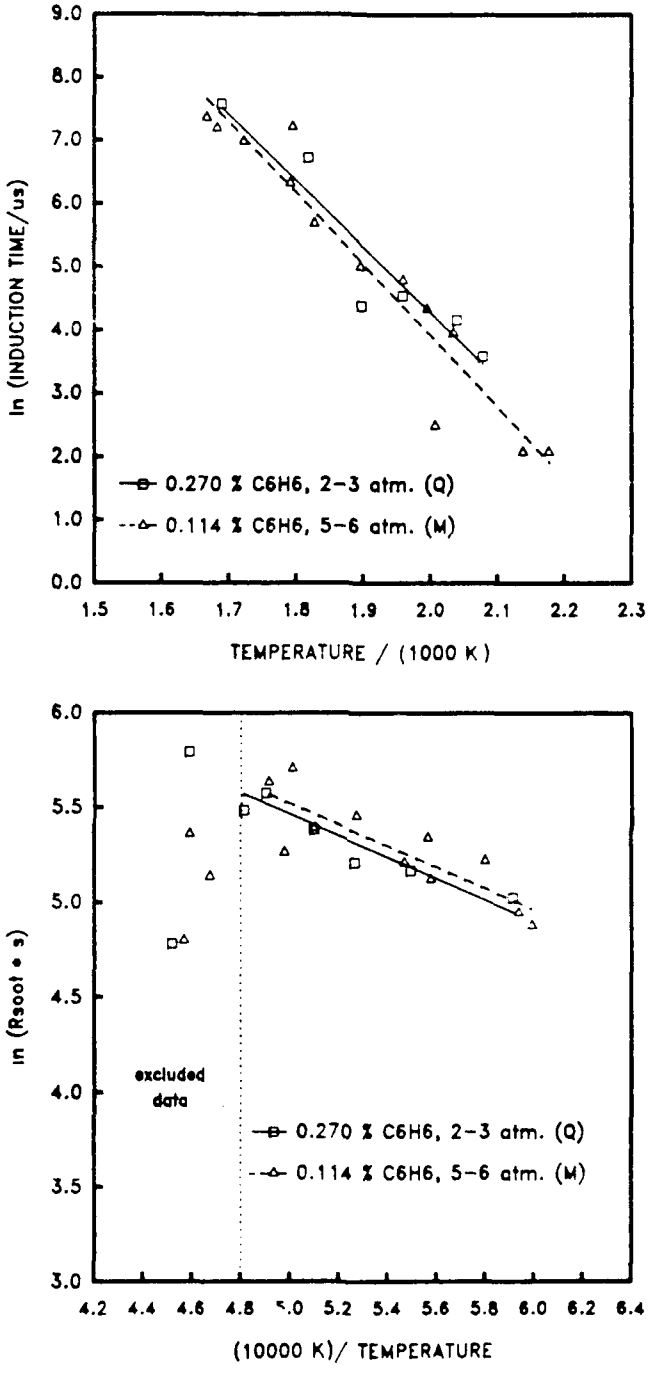

Figure 12. Effect of Pressure on Induction Times and Rates with Initial Carbon Atom Concentration Held Constant.

3. Effect of Additives at 2-3 Atmosphere Reaction Pressure

The additive of interest in this study is iron. As discussed above, iron was added to the test mixtures in the form of iron pentacarbonyl, $Fe(CO)_5$. To ensure that the CO ligands released from the iron pentacarbonyl had no effect on soot formation, it was necessary to study separately a series in which CO was the sole additive. Since the desired iron concentration in a nominal 0.3 mole percent benzene mixture was 0.557 ppm, and since each mole of iron pentacarbonyl releases five moles of carbon dioxide, a mixture of 3 ppm carbon monoxide and 3000 ppm (0.3 mole percent) benzene was an appropriate control mixture. The soot yield curves for a base-case mixture of 0.293 percent benzene (Series C), a mixture of 3 ppm carbon monoxide and 0.278 percent benzene (Series G), a mixture of 0.557 ppm iron pentacarbonyl and 0.275 percent benzene (Series H), and a mixture of 3 ppm oxygen and 0.293 percent benzene (Series CC) are shown in Figure 13. The motivation for including the last of these series, with 3 ppm oxygen, is discussed below.

Much to our surprise, the addition of a small amount of carbon monoxide to the benzene mixture (in the proportion 1 to 1000) substantially increased the soot yield. As seen in Figure 13, the maximum soot yield (at 2.0 ms) was essentially doubled, increasing from 24 percent with the base-case mixture to 44 percent with the addition of CO. The general shape of the soot-yield bells, however, was unaffected.

The addition of 0.56 ppm $Fe(CO)_5$ to a 0.275 percent benzene mixture raised the level of soot production, again without affecting the shape of the soot yield bells. The increase when compared to the base case was from 24 percent to 42 percent. It is reasonable to conclude that the increase of soot yield with the addition of iron pentacarbonyl owes to the CO ligands rather than the iron. Indeed, the presence of iron appears to decrease slightly the enhancement effect of the carbon monoxide.

To check for possible artifacts resulting from shock heating carbon monoxide or iron pentacarbonyl themselves, a separate series of measurements were made, first with a mixture of 3.0 ppm carbon monoxide in argon and then with a

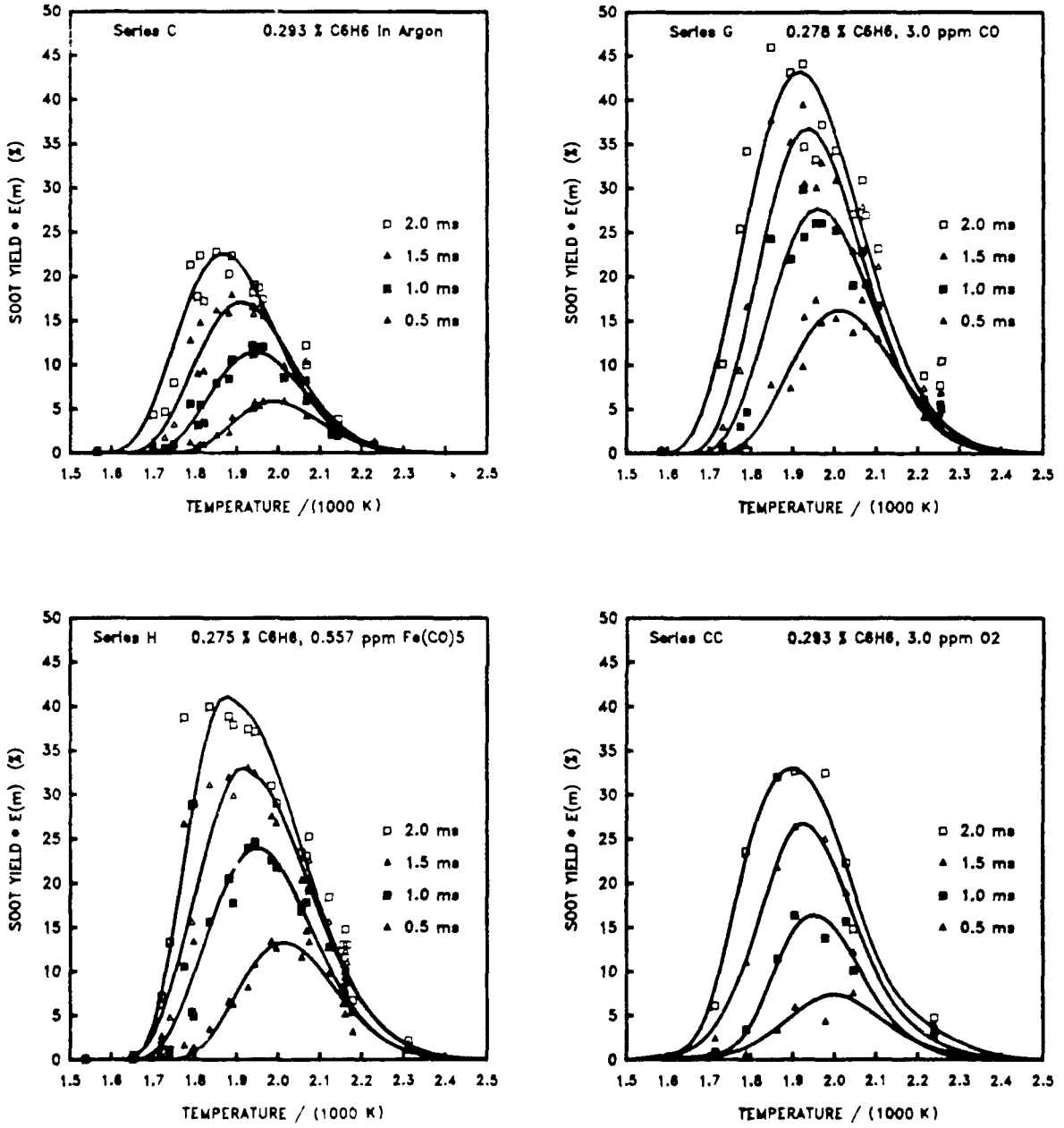

Figure 13. Effect of Carbon Monoxide, Iron Pentacarbonyl, and Oxygen as Additives During Benzene Pyrolysis at 2-3 Atmosphere Pressures.

mixture of 0.56 ppm iron pentacarbonyl in argon. Over the same temperature range used for the additive-benzene mixtures, no attenuation of the laser beam could be detected, i.e. the carbon monoxide and iron pentacarbonyl additives themselves were not contributing to the measured soot yield. Thus the observed enhancement of soot yield with these additives must owe to a modification of the complex chemical pathways for the production of soot from benzene.

At the suggestion of Dr. Michael Frenklach, oxygen was added in place of the carbon monoxide. As can be seen in Figure 13 (lower right), the addition of a small amount of oxygen did increase soot yield, but not nearly to the extent observed with the addition of carbon monoxide. The increase in soot yield is only about a third of that observed with the addition of carbon monoxide.

To aid in the comparison of the four series shown in Figure 13, the soot-yield curves at 1-ms reaction time are superimposed in Figure 14, and the induction times and rates are shown in Figure 15.

Note that the addition of 3.0 ppm of carbon monoxide (Series G) greatly increased the level of soot formation from the base case (Series C), raising it nearly three fold (from a maximum of 11.3 percent to 27.5 percent), but without changing the general shape of the curve. The iron pentacarbonyl mixture (Series H) resulted in a higher level of soot than the base case, but a lower soot yield than the carbon monoxide mixture.

The induction times for the benzene-additive mixtures are compared to those of the base-case mixture in Figure 15. The benzene-additive mixture data varied little from the base-case. An analysis of variance showed that there was no significant difference in the fitted lines at the 0.05 probability level.

The effect of additives on the rate of soot formation is also shown in Figure 15. The fitted lines to the rate data show an increase in rate with the addition of both iron pentacarbonyl and carbon monoxide. The addition of carbon monoxide increased the rate by approximately 40 percent, and the addition of iron pentacarbonyl increased the rate by approximately 26 percent. Note, however, that the addition of either carbon monoxide or iron pentacarbonyl did not effect

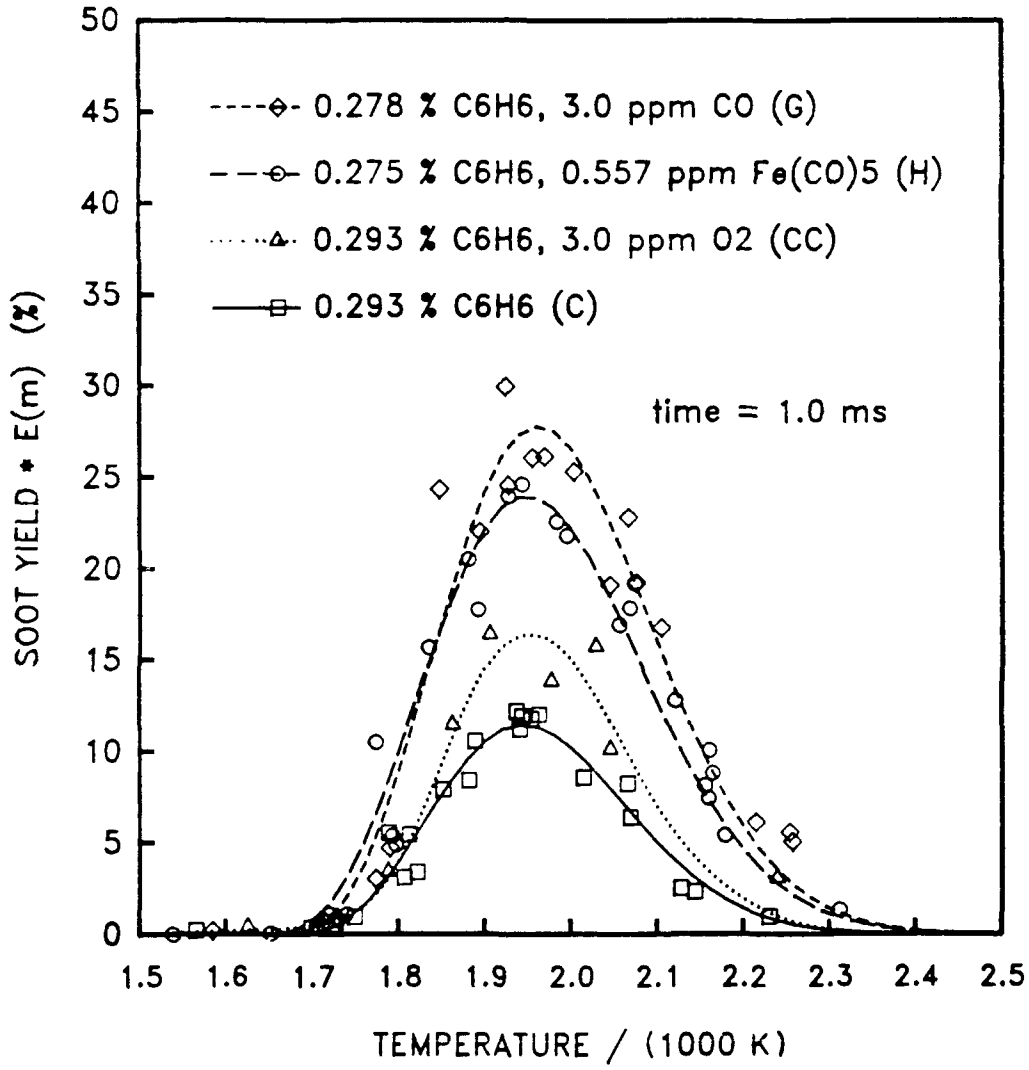

Figure 14. Comparison of Soot Yields at 1-ms Reaction Time Showing Effect of Additives During Benzene Pyrolysis at 2-3 Atmosphere Pressures.

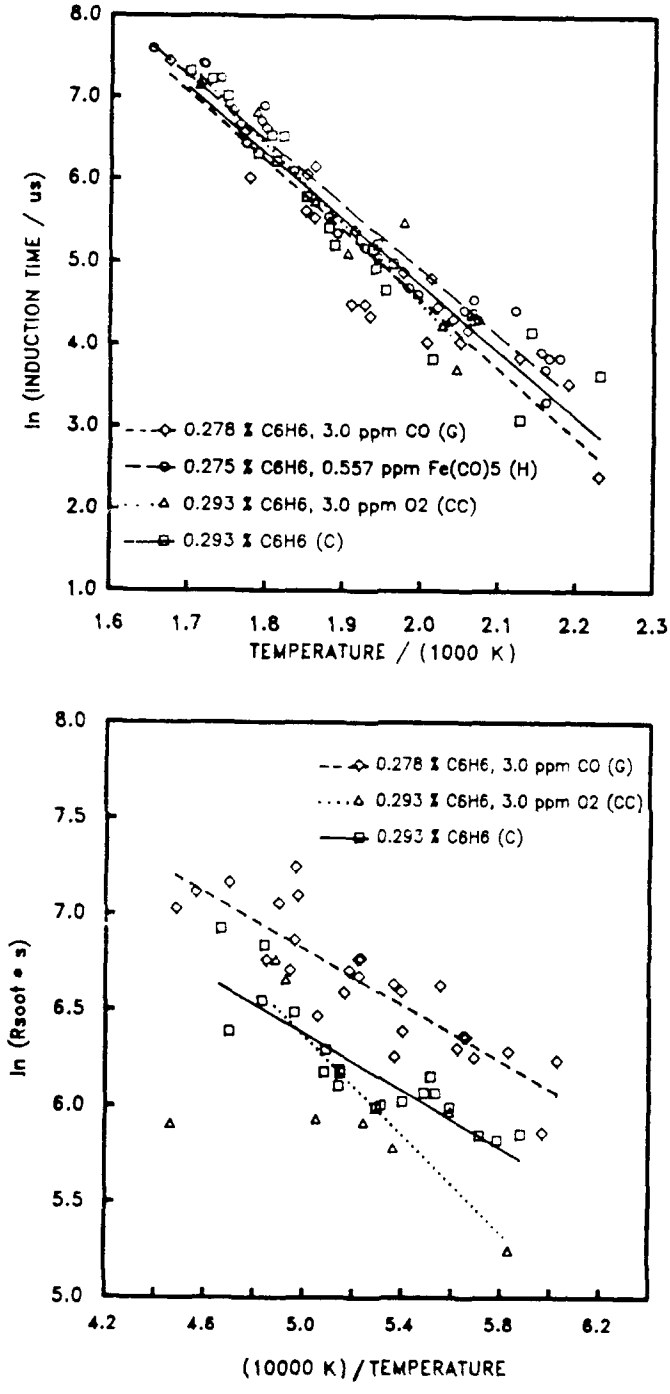

Figure 15. Effect of Additives on Induction Times and Rates of Soot Formation During Benzene Pyrolysis at 2-3 Atmosphere Pressures.

the slope of the regression line. Thus the effect of the additives is to alter the Arrhenius pre-exponential multiplier and not the activation energy. The rates found for the benzene-oxygen mixture are below those for the base-case mixture, and the slope of the regression line appears to be greater, i.e. the activation energy is increased. Although the number of data points are small and the scatter is large, the difference in the slopes of the rate regression lines for the base-case and oxygen mixtures are significant at the 0.05 level of probability. There is not an difference, however, in the intercepts of the regression lines.

The increase in soot yield with the addition of carbon monoxide and iron pentacarbonyl to mixtures of 0.275-0.293 mole percent benzene in argon motivated a series of measurements for mixtures with increased levels of benzene, carbon monoxide, and iron pentacarbonyl concentrations. The soot-yield bells for these four series are shown in Figure 16, the 1-ms curves are shown in Figure 17, and the induction times and rates are compared in Figure 18. Recall that the base-case mixture of 0.373 percent benzene was compared to the benzene mixtures of 0.308, 0.270, and 0.293 percent benzene in Figures 8-10.

As in the previous case, the addition of 3.5 ppm carbon monoxide to a mixture of 0.373 percent benzene in argon increases the soot yield. The increase is not as dramatic, however, as it was for the 0.278 percent benzene mixture. A twentyfold increase in the amount of carbon monoxide added further increases the soot yield, but not proportionately. Finally, the addition of 13.5 ppm iron pentacarbonyl to a 0.382 percent mixture of benzene in argon resulted in soot yields approximately equal to the base-case mixture. These trends can be observed by comparing the soot-yield bells for Series K, F, P, and J in Figure 16, and the 1-ms curves in Figure 17. Note in Figure 17 that the addition of 3.5 ppm carbon monoxide (Series F) increased the maximum soot yield by approximately 18 percent, while the addition of 63.8 ppm carbon monoxide increased the maximum soot yield by approximately 56 percent. Thus the percent increase in soot yield was about three fold with an 18-fold increase in carbon monoxide concentration.

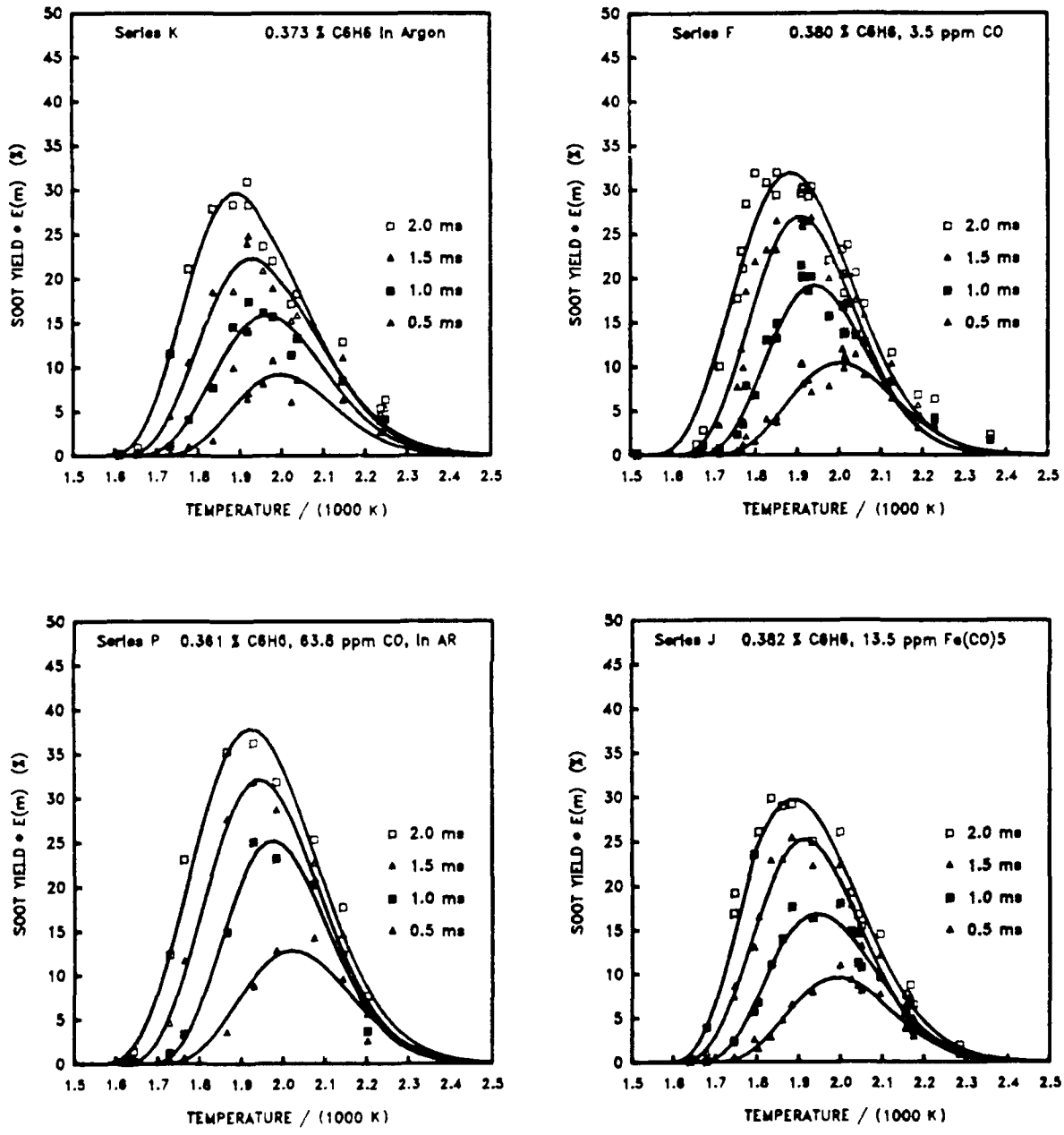

Figure 16. Effect of Additives on Soot Yield for the Pyrolysis of Benzene at Higher Benzene Concentrations.

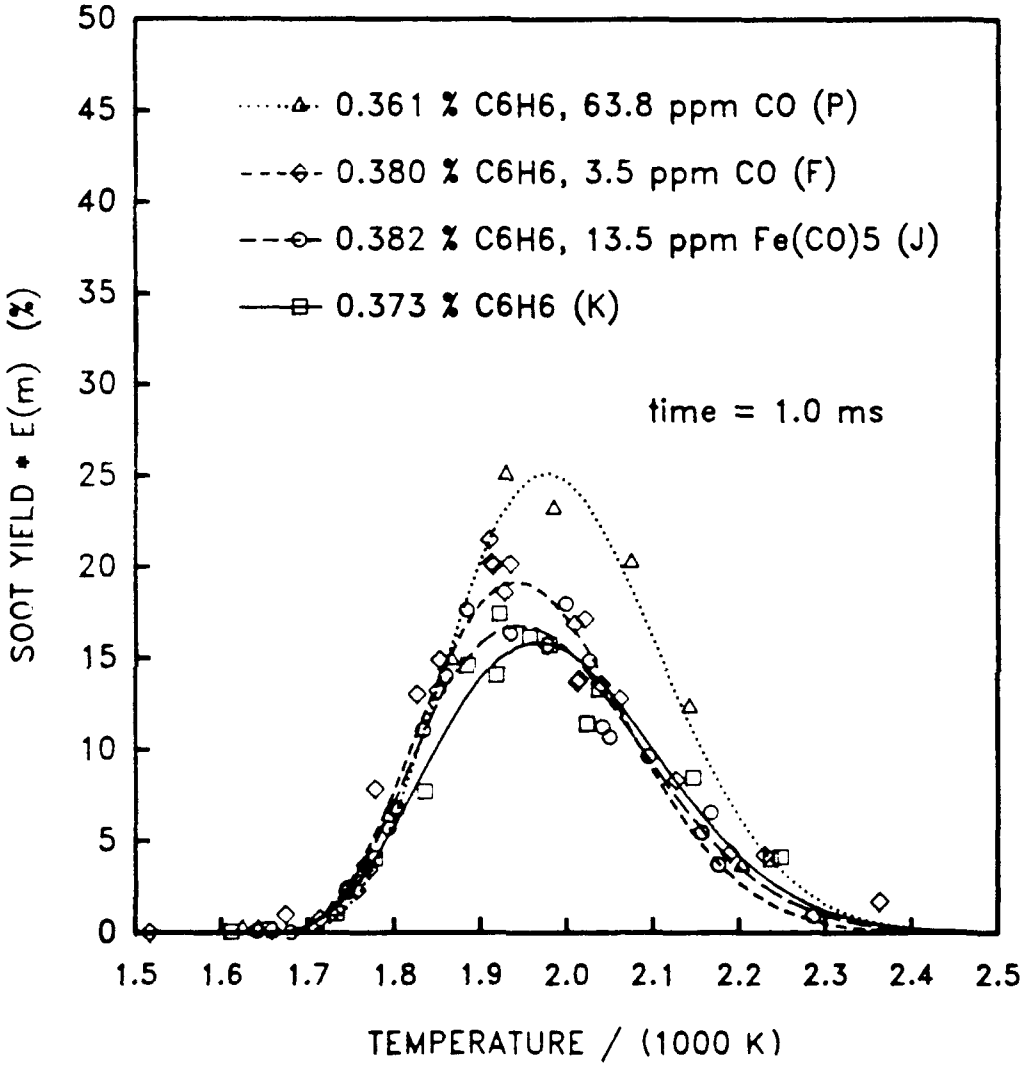

Figure 17. Comparison of Soot Yields at 1-ms Reaction Time Showing Effect of Additives at Higher Concentrations of Benzene.

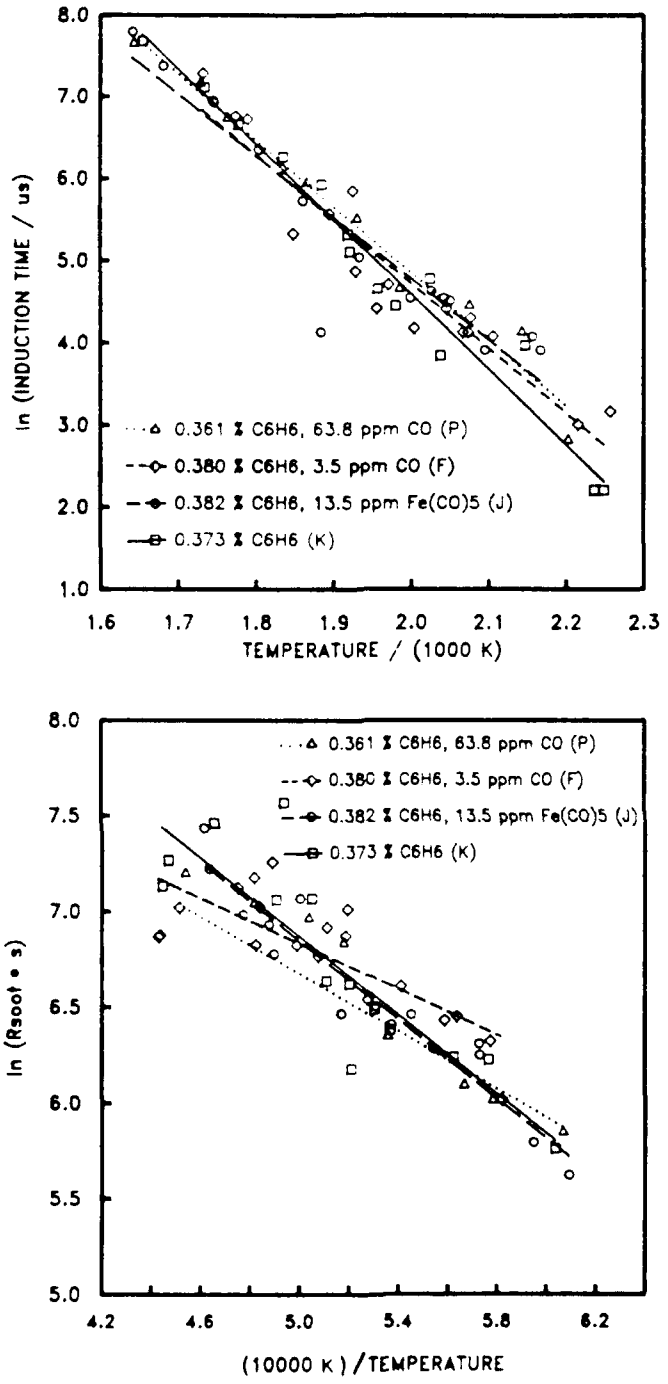

Figure 18. Effect of Additives on Induction Times and Rates of Soot Formation at Higher Concentration Levels of Benzene.

Note also in Figure 17 that the 1-ms curve for Series J (13.5 ppm iron pentacarbonyl) is essentially identical to the base-case mixture (Series K). The amount of carbon monoxide release by the 13.5 ppm iron pentacarbonyl was equivalent to 67.5 ppm, or nearly the same amount of carbon monoxide used in Series P. Thus the iron pentacarbonyl appears to reduce the enhancement of soot yield by carbon monoxide. Although this effect was also seen in the mixtures with lower concentrations of benzene, the effect is much more dramatic at higher concentrations of iron pentacarbonyl.

The induction time for these four series are indistinguishable, as seen in Figure 18. The rate regressions lines, also shown in Figure 18, reflect the behavior observed in the 1-ms curves for Series J and K, i.e. the rates are identical. In contrast the rates for Series F and P (3.5 and 63.8 ppm carbon monoxide respectively) appear to be less at higher temperatures and greater or equal at lower temperatures. However, because of the scatter in the data, neither the magnitude nor the slope of any of the four regressions lines are significantly different at the 0.05 probability level.

4. Effect of Additives at 5-7 Atmosphere Reaction Pressures

The effect of carbon monoxide and iron pentacarbonyl additives at reaction pressures from 5-7 atmospheres is indicated by the soot-yield bells for Series M, O, and N shown in Figure 19. Note that the concentration of benzene and additives have been reduced to provide approximately the same initial atom concentrations (at the elevated reaction pressure) as prevailed in the measurements at 2-3 atmospheres. As can be seen, the soot-yield bells at all reaction times are nearly identical. This can be seen more clearly in the superimposed 1-ms curves shown in Figure 20 and the induction times and rates shown in Figure 21. Although the rates for the benzene base case (Series M) appear to increase more rapidly with temperature that the rates obtained with additives, the differences in the slopes and magnitudes are not statistically significant. Note also that the rates measured at the highest temperatures have no been included in the regression analysis because of the high degree of uncertainty in measuring the slope of the laser attenuation trace obtained at elevated temperatures.

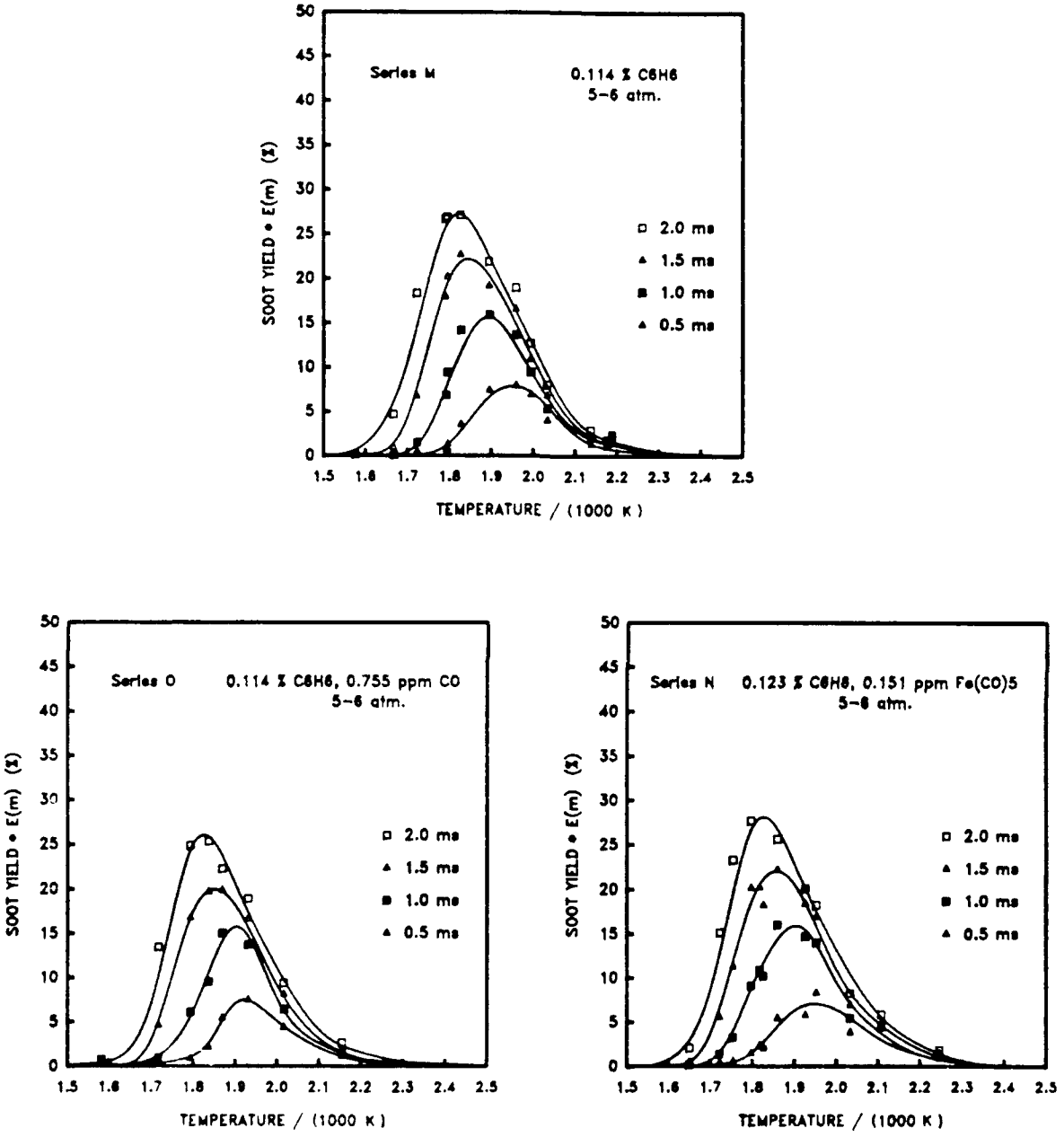

Figure 19. Effect of Carbon Monoxide and Iron Pentacarbonyl on Soot Yield During Benzene Pyrolysis at 5-7 Atmosphere Pressure.

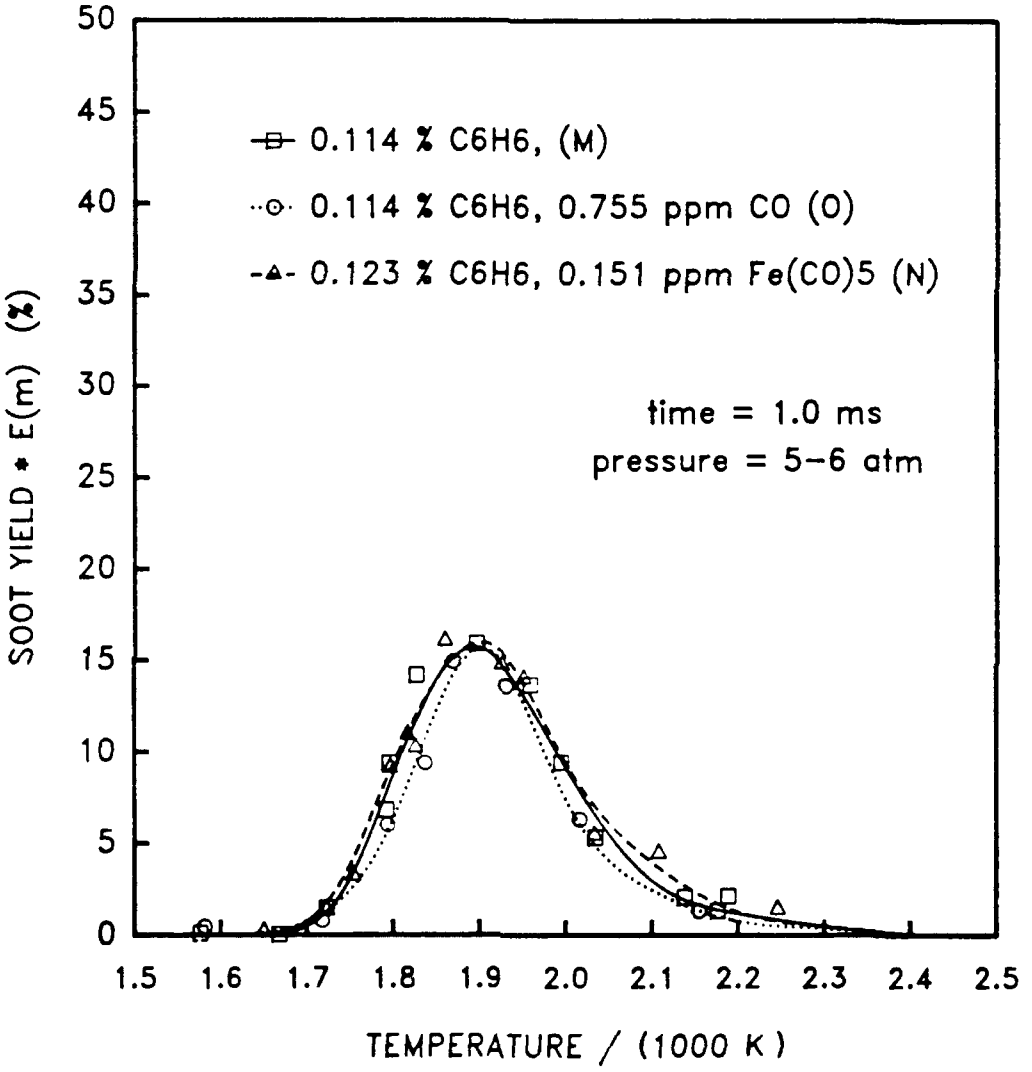

Figure 20. Comparison of Soot Yields at 1-ms Reaction Time Showing Effect of Additives at Pyrolysis Pressures from 5-7 Atmospheres.

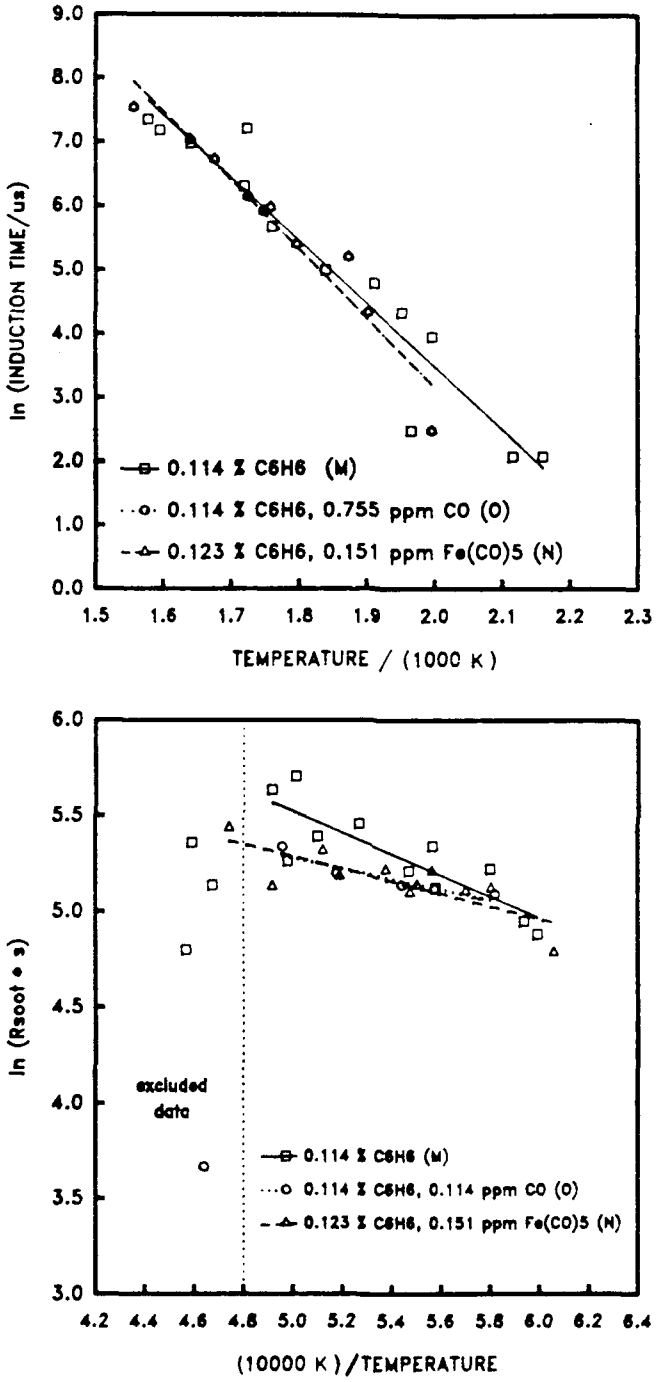

Figure 21. Effect of Additives on Induction Times and Rates for Benzene Pyrolysis at 5-7 Atmosphere Reaction Pressures.

These results show no effect of either carbon monoxide or iron pentacarbonyl on soot yield during benzene pyrolysis at 5-7 atmospheres. Thus the increase in soot production effected by carbon monoxide at 2-3 atmospheres is suppressed at 5-7 atmospheres. Also, the absence of any effect with the addition of iron pentacarbonyl supports the conjecture that iron pentacarbonyl suppressed the effect of carbon monoxide at 2-3 atmosphere reaction pressures.

C. OXIDATION MEASUREMENTS

The base-case mixtures for the oxidation measurements were approximately equimolar mixtures of benzene and oxygen in argon. Preliminary runs with stoichiometric addition of oxygen (7.5 moles oxygen per mole of benzene) showed a total absence of soot formation. Thus the rich, equimolar mixtures were used as the base case in order to provide adequate sooting, but at a lower soot yield than for the pyrolysis measurements. As with the pyrolysis measurements discussed above, two levels of reaction pressures were used.

For the lower, 2-3 atmosphere reaction pressures, the benzene concentrations were maintained near those used for the pyrolysis measurements, i.e. 0.27-0.29 mole percent. The oxygen concentration was maintained at 0.28 percent. For the higher, 5-7 atmosphere reaction pressures, the benzene concentration ranged from 0.11-0.12 percent, and the oxygen concentration was maintained at 0.12 percent. The initial fuel and oxygen atom concentrations were thus held approximately constant as the reaction pressure varied.

Both carbon monoxide and iron pentacarbonyl were used as additives. At the lower reaction pressures, two concentration levels were used for the additives; 3.0 and 62.5 ppm for carbon monoxide, and 0.5 and 11.5 ppm for iron pentacarbonyl. At the higher reaction pressures, however, only one concentration level was used -- 1.60 ppm carbon monoxide and 0.318 ppm iron pentacarbonyl. These levels provided initial atom concentrations at the elevated reaction pressures equivalent to those used at the lower, 2-3 atmosphere reaction pressures.

1. Effect of Additives at 2-3 Atmosphere Reaction Pressures

The effects of carbon monoxide and iron pentacarbonyl as additives to equimolar mixtures of benzene and oxygen in argon are illustrated by the soot-yield bells in Figure 22 and the superimposed 1-ms curves in Figure 23. The corresponding curves obtained for the pyrolysis of a mixture of 0.270 percent benzene in argon are included for comparison. The induction times and rates for the four mixtures are shown in Figure 24.

The addition of oxygen to the benzene mixtures reduces, but does not eliminate, the soot yield. As mentioned above, the sociometric amount of oxygen required for complete combustion of the benzene is $7\frac{1}{2}$ moles oxygen per mole of benzene, so an equimolar mixture is still very rich. The maximum soot yield at 1-ms reaction time was reduced by 42 percent with the addition of oxygen. The shape of the soot-yield bells, however, was not altered. As can be seen in Figure 24, the addition of oxygen increases the slope of the rate regression line, indicating an increase in the activation energy. The induction time, however, appears to be unaltered by addition of oxygen.

The results shown inn Figures 22-24 show that neither carbon monoxide (at 3 ppm) nor iron pentacarbonyl (at 0.5 ppm) affect soot production for equimolar mixtures of benzene and oxygen shock heated at 2-3 atmosphere pressures. This negative result motivated another series of measurements with the concentration levels of the additives increased by about 20 times. These results are shown in Figures 25-27. As can be seen, the soot yields, induction times, and rates with the addition of 62.5 ppm carbon monoxide and 11.5 ppm iron pentacarbonyl are indistinguishable from the corresponding results obtained with the lower concentration levels of the additives, i.e. no effect of either carbon monoxide or iron pentacarbonyl could be observed for oxidation measurements at 2-3 atmosphere reaction pressure.

2. Effect of Additives at 5-7 Atmosphere Reaction Pressures

The final series of measurements were carried out with equimolar benzene-oxygen mixtures at reaction pressures from 5-7 atmospheres. The concentration

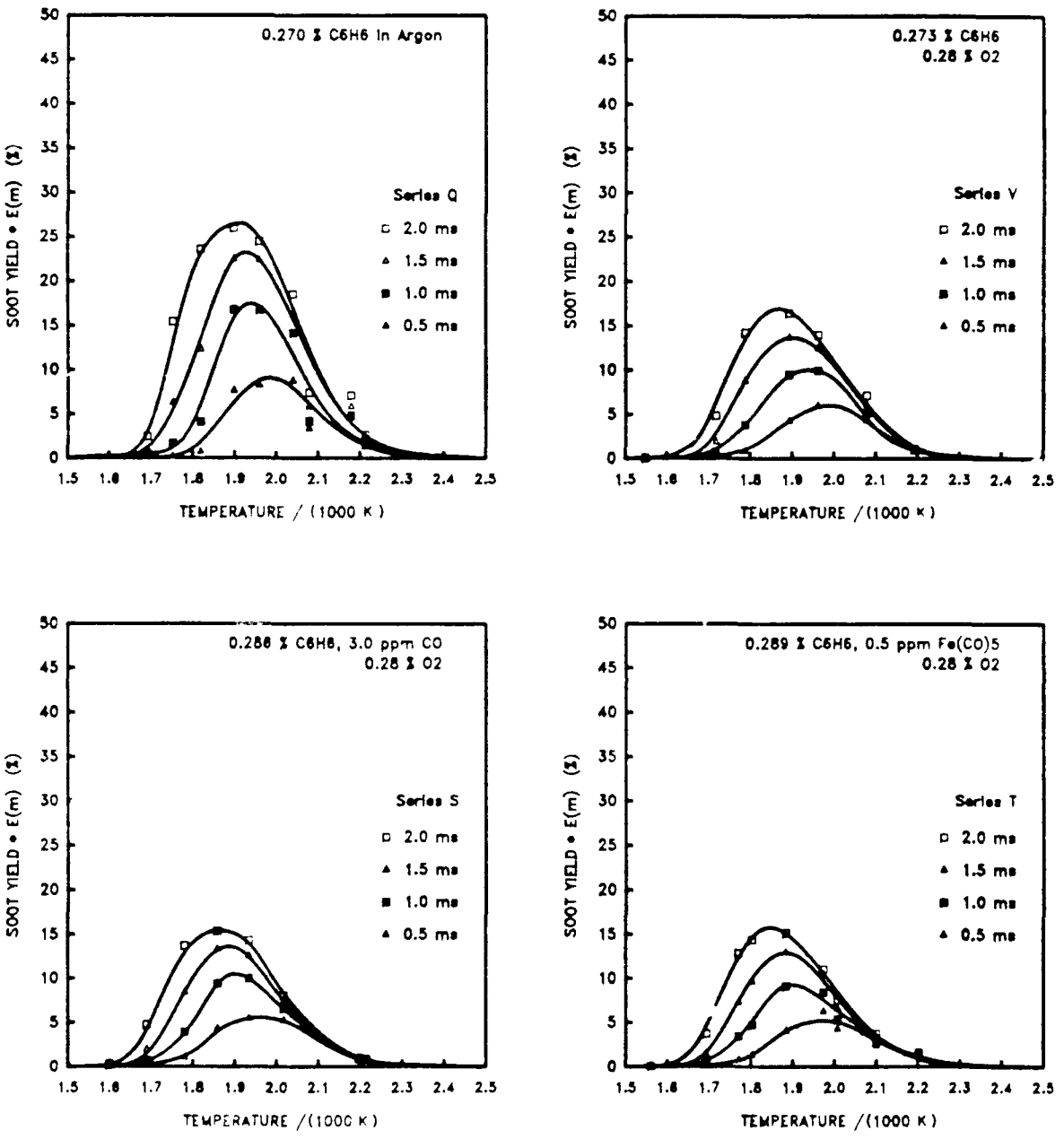

Figure 2.. Effect of Carbon Monoxide and Iron Pentacarbonyl Additives of Soot Yield During Benzene Oxidation at 2-3 Atmosphere Pressures.

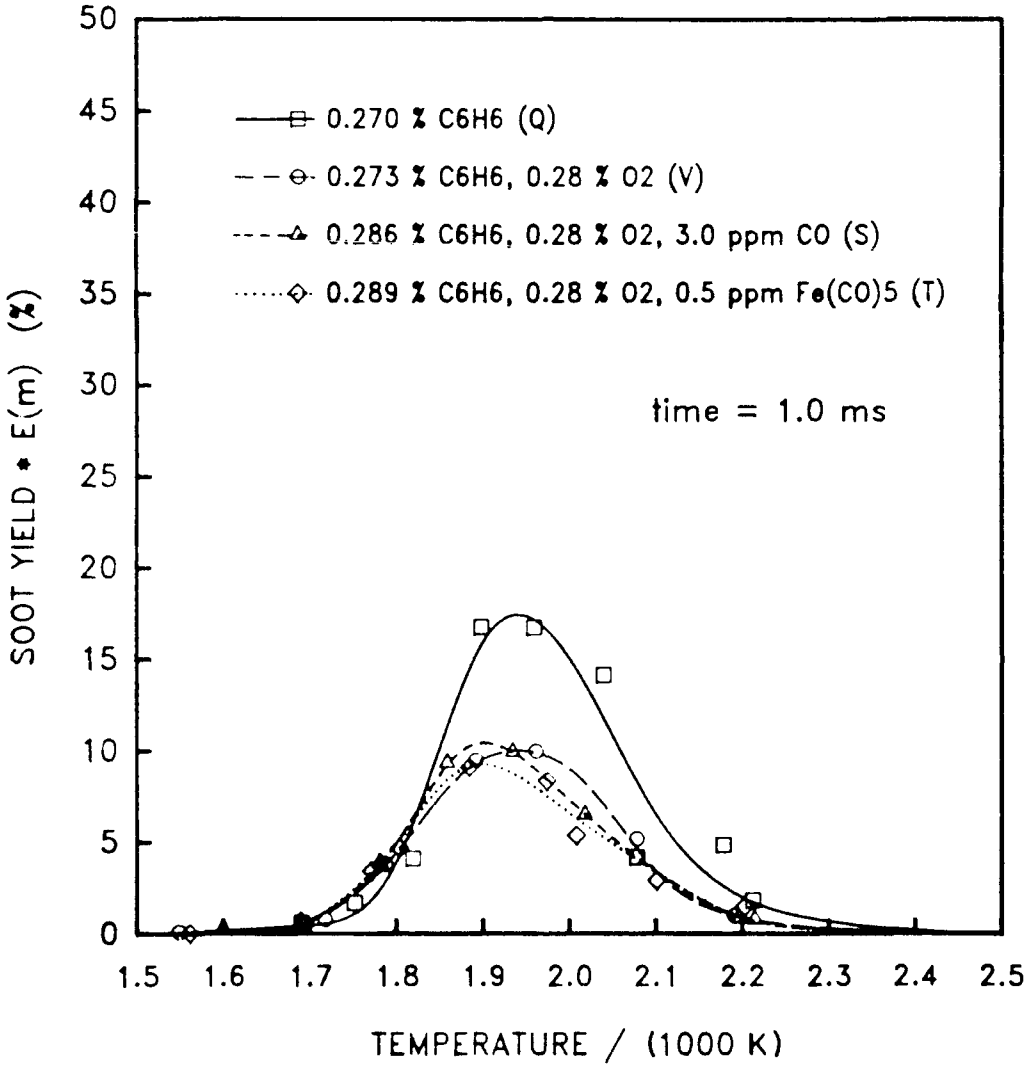

Figure 3-1. Comparison of Soot Yields at 1-ms Reaction Time Showing Effect of Additives During Benzene Oxidation at 2-3 Atmosphere Pressures.

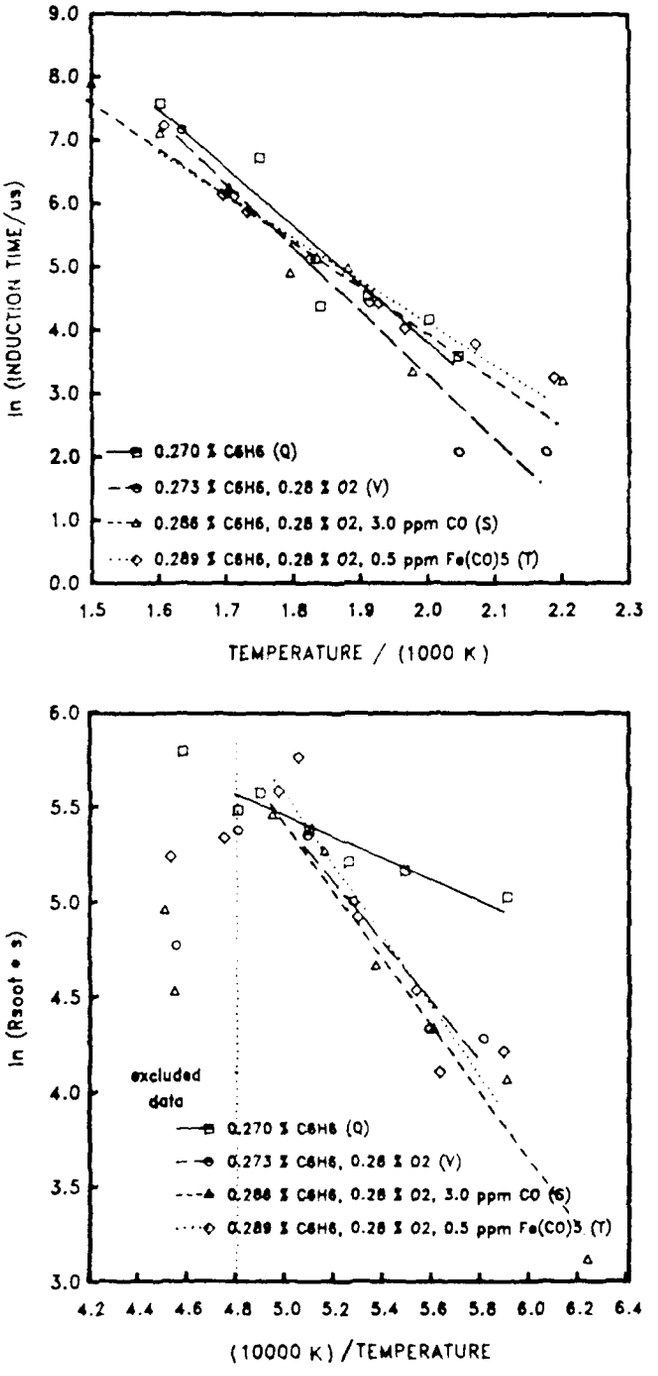

Figure 34. Effect of Additives on Induction Times and Rates of Soot Formation for Benzene Oxidation at 2-3 Atmosphere Pressures.

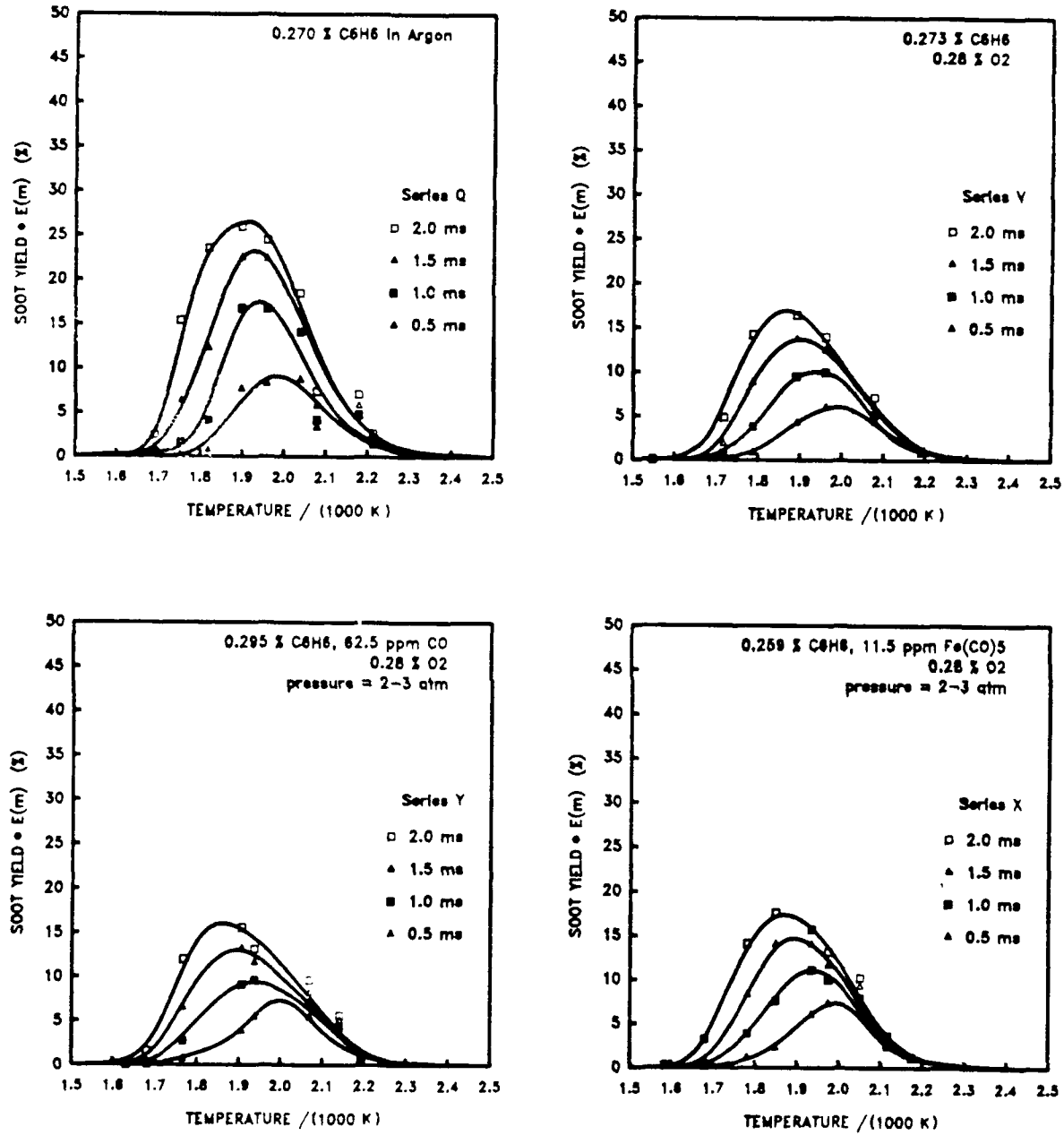

Figure 25. Effect of Increased Additive Concentrations on Soot Yield During Benzene Oxidation at 2-3 Atmosphere Pressures.

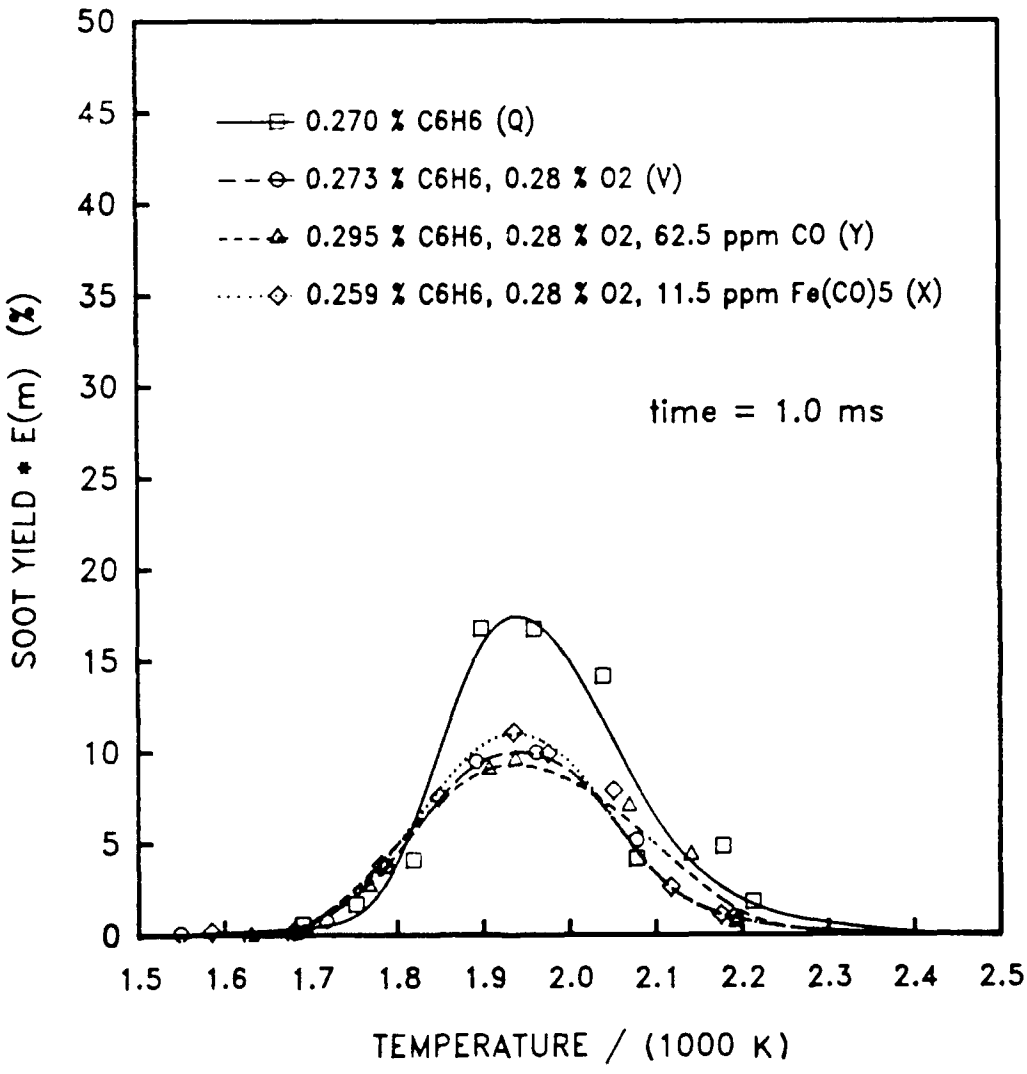

Figure 26. Comparison of Soot Yields at 1-ms Reaction Time Showing Effect of Additives at Higher Concentration Levels.

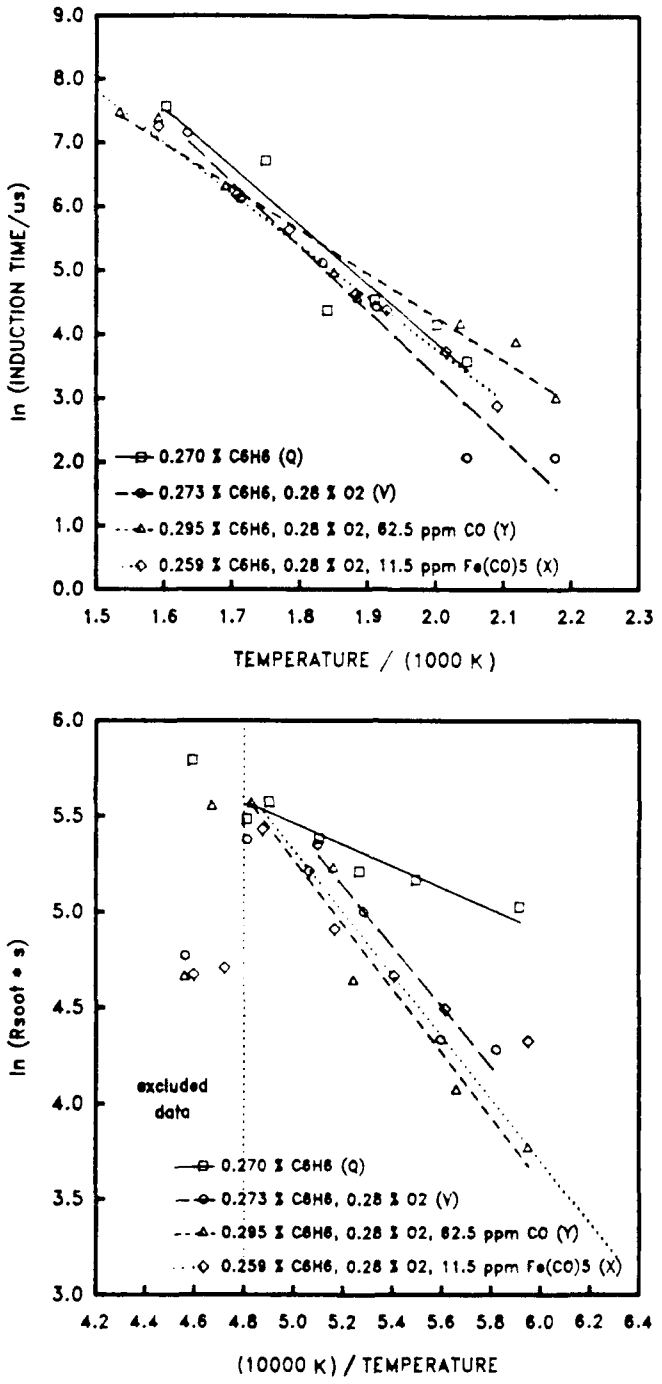

Figure 27. Effect of Higher Additive Concentations on Induction Times and Rates During Benzene Oxidation at 2-3 Atmosphere Pressures.

of benzene, oxygen, carbon monoxide, and iron pentacarbonyl were reduced proportionally such that the initial atom concentrations were equivalent to those used at reaction pressures from 2-3 atmospheres.

The results are shown in Figures 28-30. The curves obtained for benzene pyrolysis at 5-7 atmospheres (Series Q) are included for comparison. As was the case for the lower reaction pressures, the addition of an equimolar quantity of oxygen reduces soot yield. As shown in Figure 29, the maximum soot yield at 1-ms reaction time is reduced by about 30 percent. The effect of oxygen on the rate of soot formation at 5-7 atmospheres is the same as at 2-3 atmospheres, i.e. the slope of the rate regression line is increased indicating an increase in the activation energy.

In contrast to the oxidation measurements at the lower pressures, however, the addition of carbon monoxide increases soot yield. This is seen most clearly in the 1-ms curves of Figure 29. With the addition of carbon monoxide (Series BB), the maximum soot yield at 1 ms is nearly identical to the soot yield found during pyrolysis measurements (Series M), i.e., the addition of carbon monoxide at one part per 750 parts benzene nearly eliminates the soot reduction effects of the oxygen.

The addition of iron pentacarbonyl, in turn, eliminates the soot enhancement by carbon monoxide. The soot yields obtained with the addition of 0.318 ppm iron pentacarbonyl are, within the scatter of the data, identical with those obtained for benzene oxidation. Thus the effect of iron is to eliminate the enhancement of soot yield by carbon monoxide. This effect of iron was seen in the pyrolysis measurements at 2-3 atmospheres, where the iron was shown to reduce the enhancement effect of carbon monoxide, especially when the concentration of benzene was increase.

As shown in Figure 30, the addition of carbon monoxide did not affect the slope of the rate regression line, but only its magnitude. The enhancement effect by carbon monoxide (and the elimination of this effect by iron pentacarbonyl) is not through a change in the activation energy. Note also that

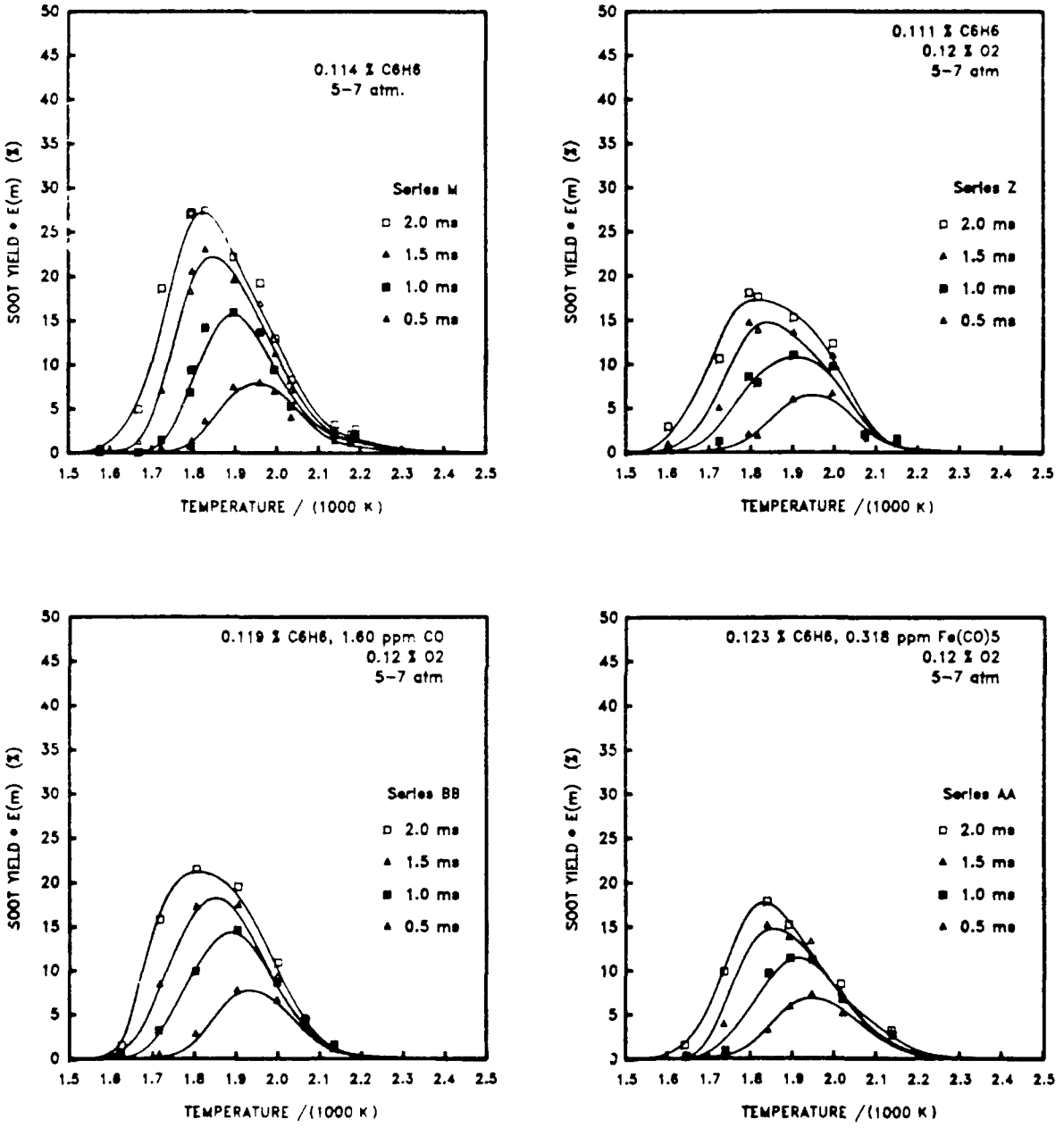

Figure 28. Effect of Carbon Monoxide and Iron Pentacarbonyl Additives on Soot Yield During Benzene Oxidation at 5-7 Atmosphere Pressures.

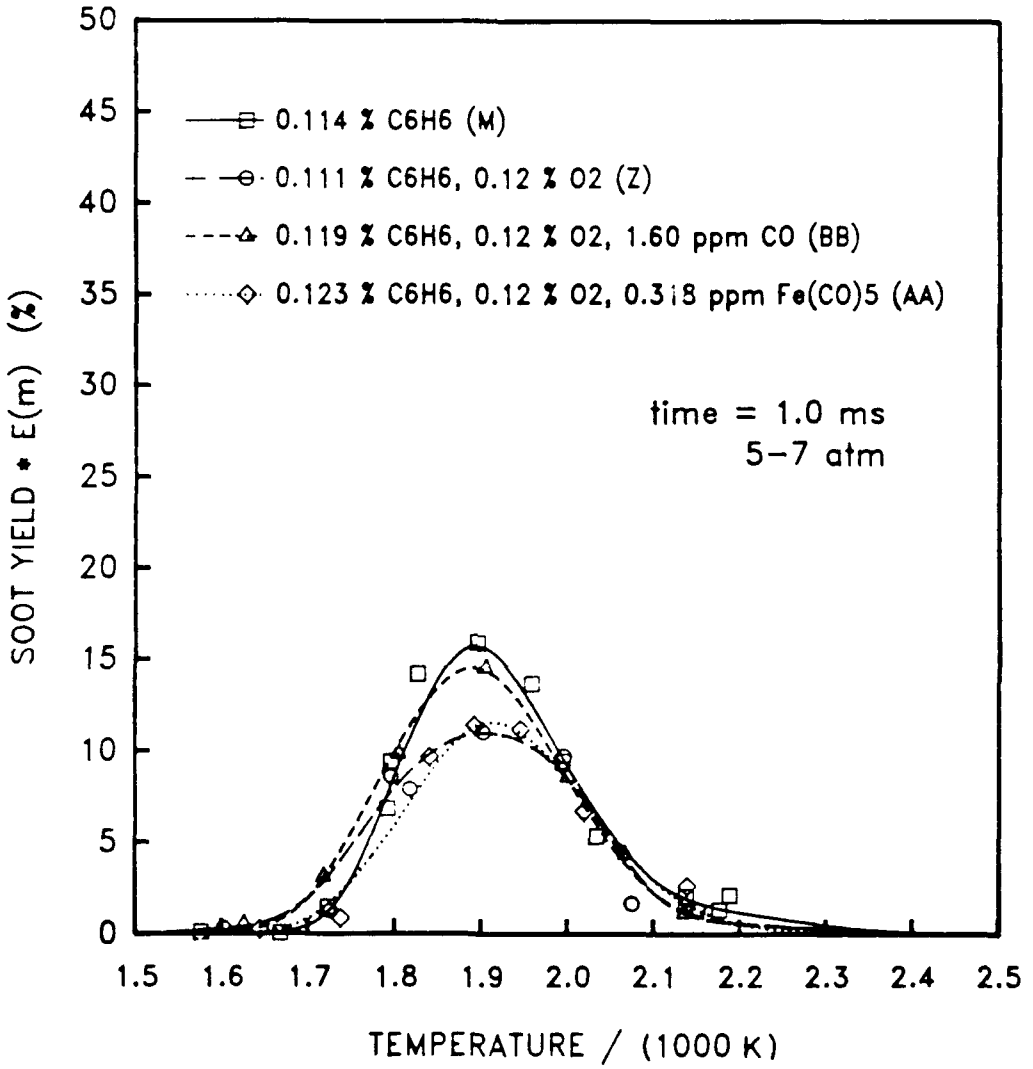

Figure 29. Comparison of Soot Yields at 1-ms Reaction Time Showing Effect of Additives During Benzene Oxidation at 5-7 Atmosphere Pressures.

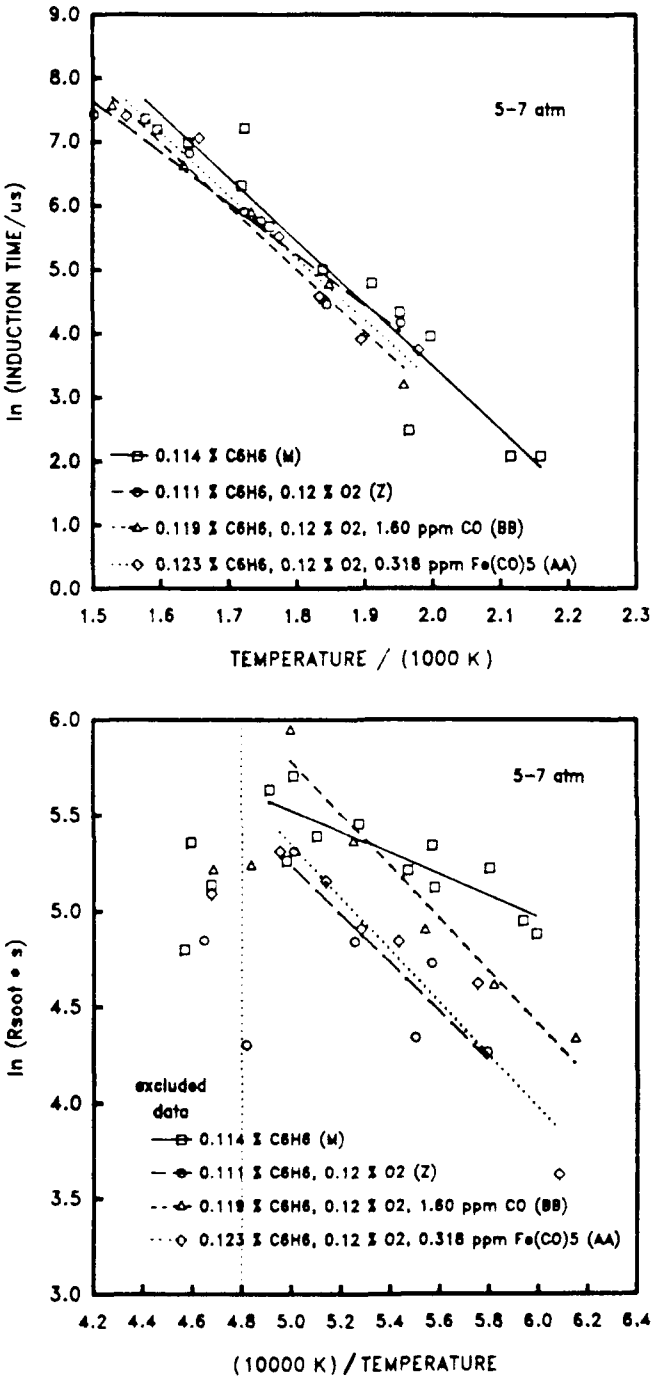

Figure 30. Effect of Additives on Induction Times and Rates During Benzene Oxidation at 5-7 Atmosphere Reaction Pressures.

neither oxygen, carbon monoxide, or iron pentacarbonyl have a significant effect of the induction time.

D. SUMMARY OF EXPERIMENTAL RESULTS

The effect on carbon monoxide on soot formation was an unexpected phenomena that partially obscured any effect of iron. The effects of carbon monoxide are summarized in Figure 31. The addition of carbon monoxide (at near-tract amounts) nearly doubled soot yield during benzene pyrolysis at 2-3 atmosphere reaction pressures, ind increase soot yield by more than 35 percent during benzene oxidation at 5-7 atmosphere reaction pressures. In terms of Arrhenius parameters, this increase was through the preexponential multiplied (frequency factor) rather than the activation energy. No effect of carbon monoxide could be observed, however, for either benzene pyrolysis at 5-7 atmospheres or benzene oxidation at 2-3 atmospheres.

The effect of iron, through the addition of iron pentacarbonyl, was to reduce the enhancement of soot yield by carbon monoxide. This effect was strongest for benzene oxidation at 5-7 atmospheres, where the enhancement by carbon monoxide was totally eliminated.

These observations cannot be explained by any existing models of soot formation chemistry. The results clearly show, however, that the effects of carbon monoxide (and the reduction of these effects by iron pentacarbonyl) are chemical in nature. This, in turn, suggests that carbon monoxide and iron pentacarbonyl might be useful chemical probes to elucidate better the complex chemical pathways to soot formation.

Some pilot studies on the morphology of the soot formed in these experiments were also carried out. These studies suffered from the difficulty in obtaining, in a single shock or even several repeated shocks, sufficient amounts of soot for analysis; the soot samples were collected on glass plates affixed to the driven end of the shock tube. Although the results of these studies are far too tentative to discuss in detail, the general observations should be mentioned.

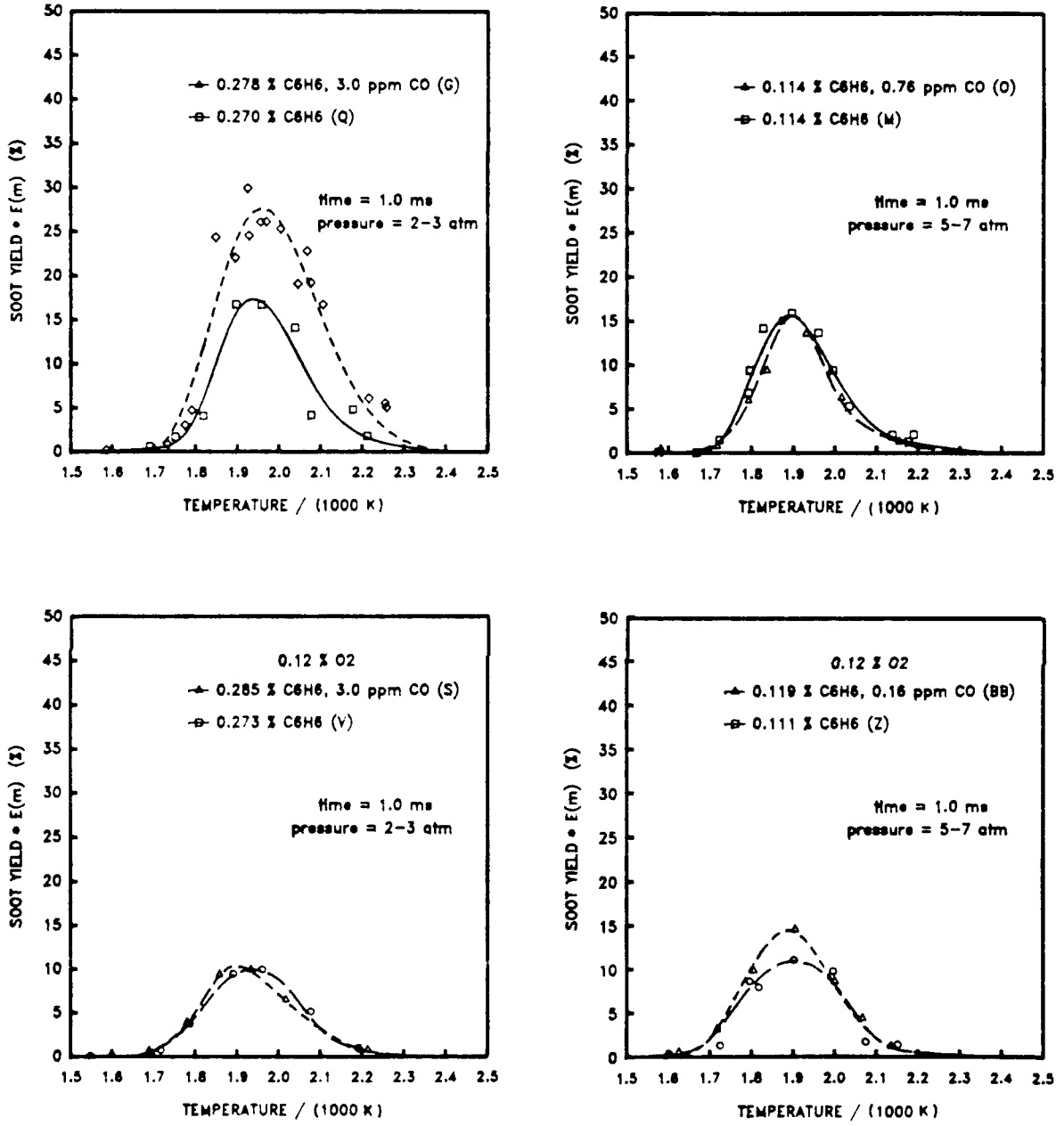

Figure 31. Summary of Effects of Carbon Monoxide on Soot Yield During Benzene Pyrolysis and Oxidation.

Transmission electron micrographs (100,000X) showed that the soot was highly agglomerated, with the component spherules in the size range of 8 to 12 nm. There appeared to be some tendency of the spherule size to diminish at higher reaction temperatures, but the addition of carbon monoxide or iron pentacarbonyl did not appear to affect the size.

A preliminary analysis of the soot samples also showed that the carbon was primarily graphitic with some aliphatic and aromatic bonds.

SECTION V

CONCLUSIONS

1. The experimental measurements carried out in this study showed no direct influence of iron on the production of soot during either benzene pyrolysis or benzene oxidation; i.e., our results show that iron has negligible influence on soot formation chemistry.

2. The use of iron pentacarbonyl in place of ferrocene led to an unexpected enhacement of soot production that partially obscurred the influence of iron. This enhancement occured for low-pressure pyrolysis and high-pressure oxidation, but not for low-pressure oxidation or high-pressure pyrolysis.

3. At the concentrations of iron pentacarbonyl used in this work, no nucleation of iron vapor could be observed when iron pentacarbonyl alone was subjected to shock heating. This indicates that the observed enhancement of soot yield by iron pentacarbonyl owes to chemical effects rather than physical effects, such as iron nuclei providing condensation sites for soot. This conjecture is strongly supported by the parallel increase in soot yield, at the same experimental conditions, when carbon monoxide alone was added to the fuel mixtures. In terms of a global Arrhenius rate model, the enhancement of soot yield by carbon monoxide (at its mediation by iron pentacarbonyl) is through the pre-exponential multiplier rather than the activation energy. Also, the influence of carbon monoxide does not appear to increase in stoiciometric proportion.

4. An indirect influence of iron was evidenced by its ability to reduce the enhancement of soot yield by carbon monoxide. For low-pressure pyrolysis, the influence of iron increased as the fuel concentration increased. For high-pressure oxidation, iron completely eliminated the enhancement of soot yield by carbon monoxide. This result suggests that the beneficial effects of ferrocene observed for some gas turbine combustors may owe to the

secondary influence of iron on stable intermediates or radicals generated along the complex chemical pathways to soot formation.

5. No influence of pressure on soot production was observed when the concentration of carbon atoms, at the reaction conditions, was held constant. This result indicates that the increase in sooting tendency with an increase in pressure observed by other investigators owes to fuel concentration rather than reaction pressure.

6. Current detailed modeling studies of the soot formation process offer no satisfactory explanation for either the enhancement of soot yield by near-trace amounts of carbon monoxide or the action by iron to reduce or eliminate this enhancement. The peculiar dependence of these phenomena on pressure and oxygen level indicates that these additives may serve as effective chemical probes to help unravel the complex, high-temperature, gas-phase reactions that comprise the combustion process.

REFERENCES

1. Hirschler, M.M., "Soot from Fires II. Mechanisms of Soot Formation," J. of Fire Sci., vol 3, p. 380, 1985.

2. Wagner, H.Gg., "Soot Formation in Combustion," Seventeenth Symposium (Int.) on Combustion, p. 3, The Combustion Institute, 1978.

3. Calcote, H.F., "Mechanisms of Soot Nucleation in Flames -- A Critical Review," Combustion and Flame, vol 42, p. 215, 1981.

4. Haynes, B.S., and H.Gg. Wagner, "Soot Formation," Prog. Energy Combust. Sci., vol 7, p. 229, 1981.

5. Wagner, H.Gg., "Soot Formation," in Particulate Carbon: Formation During Combustion, (D.C. Siegla and G.W. Smith, Eds.), Plenum, New York, 1981.

6. Longwell, J.P., "The Formation of Polycyclic Aromatic Hydrocarbons by Combustion," Nineteenth Symposium (Int.) on Combustion, p. 1339, The Combustion Institute, 1982.

7. Glassman, I., "Soot Formation in Combustion Processes," Twenty-Second Symposium (Int.) on Combustion, in press, The Combustion Institute.

8. Kern, R.D., H.J. Singh, M.A. Esslinger, and P.W. Winkeler, "Product Profiles Observed During the Pyrolysis of Toluene, Benzene, Butadiene, and Acetylene," Nineteenth Symposium (Int.) on Combustion, p. 1351, The Combustion Institute, 1982.

9. Smith, R.D., "Formation of Radicals and Complex Organic Compounds by High Temperature Pyrolysis: The Pyrolysis of Toluene," Combustion and Flame, vol 35, p. 179, 1979.

10. Mar'yasin, I.L., and Z.A. Nabutovskii, "An Investigation of the Kinetics of the Pyrolysis of Benzene in Shock Waves. I.," Kinetics & Catalysis, vol 10, p. 800, 1969.

11. Mar'yasin, I.L., and Z.A. Nabutovskii, "Investigation of the Kinetics of Carbon Black Formation During the Thermal Pyrolysis of Benzene and Acetylene in a Shock Wave. III.," Kinetics & Catalysis, vol 14, p. 139, 1973.

12. Bauer, S.H., and C.F. Aten, "Absorption Spectra of Polyatomic Molecules at High Temperatures. II. Benzene and Perfluorobenzene. Kinetics of the Pyrolysis of Benzene," The Journal of Chemical Physics, vol 39, p. 1253, 1963.

13. Asaba, T., and N. Fujii, "Shock-Tube Study of High-Temperature Pyrolysis of Benzene," Thirteenth Symposium (Int.) on Combustion, p. 155, The Combustion Institute, 1972.

14. Graham, S.C., J.B. Homer, and J.L.J. Rosenfeld, "The Formation and Coagulation of Soot Aerosols Generated by the Pyrolysis of Aromatic Hydrocarbons," Proc. Royal Soc. Lond., vol A344, p. 259, 1975.

15. Clary, D.W. "Soot Formation During Pyrolysis of Aromatic Hydrocarbons," PhD Dissertation, Louisiana State University, 1985.

16. Wang, T.S., "Soot Formation from Toluene," PhD Dissertation, Louisiana State University, 1980.

17. Frenklach, M., S. Taki, and R.A. Matula, "A Conceptual Model for Soot Formation in Pyrolysis of Aromatic Hydrocarbons," Combustion and Flame, vol 49, p. 275, 1983.

18. Frenklach, M., D.W. Clary, W.C. Gardiner, Jr., and S.E. Stein, "Detailed Kinetic Modeling of Soot Formation in Shock-Tube Pyrolysis of Acetylene," Twentieth Symposium (Int.) on Combustion, p. 43, The Combustion Institute, 1984.

19. Homann, K.H., and H.Gg. Wagner, "Some New Aspects of the Mechanism of Carbon Formation in Premixed Flames," Eleventh Symposium (Int.) on Combustion, .p 371, The Combustion Institute, 1967.

20. Davies, R.A., and D.B. Scully, "Carbon Formation from Aromatic Hydrocarbons II," Combustion and Flame, vol 10, p. 165, 1966.

21. Wang, T.S., R.A. Matula, and R.C. Farmer, "Combustion Kinetics of Soot Formation from Toluene," Eighteenth Symposium (Int.) on Combustion, p. 1149, The Combustion Institute, 1981.

22. Stein, S.E., "On the High Temperature Chemical Equilibria of Polycyclic Aromatic Hydrocarbons," J. Phys. Chem., vol 82, p. 566, 1978.

23. Bowser, R.J., and F.J. Weinberg, "Chemi-ionization during Pyrolysis," Combustion and Flame, vol 27, p. 21, 1976.

24. Abrahamson, J., and E.R. Kennedy, Twelfth Biennial Conference on Carbon, p. 169, The American Carbon Society, 1975.

25. Homann, K.H., and H. Wolf, "Charged Particles in Sooting Flames. 2. Determination of the Fraction of Charged Soot," Ber. Bunseges. Phys. Chem., vol 87, p. 1073, 1983.

26. Ball, R.T., and J.B. Howard, "Electric Charge of Carbon Particles in Flames," Thirteenth Symposium (Int.) on Combustion, p. 353, The Combustion Institute, 1971.

27. Howard, J.B., "On the Mechanism of Carbon Formation in Flames," Twelfth Symposium (Int.) on Combustion, p. 877, The Combustion Institute, 1969.

28. Abrahamson, J., "Saturated Platelets Are New Intermediates in Hydrocarbon Pyrolysis and Carbon Formation," Nature, vol 266, p. 323, 1977.

29. Frenklach, M., Clarey, D.W., Yuan, T., Gardner, W.C. Jr., and Stein, S.E., "Mechanism of Soot Formation in Acetylene-Oxygen Mixtures," Comb. Sci. and Tech., vol 50, p. 79, 1985.

30. Frenklach, M., "On the Driving Force for PAH Production," Twenty-Second Symposium (Int.) on Combustion, in press, The Combustion Institute, 1988.

31. Westmorland, P.R., "The Importance of Obvious and Disguised Association Reactions in Combustion," paper presented at 1988 Technical Meeting, The Eastern Section of the Combustion Institute, Clearwater Beach, Florida, 5 - 7 December 1988.

32. Smith, George M., "A Simple Nucleation/Depletion Model for the Spherule Size of Particulate Carbon," Combustion and Flame, vol 48, p. 265, 1982.

33. La Cava, A., and D.L. Trimm, Letter to Editor, Carbon, vol 16, p. 504, 1978.

34. Prado, G.P., and J.B. Howard, "Formation of Large Hydrocarbon Ions in Sooting Flames," Advances in Chemistry Series - Evaporation and Combustion of Fuels, p. 154, American Chemical Society, 1978.

35. Levy, A., "Unresolved Problems in SO_x, NO_x, and Soot Control in Combustion," Nineteenth Symposium (Int.) on Combustion, p. 1223, The Combustion Institute, 1982.

36. Fujii, N., and T. Asaba, "Shock-Tube Study of the Reaction of Rich Mixtures of Benzene and Oxygen," Fourteenth Symposium (Int.) on Combustion, p. 433, The Combustion Institute, 1973.

37. Venkat, C., K. Brezinsky, and I. Glassman, "High Temperature Oxidation of Aromatic Hydrocarbons," Nineteenth Symposium (Int.) on Combustion, p. 143, The Combustion Institute, 1982.

38. Glassman, I., and P. Yaccarino, "The Temperature Effect in Sooting Diffusion Flames," Eighteenth Symposium (Int.) on Combustion, p. 1175, The Combustion Institute, 1981.

39. Frenklach, M., "Shock Tube Study of the Fuel Structure Effects on the Chemical Kinetic Mechanisms Responsible for Soot Formation," NASA Report CR-174661, 1983.

40. Frenklach, M., D.W. Clary, and M.K. Ramachandra, "Shock Tube Study of the Fuel Structure Effects on the Chemical Kinetic Mechanisms Responsible for Soot Formation," NASA Report CR-174880, 1985.

41. Hirschler, M.M., "Soot from Fires, III. Soot Suppression," J. of Fire Sci., vol 4, p. 42, 1986.

42. Bulewicz, E.M., D.G. Evans, and P.J. Padley, "Effects of Metallic Additives on Soot Formation Processes in Flames," Fifteenth Symposium (Int.) on Combustion, p. 1461, The Combustion Institute, 1975.

43. Haynes, B.S., H. Jander, and H.Gg. Wagner, "The Influence of Gaseous Additives on the Formation of Soot in Premixed Flames," Nineteenth Symposium (Int.) on Combustion, p. 1379, The Combustion Institute, 1982.

44. Street, J.C., and A. Thomas, "Carbon Formation in Premixed Flames," Fuel, vol 34, p. 4, 1955.

45. Brooks, C.T., "Some Chemical Aspects of Processes Occurring in the Gas Recycle Hydrogenator," I.G.E. Journal, vol 6, p. 492, 1966.

46. Schug, K.P., Y. Manheimer-Timnat, P. Yaccarino, and I. Glassman, "Sooting Behavior in Gaseous Hydrocarbon Diffusion Flames and the Influence of Additives," Combustion Science and Technology, vol 22, p. 235, 1980.

47. Du, D.-X., Axelbaum, R.L., and Law, C.K., "The Influence of Gaseous Additives on the Sooting Limit of Strained Diffusion Flames," paper presented at 1988 Technical Meeting, The Eastern Section of the Combustion Institute, Clearwater Beach, Florida, 5-7 December 1988.

48. Graham S.M., and J.M. Goodings, "Metallic Ions in Hydrocarbon Flames. II. Mechanisms for the Reduction of $C_3H_3^+$ by Metals in Relation to Soot Suppression," International Journal of Mass Spectrometry and Ion Processes, vol 56, p. 205, 1984.

49. Haynes, B.S., H. Jander, and H.Gg. Wagner, "The Effect of Metal Additives on the Formation of Soot in Premixed Flames," Seventeenth Symposium (Int.) on Combustion, p.1365, The Combustion Institute, 1978.

50. Ndubizu, C.C., and B.T. Zinn, "Effects of Metal Additives upon Soot Formation in Polymer Diffusion Flames," Nineteenth Symposium (Int.) on Combustion, p. 310, The Combustion Institute, 1982.

51. Michael, A., M. Bert, T. Van Hoang, P. Bussiere, and A. Guyot, "Main Function of Iron Compounds as Smoke Suppressants in Poly(Vinyl Chloride) Combustion," J. Applied Polymer Science, vol 28, p. 1673, 1983.

52. Feugier, A., "Effect of Metal Additives on the Amount of Soot Emitted by Premixed Hydrocarbon Flames," Advances in Chemistry Series: Evaporation da Combustion of Fuels, p. 178, American Chemical Society, 1978.

53. Cotton, D.H., N.J. Friswell, and D.R. Jenkins, "The Suppression of Soot Emission from Flames by Metal Additives," Combustion and Flame, vol 17, p. 87, 1971.

54. Loveland, O.M., A.F Klarman, J. Tarquinio, and T.L. Stoddart, The Use of Fuel Additives to Control Plume Opacity of Turbine Engine Test Cells, ESL-TR-83-08, Engineering and Services Laboratory, Air Force Engineering and Services Center, Tyndall Air Force Base, Florida, 1983.

55. Klarman, A.F., "Evaluation of the Extended Use of Ferrocene for Test Cell Smoke Abatement: Engine and Enviromental Test Results," Navy Report No. NAPTC-PE-110, 1977.

56. Bonczyk, P.A., "Investigation of Fuel Additive Effects on Sooting Flames," Air Force Report UTRC/R86-956545F, 1986.

57. Samuelsen, G.S., R.L. Hack, R.M. Himes, and M. Azzazy, Effects of Fuel Specification and Additives on Soot Formation, ESL-TR-83-17, Engineering and Services Laboratory, Air Force Engineering and Services Center, Tyndall Air Force Base, Florida, December, 1983.

58. Ritrievi, K.E., Longwell, J.P., and Sarofim, A.F., "The Effects of Ferrocene Addition on Soot Particle Inception and Growth in Premixed Ethylene Flames," Combustion and Flame, vol 70, p. 17, 1987.

59. Cheung, C. K. Li, "Application of Laser-Doppler Velocimetry to Shock Tube Studies," M.S. Thesis, Louisiana State University, 1981.

60. Hsu, J., "Soot Formation from Chlorinated Hydrocarbons," M.S. Thesis, Louisiana State University, 1985.

61. Miller, D. L., "High Temperature Combustion of Selected Chlorinated Hydrocarbons," PhD Dissertation, Louisiana State University, 1984.

62. Kerker, M., The Scattering of Light and Other Electromagnetic Radiation, Academic Press, New York, 1969.

63. Donnet, J.B., J. Lahaye, A. Voet, and G. Prado, "Are Carbon Blacks Formed From Liquid Crystal Structures?," Carbon, vol 12, p. 212, 1974.

64. Bornside, D.E., "Ignition in Methane-Additive Mixtures," M.S. Thesis, Louisiana State University, 1983.

65. Miller, D.L., M. Frenklach, P.J. Laughlin, and D.W. Clary, "Transferring Data from a Nicolet Digital Oscilloscope to an IBM Mainframe Computer Using an Apple II+ Microcomputer, Part II," Computer Appl. Lab., vol 4, p. 260, 1984.

APPENDIX A

DETAILS OF EXPERIMENTAL DATA

This appendix contains tables listing the details of the experimental data. For each experimental series, the following parameters are tabulated:

EXP. NO. : this number identifies the experimental series and the track of the floppy disk on which the pressure and laser attenuation data are stored.

T_5 : temperature behind the reflected shock wave

SOOT YIELD : percentage of fuel converted to soot * E(m)

DELAY : induction time for soot formation

RATE : rate of soot formation

P_5 : pressure behind the reflected shock wave

T_1 : room temperature

C_5 : molar concentration behind the reflected shock wave

$[C]_5$: concentration of carbon atoms behind the reflected shock wave

TABLE A-1 DETAILS OF EXPERIMENTAL DATA

Series C
Mixture Composition: C_6H_6 = 0.293 %
Additive = 00.000
Argon = 99.707 %

RUN	EXP	T_s	SOOT YIELD = E(M) (%), AT TIME (ms)								DELAY	RATE	P_s	T_s	C_s	$[C]_s \times 10^{-17}$
NO.	NO.	(K)	0.25	0.50	0.75	1.00	1.25	1.50	1.75	2.00	(μsec)	(ms^{-1})	(atm)	(C)	($kmol/m^3$)	($atom/cm^3$)
1	C11H2	1565.7	0.10	0.22	-0.01	0.21	0.10	0.21	0.17	0.13	0.0	0.000	1.88	21.5	14.67	1.55
2	C13H1	1700.4	0.02	0.10	0.20	0.36	0.78	1.20	2.42	4.35	1516.0	0.349	2.08	21.2	14.93	1.58
3	C12H2	1728.4	0.06	0.29	0.46	0.53	1.04	1.66	2.77	4.68	1370.0	0.338	2.16	21.2	15.26	1.61
4	C12H1	1750.1	0.11	0.20	0.34	0.93	1.68	3.12	5.26	7.95	1112.0	0.347	2.19	21.0	15.29	1.62
5	C08H2	1789.4	0.36	1.11	2.99	5.53	8.53	12.68	17.07	21.27	554.0	0.400	2.16	21.2	14.74	1.56
6	C14H1	1806.6	0.19	0.60	1.40	3.08	5.61	8.86	13.53	17.68	692.0	0.431	2.24	21.5	15.08	1.60
7	C04H1	1812.6	0.05	0.85	2.78	5.43	9.78	14.65	19.25	22.33	504.0	0.469	2.29	21.0	14.46	1.53
8	C08H1	1822.4	0.27	0.85	1.78	3.38	5.88	9.19	13.55	17.18	682.0	0.431	2.23	21.2	14.94	1.58
9	C11H1	1851.8	0.47	1.95	4.74	7.90	12.09	16.11	20.00	22.77	328.0	0.412	2.24	21.5	14.78	1.56
10	C03H2	1881.7	0.54	2.20	4.97	8.40	12.23	15.69	18.08	20.24	224.0	0.405	2.30	20.8	14.93	1.58
11	C07H2	1889.2	1.55	3.94	6.80	10.56	14.45	17.82	20.23	22.33	182.0	0.401	2.33	21.2	15.01	1.59
12	C06H2	1938.2	1.39	4.98	8.80	12.19	14.36	16.49	18.18	-1.00	174.0	0.487	2.35	21.5	14.77	1.56
13	C04H2	1941.5	1.69	4.93	8.54	11.21	13.60	15.64	17.03	18.16	138.0	0.479	2.39	21.2	14.98	1.59
14	C07H1	1944.3	1.84	5.62	9.06	11.90	14.61	16.43	18.21	19.01	1840.0	0.448	2.37	20.0	14.86	1.57
15	C03H1	1954.7	1.63	5.22	8.58	11.77	14.48	16.35	17.64	18.68	106.0	0.481	2.36	20.0	14.73	1.56
16	C06H1	1963.9	2.12	5.74	9.05	12.00	14.07	15.43	16.62	17.40	146.0	0.540	2.39	21.0	14.80	1.57
17	C05H1	2014.9	3.44	5.84	7.50	8.56	9.05	9.79	10.69	-1.00	46.0	0.656	2.50	21.2	15.10	1.60
18	C05H2	2065.7	3.99	5.75	7.09	8.22	9.24	10.31	11.38	12.21	80.0	0.931	2.52	20.4	14.89	1.58
19	C02H2	2069.2	2.50	4.11	5.53	6.37	6.97	8.18	9.18	9.98	74.0	0.697	2.52	20.0	14.86	1.57
20	C01H1	2128.0	1.42	1.91	2.44	2.51	2.98	3.68	4.03	-1.00	22.0	0.593	2.53	18.0	14.49	1.53
21	C01H2	2144.0	1.47	1.73	2.08	2.32	2.83	3.07	3.54	3.79	64.0	0.016	2.57	20.0	14.63	1.55
22	C13H2	2231.2	0.97	0.79	0.86	0.96	1.24	1.27	1.45	-1.00	64.0	0.000	2.68	21.5	14.66	1.55

TABLE A-1 DETAILS OF EXPERIMENTAL DATA (Continued)

Series D
Mixture Composition: C_6H_6 = 0.208 %
Additive = 00.000
Argon = 99.792 %

RUN	EXP	T_s	SOOT YIELD * E(M) (%), AT TIME (ms)								DELAY	RATE	P_s	T_1	C_s	$[C]_s \times 10^{-17}$
NO.	NO.	(K)	0.25	0.50	0.75	1.00	1.25	1.50	1.75	2.00	(usec)	(ms^{-1})	(atm)	(C)	(mol/m^3)	($atom/cm^3$)
1	D08H1	1685.3	0.16	0.12	0.23	0.19	0.29	0.63	0.97	1.66	1788.0	0.039	2.18	20.2	15.79	1.19
2	D07H2	1733.1	-1.00	0.01	0.[illegible]	0.33	0.60	1.29	2.47	4.44	1486.0	0.061	2.26	19.6	15.80	1.19
3	D07H1	1739.7	0.22	0.18	[illegible]	0.66	1.78	2.95	4.92	7.95	1292.0	0.073	2.25	20.0	15.75	1.18
4	D06H2	1764.9	0.41	0.33	0 [illegible]	1.29	2.61	4.85	7.67	11.27	1068.0	0.075	2.28	19.8	15.74	1.18
5	D11H1	1771.7	0.25	0.52	0.69	1.11	2.40	4.82	8.00	12.24	1086.0	0.067	2.16	20.0	14.83	1.11
6	D08H2	1778.9	0.48	0.79	1.22	2.54	4.53	7.17	11.12	14.69	842.0	0.067	2.18	19.8	14.94	1.12
7	D11H2	1797.4	0.31	0.72	1.68	3.66	6.90	11.21	15.76	19.82	718.0	0.078	2.30	20.2	15.61	1.17
8	D09H2	1813.5	0.75	2.80	6.04	9.45	13.67	17.38	20.46	-1.00	258.0	0.094	2.10	22.0	14.14	1.06
9	D04H1	1843.9	-0.45	1.66	4.23	6.93	10.77	14.62	18.10	20.44	384.0	0.090	2.21	21.0	14.58	1.10
10	D13H2	1853.9	0.53	1.51	4.05	7.33	12.06	16.56	20.51	23.30	394.0	0.069	2.36	20.4	15.52	1.17
11	D06H1	1858.3	0.96	3.18	6.36	9.66	13.78	16.74	19.48	21.54	202.0	0.078	2.37	20.0	15.53	1.17
12	D05H1	1860.2	1.06	3.59	6.54	10.46	14.51	17.08	19.28	20.89	292.0	0.084	2.18	21.6	14.28	1.07
13	D03H2	1881.8	0.72	2.80	5.81	9.30	12.83	15.79	17.81	19.37	234.0	0.093	2.25	20.8	14.55	1.09
14	D14H2	1939.2	1.04	3.53	8.08	12.70	16.65	19.76	22.03	23.61	266.0	0.095	2.49	21.0	15.53	1.17
15	D05H2	1952.0	0.92	3.75	6.55	9.67	12.42	14.91	16.57	18.08	142.0	0.059	2.53	19.8	15.83	1.19
16	D03H1	1970.9	1.78	4.43	6.77	8.66	9.99	11.37	12.41	13.39	144.0	0.064	2.37	20.6	14.67	1.10
17	D02H2	2001.0	2.39	6.04	9.09	11.07	12.49	13.63	14.45	-1.00	98.0	0.100	2.39	20.6	14.59	1.10
18	D02H1	2019.8	2.00	4.71	6.28	7.96	8.94	9.78	10.41	11.14	60.0	0.063	2.40	20.2	14.49	1.09
19	D01H2	2080.6	3.15	4.94	5.63	6.33	6.97	7.80	8.44	-1.00	78.0	0.060	2.45	21.0	14.51	1.09
20	D15H1	2113.0	2.59	3.44	4.38	4.93	5.59	6.49	7.32	7.70	42.0	0.123	2.69	21.0	15.52	1.17
21	D01H1	2173.5	1.72	2.00	2.39	2.58	3.25	3.59	3.92	-1.00	14.0	0.130	2.60	20.8	14.58	1.10

TABLE A-1 DETAILS OF EXPERIMENTAL DATA (Continued)

Series F
Mixture Composition: C_6H_6 = 0.380 %
Additive = 3.5 ppm CO
Argon = 99.620 %

RUN	EXP	T_s	SOOT YIELD • E(M) (%), AT TIME (ms)								DELAY	RATE	P_s	T_1	C_s	$[C]_s \times 10^{-17}$
NO.	NO.	(K)	0.25	0.50	0.75	1.00	1.25	1.50	1.75	2.00	(μsec)	(ms^{-1})	(atm)	(C)	(mol/m^3)	($atom/cm^3$)
1	F14H1	1517.3	0.00	0.00	0.00	0.00	0.00	0.00	0.04	0.18	0.0	0.000	1.82	19.9	14.65	1.46
2	F13H2	1658.9	0.27	0.07	0.11	0.12	0.19	0.26	0.56	1.19	1894.0	0.513	2.13	19.0	15.62	1.55
3	F16H2	1674.8	0.38	0.30	0.36	1.00	1.02	0.86	1.41	2.78	1590.0	0.353	2.15	20.0	15.63	1.55
4	F16H1	1715.2	0.02	0.00	0.36	0.75	1.70	3.27	6.02	10.03	1162.0	0.536	2.24	20.0	15.91	1.58
5	F15H2	1757.2	0.34	0.44	1.05	2.30	4.61	7.56	11.67	17.69	792.0	0.521	2.30	19.8	15.98	1.59
6	F15H1	1767.0	0.35	0.54	1.51	3.69	7.15	11.92	17.89	23.08	658.0	0.579	2.31	18.6	15.91	1.58
7	F13H1	1771.4	0.72	1.11	1.94	3.44	6.07	9.79	15.48	21.08	586.0	0.542	2.32	18.0	15.93	1.58
8	F14H2	1778.4	0.48	1.99	4.46	7.85	12.77	18.40	23.69	28.44	310.0	0.545	2.31	19.0	15.86	1.58
9	F07H2	1800.0	0.95	1.42	3.08	6.74	13.17	21.77	28.87	31.92	620.0	0.757	2.25	18.4	15.23	1.51
10	F12H2	1851.0	1.20	4.17	8.16	13.22	18.54	23.10	26.77	29.43	196.0	0.596	2.41	17.8	15.90	1.58
11	F02H2	1851.9	1.07	3.56	8.34	14.91	21.36	26.41	29.89	31.99	326.0	0.735	2.31	18.7	15.23	1.51
12	F08H1	1862.6	0.92	2.67	6.68	12.88	20.99	27.52	32.63	35.17	362.0	0.762	2.36	18.4	15.47	1.54
13	F01H2	1862.8	1.68	3.97	8.62	13.02	18.30	23.09	27.85	30.84	178.0	0.522	2.33	18.2	15.25	1.51
14	F03H1	1910.6	4.09	10.30	17.24	21.50	24.64	26.65	28.42	29.64	54.0	0.873	2.42	18.7	15.46	1.54
15	F04H2	1912.7	4.51	10.18	15.93	20.23	23.27	25.94	28.11	30.11	18.0	0.796	2.47	18.0	15.76	1.57
16	F11H1	1915.0	2.69	7.95	14.84	20.08	23.85	25.74	28.28	30.30	150.0	0.869	2.45	18.4	15.62	1.55
17	F01H1	1927.8	3.24	8.34	13.81	18.63	22.74	26.32	28.67	29.26	54.0	0.819	2.48	17.8	15.70	1.56
18	F05H1	1934.7	3.19	7.02	13.66	20.20	24.42	26.83	28.72	30.42	46.0	0.731	2.50	18.2	15.77	1.57
19	F06H1	1976.8	3.66	7.71	12.06	15.72	17.87	19.90	21.68	22.07	84.0	0.645	2.58	18.4	15.90	1.58
20	F02H1	2008.6	6.57	11.87	15.02	16.87	17.99	20.18	21.54	23.23	32.0	0.209	2.57	18.5	15.60	1.55
21	F03H2	2013.1	5.74	9.64	11.99	13.70	14.74	16.50	17.32	18.29	78.0	0.403	2.57	18.0	15.54	1.54
22	F06H2	2015.1	6.62	11.03	12.76	13.84	15.49	17.03	18.88	20.43	32.0	0.959	2.58	17.8	15.60	1.55
23	F06H1	2021.2	4.84	10.39	14.35	17.14	18.72	20.36	21.58	23.79	52.0	0.820	2.57	18.0	15.50	1.54
24	F05H2	2041.2	6.98	11.28	13.37	13.56	14.01	17.46	19.03	20.63	44.0	0.163	0.26	18.6	15.67	1.56
25	F08H2	2061.7	5.59	8.95	10.70	12.79	14.02	15.76	16.74	17.10	38.0	0.864	2.67	18.8	15.77	1.57
26	F07H1	2127.0	4.93	6.32	7.49	8.33	9.23	10.30	11.35	11.64	26.0	0.294	2.76	17.8	15.80	1.57
27	F12H1	2190.5	2.50	3.00	3.47	4.33	4.97	5.58	6.04	6.86	18.0	0.231	2.83	18.0	15.72	1.56
28	F11H2	2230.3	2.68	3.24	3.50	4.23	4.83	5.31	5.75	6.34	5.0	0.130	2.88	18.0	15.24	1.51

TABLE A-1 DETAILS OF EXPERIMENTAL DATA (Continued)

Series G
Mixture Composition: C_6H_6 = 0.278 %
Additive = 3.0 ppm CO
Argon = 99.722 %

RUN	EXP	T_s	SOOT YIELD * E(M) (%), AT TIME (ms)								DELAY	RATE	P_s	T_s	C_s	$[C]_s \times 10^{-17}$
NO.	NO.	(K)	0.25	0.50	0.75	1.00	1.25	1.50	1.75	2.00	(μsec)	(ms^{-1})	(atm)	(C)	(mol/m^3)	($atom/cm^3$)
1	G12H2	1584.8	0.53	0.36	0.22	0.19	0.09	0.15	0.22	0.15	0.0	0.000	2.01	19.0	15.42	2.12
2	G11H2	1731.7	0.87	0.62	0.77	0.82	1.59	2.90	5.74	10.15	1320.0	0.558	2.23	19.0	15.70	2.15
3	G12H1	1774.2	0.17	0.47	1.21	3.03	5.69	9.31	16.32	25.44	726.0	0.636	2.28	19.0	15.69	2.15
4	G01H1	1789.7	0.53	0.84	1.83	4.71	9.78	16.57	25.61	34.29	698.0	0.622	2.29	23.0	15.62	2.14
5	G01H2	1848.5	2.55	7.71	15.57	24.35	31.87	37.71	42.37	46.01	142.0	0.742	2.33	23.0	15.36	2.11
6	G11H1	1894.8	2.02	7.36	14.41	22.02	29.08	35.21	39.82	43.17	188.0	0.695	2.43	19.0	15.63	2.15
7	G14H1	1925.1	1.82	9.77	21.59	29.92	34.98	39.41	41.80	44.12	256.0	0.110	2.40	17.5	15.22	2.09
8	G02H2	1928.2	7.28	15.40	21.28	24.53	27.73	30.51	32.58	34.77	84.0	0.965	2.46	22.6	15.53	2.13
9	G14H2	1955.6	8.42	17.26	22.51	26.06	28.45	30.01	32.11	33.31	50.0	0.008	2.43	17.5	15.17	2.08
10	G05H2	1970.5	6.48	14.77	21.54	26.11	29.27	32.88	35.77	37.28	70.0	0.868	2.51	25.0	15.55	2.13
11	G02H1	2003.7	7.75	15.25	20.77	25.30	27.83	30.89	32.70	34.35	38.0	0.919	2.55	23.0	15.52	2.13
12	G16H1	2045.1	8.72	13.63	16.73	19.07	20.83	22.85	24.37	27.13	50.0	0.418	2.54	16.4	15.39	2.11
13	G04H1	2066.6	10.41	17.31	22.12	22.81	25.39	27.85	29.39	30.99	36.0	0.125	2.53	25.0	14.91	2.05
14	G03H1	2076.3	8.78	14.33	17.07	19.21	21.14	23.23	24.93	26.97	44.0	0.309	2.65	22.4	15.53	2.13
15	G13H2	2105.4	8.99	12.90	14.63	16.74	18.58	21.07	21.90	23.20	34.0	0.243	2.69	18.0	15.60	2.14
16	G15H2	2215.5	3.33	4.06	4.98	6.10	6.63	7.37	7.81	8.82	10.0	0.120	2.83	16.4	15.56	2.14
17	G04H2	2253.8	3.90	4.45	5.04	5.56	6.06	6.78	7.32	7.74	0.0	0.000	2.82	25.0	15.27	2.10
18	G05H1	2256.9	3.24	3.45	4.16	5.06	6.21	6.82	8.29	10.49	12.0	0.961	2.86	25.2	15.45	2.12

TABLE A-1 DETAILS OF EXPERIMENTAL DATA (Continued)

Series H
Mixture Composition: C_6H_6 = 0.275 %
Additive = 0.557 ppm $Fe(CO)_5$
Argon = 99.725 %

RUN	EXP	T_s	SOOT YIELD = E(M) (%), AT TIME (ms)								DELAY	RATE	P_s	T_1	C_s	$[C]_s \times 10^{-17}$
NO.	NO.	(K)	0.25	0.50	0.75	1.00	1.25	1.50	1.75	2.00	(μsec)	(ms^{-1})	(atm)	(C)	(mol/m^3)	($atom/cm^3$)
1	H08H1	1539.3	0.67	0.19	0.03	0.00	0.01	0.13	0.28	0.12	0.0	0.000	1.91	23.0	15.13	1.49
2	H11H2	1653.3	0.27	0.23	0.24	0.07	0.00	0.07	0.20	0.50	1884.0	0.104	2.14	23.6	15.75	1.55
3	H07H1	1718.1	1.28	0.80	0.81	0.69	1.25	1.99	3.68	6.21	1520.0	0.411	2.22	23.0	15.75	1.55
4	H11H1	1719.8	0.47	0.40	0.85	1.10	1.59	2.58	4.40	7.19	1516.0	0.423	2.24	23.4	15.86	1.56
5	H08H2	1740.5	0.32	0.59	0.54	1.07	2.32	4.66	8.00	13.34	1242.0	0.456	2.2[illegible]	23.2	15.77	1.56
6	H06H2	1774.3	0.49	1.50	5.06	10.50	18.47	26.55	33.14	38.74	502.0	0.592	2.21	22.6	15.17	1.50
7	H07H2	1793.4	0.32	0.95	2.57	5.36	9.50	15.49	22.30	28.85	686.0	0.479	2.30	23.0	15.66	1.54
8	H04H1	1797.1	0.70	1.23	2.31	4.86	8.36	13.32	21.37	28.91	848.0	0.505	2.27	25.2	15.36	1.51
9	H05H2	1835.0	0.93	3.36	8.57	15.65	24.01	31.03	36.08	39.97	342.0	0.642	2.32	22.8	15.40	1.52
10	H05H1	1881.2	1.81	6.48	13.04	20.51	25.79	31.89	36.09	38.89	180.0	0.638	2.39	22.8	15.46	1.52
11	H06H1	1892.4	2.13	6.14	11.27	17.74	24.27	29.76	34.62	37.91	144.0	0.556	2.42	22.6	15.58	1.54
12	H02H1	1927.9	2.39	8.09	16.34	23.93	29.19	32.94	35.57	37.46	118.0	0.719	2.46	25.0	15.04	1.48
13	H02H2	1943.9	3.80	10.70	18.16	24.60	29.28	32.37	34.77	37.12	102.0	0.690	2.49	23.6	15.59	1.54
14	H04H2	1984.5	5.93	13.29	18.69	22.57	25.16	27.42	29.20	30.98	68.0	0.906	2.60	22.6	15.98	1.58
15	H01H2	1996.1	5.29	12.52	18.17	21.79	24.44	26.66	28.17	29.03	62.0	0.799	2.46	25.0	15.04	1.48
16	H12H2	2055.9	6.59	11.51	14.72	16.88	18.78	20.29	21.85	23.43	50.0	0.794	2.74	23.8	15.51	1.53
17	H03H1	2068.0	8.38	14.51	16.97	17.81	18.80	20.36	20.77	23.08	58.0	0.793	2.64	23.6	15.56	1.53
18	H03H2	2073.8	7.27	13.28	16.86	19.16	21.07	22.50	23.26	25.26	44.0	0.881	2.62	25.4	15.39	1.52
19	H12H1	2122.2	6.38	9.67	11.03	12.75	14.18	15.54	16.74	18.41	50.0	0.770	2.70	23.8	15.51	1.53
20	H13H1	2155.7	4.58	6.21	7.22	8.10	9.28	10.66	11.67	13.05	28.0	0.034	2.74	23.8	15.51	1.53
21	H13H2	2160.5	3.91	5.01	6.20	7.40	8.35	9.23	10.47	11.48	22.0	0.842	2.73	23.0	15.43	1.52
22	H15H1	2161.4	5.38	7.03	8.34	10.03	11.22	12.23	13.11	14.77	14.0	0.925	2.66	23.4	15.01	1.48
23	H14H2	2165.0	4.43	6.40	7.64	8.78	10.07	10.92	11.76	13.00	26.0	0.710	2.69	23.2	15.17	1.50
24	H14H1	2179.1	2.89	3.03	3.94	5.38	6.44	5.53	5.95	6.69	26.0	0.718	2.75	23.0	15.39	1.52
25	H15H2	2312.7	0.86	0.97	1.16	1.31	1.51	1.64	1.99	2.12	0.0	0.000	2.90	23.0	15.27	1.51

TABLE A-1 DETAILS OF EXPERIMENTAL DATA (Continued)

Series J
Mixture Composition: C_6H_6 = 0.382 %
Additive = 13.50 ppm $Fe(CO)_5$
Argon = 99.618 %

RUN NO.	EXP NO.	T_s (K)	SOOT YIELD = E(M) (%), AT TIME (ms) 0.25	0.50	0.75	1.00	1.25	1.50	1.75	2.00	DELAY (μsec)	RATE (ms^{-1})	P_s (atm)	T_s (C)	C_s (mol/m^3)	[C], X 10^{-17} (atom/cm^3)
1	J11H2	1641.5	0.17	0.10	0.17	0.09	0.15	0.21	0.24	0.30	2366.0	0.277	2.03	23.2	15.09	2.03
2	J07H2	1680.9	0.12	0.12	0.00	0.03	0.54	0.97	2.01	3.88	1464.0	0.329	2.19	22.8	15.85	2.13
3	J08H1	1745.4	0.33	0.36	0.97	2.22	4.25	7.27	11.81	16.91	902.0	0.519	2.26	23.0	15.79	2.12
4	J11H1	1746.2	0.70	0.47	1.10	2.40	4.85	8.51	13.72	19.19	882.0	0.550	2.24	23.2	15.65	2.10
5	J03H1	1794.3	1.32	2.46	3.49	5.70	9.66	12.96	19.15	23.54	532.0	0.000	2.31	26.0	15.69	2.11
6	J12H1	1804.0	0.34	1.37	3.71	6.73	11.13	16.43	21.89	26.08	454.0	0.536	2.34	23.2	15.84	2.13
7	J08H2	1833.0	0.83	2.69	6.01	11.07	17.19	22.81	27.24	29.89	350.0	0.640	2.37	23.2	15.77	2.12
8	J02H2	1860.8	1.22	4.64	9.32	14.00	19.22	22.91	26.63	28.99	224.0	0.606	2.39	26.5	15.67	2.11
9	J01H2	1933.8	3.64	7.80	12.80	16.37	19.63	22.18	24.08	25.04	102.0	0.642	2.47	27.6	15.58	2.09
10	J01H1	1998.7	5.50	10.85	14.56	17.98	20.25	22.28	24.53	26.07	58.0	0.173	2.59	26.0	15.82	2.13
11	J03H2	2025.8	4.79	9.23	12.52	14.85	16.13	17.70	18.79	19.20	64.0	0.003	2.61	26.0	15.69	2.11
12	J04H1	2041.9	5.10	8.53	10.23	11.24	12.49	14.40	15.81	16.73	58.0	0.877	2.64	23.2	15.79	2.12
13	J04H2	2049.8	5.03	7.97	9.45	10.69	11.79	13.07	13.85	15.38	56.0	0.024	2.60	23.6	15.48	2.08
14	J05H1	2095.0	5.57	7.61	8.73	9.63	10.60	12.00	13.22	14.53	28.0	0.077	2.66	23.4	15.49	2.08
15	J06H1	2156.6	2.54	3.68	4.71	5.46	6.09	6.33	6.55	7.62	34.0	0.368	2.75	23.0	15.57	2.09
16	J05H2	2166.6	3.66	4.80	5.81	6.56	7.19	7.43	7.65	8.71	28.0	0.694	2.78	23.4	15.66	2.10
17	J06H2	2176.2	2.59	2.80	3.41	3.77	4.38	4.83	5.52	6.51	0.0	0.000	2.77	23.0	15.51	2.08
18	J07H1	2286.0	0.62	0.82	0.78	0.91	1.25	1.40	1.63	1.91	0.0	0.000	2.93	22.6	15.62	2.10

TABLE A-1 DETAILS OF EXPERIMENTAL DATA (Continued)

Series K
Mixture Composition: C_6H_6 = 0.373 %
Additive = 00.000
Argon = 99.627 %

RUN	EXP	T_s	SOOT YIELD * E(M) (%), AT TIME (ms)								DELAY	RATE	P_s	T_s	C_s	$[C]_s \times 10^{-17}$
NO.	NO.	(K)	0.25	0.50	0.75	1.00	1.25	1.50	1.75	2.00	(μsec)	(ms^{-1})	(atm)	(C)	(mol/m^3)	($atom/cm^3$)
1	K03H2	1612.1	0.00	0.07	0.07	0.05	0.00	0.00	0.11	0.16	0.0	0.000	2.09	25.0	15.77	2.12
2	K04H1	1656.4	0.21	0.03	0.11	0.15	0.25	0.37	0.50	0.92	2074.0	0.318	2.13	25.0	15.69	2.11
3	K04H2	1734.2	0.12	0.15	0.53	1.05	2.32	4.33	7.36	11.53	1090.0	0.507	2.24	25.0	15.77	2.12
4	K05H1	1778.0	0.31	0.96	2.24	4.05	6.73	10.45	16.11	21.12	646.0	0.513	2.30	25.0	15.76	2.12
5	K08H1	1835.6	0.45	1.66	4.12	7.71	12.74	18.42	23.71	27.92	412.0	0.591	2.37	27.0	15.75	2.12
6	K05H2	1885.5	6.15	9.86	12.82	14.59	16.29	18.51	20.59	21.38	140.0	0.655	2.41	26.0	15.61	2.10
7	K07H2	1919.1	2.13	6.31	10.21	14.07	19.15	23.78	27.76	30.96	140.0	0.482	2.48	26.5	15.76	2.12
8	K01H2	1921.7	8.42	17.26	22.51	26.06	28.45	30.01	32.11	33.31	110.0	0.750	2.45	24.8	15.54	2.09
9	K02H1	1970.5	6.48	14.77	21.54	26.11	29.27	32.88	35.77	37.28	70.0	0.868	2.51	25.0	15.55	2.10
10	K03H1	2003.7	7.75	15.25	20.77	25.30	27.83	30.89	32.70	34.35	38.0	0.919	2.55	23.0	15.52	2.09
11	K01H1	2045.1	8.72	13.63	16.73	19.07	20.83	22.85	24.37	27.13	50.0	0.418	2.54	16.4	15.39	2.07
12	K02H2	2066.6	10.41	17.31	22.12	22.81	25.39	27.85	29.39	30.99	36.0	0.125	2.53	25.0	14.91	2.01
13	K06H2	2076.3	8.78	14.33	17.07	19.21	21.14	23.23	24.93	26.97	44.0	0.309	2.65	22.4	15.53	2.09
14	K08H2	2105.4	8.99	12.90	14.63	16.74	18.58	21.07	21.90	23.20	34.0	0.243	2.69	18.0	15.60	2.10
15	K06H1	2253.8	3.90	4.45	5.04	5.56	6.06	6.78	7.32	7.74	0.0	0.000	2.82	25.0	15.27	2.06

TABLE A-1 DETAILS OF EXPERIMENTAL DATA (Continued)

Series L
Mixture Composition: C_6H_6 = 0.373 %
Additive = 0.0
Argon = 99.627 %

RUN	EXP	T_s	SOOT YIELD * E(M) (%), AT TIME (ms)								DELAY	RATE	P_s	T_s	C_s	$[C]_s \times 10^{-17}$
NO.	NO.	(K)	0.25	0.50	0.75	1.00	1.25	1.50	1.75	2.00	(μsec)	(ms^{-1})	(atm)	(C)	(mol/m^3)	($atom/cm^3$)
1	L04H2	1669.5	0.56	0.67	0.78	1.24	2.27	4.81	9.37	15.57	1052.0	294.3	4.22	23.0	30.84	4.15
2	L05H1	1734.4	0.97	1.40	2.90	6.47	12.43	19.01	25.13	30.55	504.0	340.4	4.35	23.0	30.59	4.12
3	L05H2	1760.0	2.16	8.46	17.68	25.15	30.00	33.66	36.37	39.18	---	---	4.34	23.0	30.03	4.05
4	L08H1	1793.3	0.77	2.63	7.38	15.39	22.54	27.16	32.32	35.33	328.0	409.2	4.55	22.4	30.93	4.17
5	L07H1	1817.8	1.57	6.61	13.93	20.51	26.32	31.70	34.93	38.48	164.0	443.3	4.59	22.2	30.76	4.14
6	L07H2	1845.5	2.69	8.71	17.49	23.91	28.81	32.66	35.58	36.53	108.0	454.2	4.66	22.6	30.79	4.15
7	L06H2	1848.4	1.63	5.36	10.60	14.93	17.71	20.06	22.27	24.03	146.0	374.5	4.68	22.1	30.89	4.16
8	L06H1	1876.0	5.00	14.76	23.07	26.90	30.07	33.08	35.26	37.15	86.0	600.0	4.47	22.1	30.74	4.14
9	L08H2	1912.5	4.69	13.82	21.96	26.39	29.33	33.17	36.10	37.98	96.0	698.4	4.83	22.0	30.93	4.17
10	L04H1	1964.6	10.69	19.34	23.00	25.22	27.11	28.43	29.47	31.95	20.0	1033.9	5.05	23.0	31.34	4.22
11	L02H2	1981.0	6.84	16.37	21.72	24.36	26.46	28.55	29.79	31.68	64.0	736.4	5.00	23.8	30.77	4.15
12	L03H1	2084.2	10.97	15.20	17.26	18.83	20.52	22.12	24.29	26.29	30.0	1479.4	5.20	22.8	30.38	4.09
13	L03H2	2203.6	6.57	7.89	9.33	11.36	12.37	13.79	15.01	16.62	0.0	962.5	5.53	22.8	30.58	4.12
14	L02H1	2259.1	3.07	4.28	5.11	6.09	7.04	7.82	9.18	10.04	0.0	1118.8	5.64	23.8	30.45	4.10

TABLE A-1 DETAILS OF EXPERIMENTAL DATA (Continued)

Series M
Mixture Composition: C_6H_6 = 0.114 %
Additive = 0.0
Argon = 99.886 %

RUN	EXP	T_s	SOOT YIELD * E(M) (%), AT TIME (ms)								DELAY	RATE	P_s	T_1	C_s	$[C]_s \times 10^{-17}$
NO.	NO.	(K)	0.25	0.50	0.75	1.00	1.25	1.50	1.75	2.00	(μsec)	(ms^{-1})	(atm)	(C)	(mol/m^3)	($atom/cm^3$)
1	M07H1	1576.6	0.53	0.41	0.21	0.10	0.13	0.25	0.38	0.25	---	---	4.90	23.0	37.86	1.56
2	M07H2	1668.4	0.00	0.05	0.03	0.00	0.31	1.04	2.49	4.81	1556.0	131.8	5.17	23.2	37.77	1.56
3	M01H1	1683.8	2.51	3.99	3.46	2.51	2.75	3.68	5.00	8.34	1316.0	141.1	5.22	22.0	37.81	1.56
4	M01H2	1723.5	0.45	0.48	0.70	1.47	3.31	6.87	12.56	18.48	1072.0	185.4	5.24	22.1	37.02	1.52
5	M08H1	1792.3	0.33	0.65	2.76	6.83	12.17	18.07	23.20	26.85	5520.0	167.7	5.49	23.2	37.36	1.54
6	M05H1	1796.0	0.65	1.26	4.34	9.40	15.37	20.31	24.45	27.08	1352.0	208.6	5.49	22.0	37.29	1.54
7	M02H1	1827.8	0.95	3.51	8.26	14.20	19.39	22.80	25.32	27.27	292.0	183.1	5.56	22.5	37.05	1.53
8	M02H2	1896.9	2.23	7.39	12.73	15.91	17.64	19.29	20.76	22.01	148.0	233.8	5.76	23.0	37.00	1.52
9	M05H2	1959.7	3.27	7.93	11.62	13.67	15.27	16.70	17.89	19.10	120.0	219.2	5.98	22.5	37.19	1.53
10	M03H1	1995.3	3.97	6.90	8.20	9.44	10.32	11.03	12.10	12.84	76.0	300.0	6.05	23.0	36.97	1.52
11	M03H2	2007.5	1.53	1.84	2.08	2.48	2.59	2.99	2.93	3.27	12.0	192.9	5.98	23.0	36.30	1.49
12	M06H2	2034.6	3.22	3.98	4.79	5.32	6.45	6.94	7.88	8.18	52.0	279.2	6.18	23.0	37.02	1.52
13	M04H1	2138.5	1.18	1.29	1.64	2.06	2.13	2.44	2.84	3.03	8.0	170.0	6.52	23.0	37.13	1.53
14	M04H2	2177.2	0.89	0.96	1.14	1.32	1.73	1.66	1.64	1.94	8.0	212.5	6.51	23.1	36.44	1.50
15	M06H1	2189.1	1.38	1.75	1.81	2.12	1.79	2.09	2.24	2.53	0.0	121.4	6.82	23.0	38.00	1.56

TABLE A-1 DETAILS OF EXPERIMENTAL DATA (Continued)

Series N
Mixture Composition: C_6H_6 = 0.123 %
Additive = 0.151 ppm $Fe(CO)_5$
Argon = 99.877 %

RUN NO	EXP NO.	T_s (K)	SOOT YIELD * E(M) (%), AT TIME (ms) 0.25	0.50	0.75	1.00	1.25	1.50	1.75	2.00	DELAY (usec)	RATE (ms^{-1})	P_s (atm)	T_1 (C)	C_s (mol/m^3)	$[C]_s \times 10^{-17}$ ($atom/cm^3$)
1	N05H1	1650.2	0.13	0.14	0.14	0.23	0.26	0.52	1.23	2.11	1882.0	119.9	4.78	20.6	35.30	1.57
2	N04H2	1722.6	0.40	0.40	0.96	1.42	2.75	5.60	9.99	15.21	1134.0	167.2	4.97	21.0	35.16	1.56
3	N05H2	1753.9	0.36	0.53	1.45	3.28	6.72	11.34	17.45	23.34	836.0	164.7	5.00	22.3	34.77	1.54
4	N01H1	1796.9	0.59	1.40	4.67	14.92	20.22	24.41	27.74	30.50	470.0	182.8	5.10	24.0	34.58	1.54
5	N03H2	1817.0	0.68	2.26	5.97	10.97	16.26	20.28	23.71	-1.00	372.0	170.1	5.15	22.0	34.53	1.53
6	N01H2	1826.2	0.74	1.97	6.06	10.26	15.01	18.29	19.69	-1.00	396.0	163.5	5.13	22.5	34.24	1.52
7	N04H1	1859.5	1.83	5.39	10.68	16.08	19.79	22.29	24.16	25.69	222.0	184.0	5.28	22.0	34.61	1.54
8	N03H1	1926.4	1.70	5.73	11.10	14.78	17.22	18.42	19.98	20.16	1820.0	177.9	5.52	22.0	34.90	1.55
9	N06H1	1951.9	3.37	8.26	11.77	14.04	15.52	16.96	17.62	18.29	76.0	203.0	5.59	20.0	34.91	1.55
10	N02H1	2033.5	3.00	3.77	4.88	5.49	6.41	6.99	7.53	8.29	12.0	168.8	5.78	22.0	34.67	1.54
11	N02H2	2108.1	4.32	4.26	4.61	4.49	4.43	4.87	5.33	5.88	0.0	229.2	5.98	22.0	34.58	1.54
12	N06H2	2246.1	1.06	0.87	1.43	1.44	1.65	1.51	1.65	1.87	---	---	6.39	20.2	34.66	1.54

TABLE A-1 DETAILS OF EXPERIMENTAL DATA (Continued)

Series O
Mixture Composition: C_6H_6 = 0.114 %
Additive = 0.755 ppm CO
Argon = 99.886 %

RUN	EXP	T_s	SOOT YIELD * E(M) (%), AT TIME (ms)								DELAY	RATE	P_s	T_1	C_s	$[C]_s \times 10^{-17}$
NO.	NO.	(K)	0.25	0.50	0.75	1.00	1.25	1.50	1.75	2.00	(μsec)	(ms^{-1})	(atm)	(C)	(mol/m')	(atom/cm')
1	014H1	1581.7	0.58	0.41	0.27	0.49	0.47	0.29	0.37	0.64	---	---	4.82	24.2	37.11	1.53
2	011H1	1717.8	0.14	0.19	0.43	0.83	2.03	4.53	8.41	13.37	1188.0	162.7	5.23	22.8	37.12	1.53
3	013H2	1793.7	0.30	0.88	2.49	6.03	11.22	16.67	21.22	22.78	674.0	166.7	5.49	22.6	37.28	1.54
4	011H2	1837.1	1.33	2.11	5.18	9.44	15.21	19.58	23.08	25.24	410.0	169.9	5.57	24.0	36.95	1.52
5	014H2	1869.4	1.01	5.42	10.77	14.96	17.87	19.76	21.10	22.17	---	---	5.63	22.8	36.72	1.51
6	012H1	1931.3	2.73	7.47	11.30	13.63	15.37	16.52	17.46	18.82	94.0	180.6	5.81	24.3	36.69	1.51
7	012H2	2016.6	3.16	4.39	5.48	6.34	7.21	8.04	8.57	9.31	62.0	207.7	6.05	24.2	36.58	1.51
8	013H1	2155.1	0.94	1.14	1.38	1.36	1.67	1.69	2.08	2.56	0.0	39.1	6.47	24.8	36.58	1.51

TABLE A-1 DETAILS OF EXPERIMENTAL DATA (Continued)

Series P
Mixture Composition: C_6H_6 = 0.362 %
Additive = 63.80 ppm CO
Argon = 99.639 %

RUN	EXP	T_s	SOOT YIELD * E(M) (%), AT TIME (ms)								DELAY	RATE	P_s	T_1	C_s	$[C]_s \times 10^{-17}$
NO.	NO.	(K)	0.25	0.50	0.75	1.00	1.25	1.50	1.75	2.00	(μsec)	(ms^{-1})	(atm)	(C)	(mol/m^3)	($atom/cm^3$)
1	P03H2	1624.6	0.69	0.60	0.37	0.18	0.26	0.23	0.27	0.44	0.0	0.000	2.24	25.4	16.79	2.19
2	P04H1	1642.9	-1.00	0.14	0.18	0.18	0.23	0.39	0.66	1.34	2006.0	0.047	2.22	25.8	16.44	2.14
3	P05H1	1729.4	0.27	0.45	0.68	1.18	2.40	4.51	7.68	12.36	1148.0	0.055	2.36	26.0	16.64	2.17
4	P04H2	1764.1	0.22	0.57	1.76	3.73	7.15	11.59	16.67	23.11	706.0	0.060	2.39	26.0	16.50	2.15
5	P03H1	1866.0	0.74	3.49	8.10	14.90	21.80	27.53	32.30	35.28	288.0	0.077	2.53	25.0	16.53	2.16
6	P01H2	1930.5	2.01	8.65	18.24	25.04	29.27	31.67	34.09	36.25	174.0	0.126	2.58	25.8	16.28	2.12
7	P05H2	1984.7	5.35	12.73	18.82	23.19	26.18	28.58	30.19	31.81	66.0	0.143	2.66	26.4	16.32	2.13
8	P01H2	2075.4	7.01	14.13	17.96	20.25	21.31	22.60	24.32	25.29	52.0	0.155	2.80	26.0	16.43	2.14
9	P02H1	2143.2	6.53	9.46	10.94	12.30	13.79	14.51	16.04	17.70	36.0	0.067	2.87	26.2	16.30	2.13
10	P02H2	2203.1	2.22	2.42	3.19	3.63	4.27	5.48	7.01	7.63	8.0	0.181	2.92	26.4	16.16	2.11

TABLE A-1 DETAILS OF EXPERIMENTAL DATA (Continued)

Series Q
Mixture Composition: C_6H_6 = 0.270 %
Additive = 0.0
Argon = 99.730 %

RUN NO.	EXP NO.	T_s (K)	SOOT YIELD * E(M) (%), AT TIME (ms) 0.25	0.50	0.75	1.00	1.25	1.50	1.75	2.00	DELAY (μsec)	RATE (ms^{-1})	P_s (atm)	T_1 (C)	C_s (mol/m³)	$[C]_s \times 10^{-17}$ (atom/cm³)
1	Q01H2	1602.1	0.09	0.00	0.00	0.07	0.00	0.04	0.00	0.00	---	---	2.13	21.0	16.20	1.58
2	Q01H1	1690.4	0.49	0.38	0.41	0.60	1.45	0.95	1.42	2.44	1945.0	152.5	2.23	20.8	16.12	1.57
3	Q05H2	1752.3	0.39	0.21	0.85	1.69	3.40	6.26	10.56	15.42	---	---	2.31	21.2	16.08	1.57
4	Q02H1	1819.2	0.28	0.71	1.90	4.09	7.14	12.28	18.36	23.58	828.0	175.5	2.41	21.0	16.18	1.58
5	Q03H2	1898.2	2.88	7.63	12.63	16.75	20.00	22.43	24.01	25.95	80.0	183.0	2.43	21.5	15.63	1.52
6	Q02H2	1959.4	3.24	8.22	13.05	16.72	19.78	22.35	23.84	24.45	94.0	217.5	2.56	21.0	15.90	1.55
7	Q03H1	2039.5	4.39	8.73	12.23	14.13	15.14	16.30	17.14	18.50	64.0	263.5	2.65	21.3	15.81	1.54
8	Q04H1	2078.2	2.78	3.29	3.58	4.17	5.12	5.82	6.66	7.41	36.0	240.6	2.66	21.3	15.62	1.52
9	Q05H1	2178.6	4.01	4.53	5.06	4.83	5.32	5.78	6.55	7.08	0.0	327.8	2.83	21.5	15.81	1.54
10	Q04H2	2212.7	1.29	1.27	1.72	1.81	2.06	2.32	2.21	2.63	0.0	119.2	2.85	21.3	15.68	1.53

TABLE A-1 DETAILS OF EXPERIMENTAL DATA (Continued)

Series S
Mixture Composition: C_6H_6 = 0.286 %
Oxygen = 0.28 %
Additive = 3.0 ppm CO
Argon = 99.714 %

RUN NO.	EXP NO.	T_s (K)	SOOT YIELD * E(M) (%), AT TIME (ms) 0.25	0.50	0.75	1.00	1.25	1.50	1.75	2.00	DELAY (μsec)	RATE (ms^{-1})	P_s (atm)	T_1 (C)	C_s (mol/m³)	[C], X 10^{-17} (atom/cm³)
1	S04II1	1600.1	0.18	0.17	0.33	0.33	0.00	0.13	0.15	0.13	2630.0	22.5	1.98	19.6	15.11	1.56
2	S03II2	1689.7	0.35	0.43	0.43	0.71	1.19	1.92	3.03	4.76	1194.0	58.1	2.08	20.0	14.99	1.55
3	S03II1	1780.8	0.34	1.05	2.49	3.89	6.19	8.38	11.23	13.71	5120.0	75.8	2.19	19.0	14.99	1.55
4	S02II2	1858.7	1.13	4.28	6.97	9.38	11.84	13.30	14.56	15.37	132.0	105.7	2.25	20.5	14.75	1.52
5	S04II2	1934.5	2.19	5.43	8.05	9.97	11.34	12.52	13.35	14.30	142.0	192.9	2.36	19.8	14.90	1.54
6	S01II1	2017.7	3.92	5.24	6.13	6.54	7.01	7.41	8.03	8.09	28.0	233.3	2.43	20.3	14.66	1.51
7	S01II2	2196.5	0.91	0.85	0.89	0.89	0.99	1.05	0.99	1.01	0.0	92.3	2.67	20.5	14.82	1.53
8	S02II1	2214.3	0.60	0.77	0.77	0.82	0.83	0.90	0.71	0.90	24.0	141.7	2.65	20.8	14.57	1.51

TABLE A-1 DETAILS OF EXPERIMENTAL DATA (Continued)

Series T
Mixture Composition: C_6H_6 = 0.280 %
Oxygen = 0.28 %
Additive = 0.5 ppm $Fe(CO)_5$
Argon = 99.720 %

RUN	EXP	T_s	SOOT YIELD * E(M) (%), AT TIME (ms)								DELAY	RATE	P_s	T_1	C_s	$[C]_s \times 10^{-17}$
NO.	NO.	(K)	0.25	0.50	0.75	1.00	1.25	1.50	1.75	2.00	(μsec)	(ms^{-1})	(atm)	(C)	(mol/m^3)	($atom/cm^3$)
1	T04H1	1561.2	0.02	0.12	0.05	0.07	0.00	0.13	0.07	0.05	---	---	1.98	19.0	15.42	1.56
2	T03H2	1694.0	0.29	0.18	0.32	0.52	0.91	1.40	2.42	3.77	1384.0	68.0	2.16	19.0	15.56	1.57
3	T05H1	1771.3	0.37	0.80	1.95	3.45	5.36	7.35	10.33	12.92	466.0	60.9	2.26	20.5	15.58	1.58
4	T03H1	1803.4	0.50	1.28	2.97	4.70	7.01	9.63	12.17	14.39	356.0	93.4	2.30	18.8	15.57	1.57
5	T04H2	1884.3	1.10	4.02	6.63	9.13	11.47	12.97	14.45	15.17	168.0	137.0	2.39	19.0	15.49	1.57
6	T01H1	1973.8	4.02	6.27	7.50	8.38	9.83	9.69	10.46	11.05	84.0	318.4	2.48	17.8	15.32	1.55
7	T01H2	2007.8	3.21	4.30	4.94	5.39	6.12	6.59	7.09	7.56	56.0	265.8	2.49	18.0	15.10	1.53
8	T02H2	2100.8	2.02	2.42	2.78	2.94	3.03	3.33	3.66	3.72	44.0	208.3	2.66	18.4	15.42	1.56
9	T02H1	2202.4	1.30	1.39	1.31	1.50	1.37	1.55	1.53	1.61	260.0	189.3	2.78	18.0	15.39	1.56

TABLE A-1 DETAILS OF EXPERIMENTAL DATA (Continued)

Series V
Mixture Composition: C_6H_6 = 0.273 %
Oxygen = 0.28 %
Add't'v = 0.0
Argon = 99.727 %

RUN	EXP	T_s	SOOT YIELD * E(M) (%), AT TIME (ms)								DELAY	RATE	P_s	T_1	C_s	$[C]_s \times 10^{-17}$
NO.	NO.	(K)	0.25	0.50	0.75	1.00	1.25	1.50	1.75	2.00	(μsec)	(ms^{-1})	(atm)	(C)	(mol/m^3)	($atom/cm^3$)
1	V03H2	1549.0	0.00	0.00	0.00	0.11	0.00	0.00	0.11	0.00	---	---	2.02	19.0	15.91	1.57
2	V03H1	1717.8	0.27	0.38	0.52	0.78	1.21	1.88	3.14	4.85	1276.0	72.4	2.26	20.8	16.01	1.58
3	V02H2	1787.1	0.28	0.86	2.02	3.78	6.09	8.81	11.79	14.26	456.0	76.2	2.32	20.8	15.82	1.56
4	V04H1	1891.9	1.17	4.24	6.84	9.48	11.73	13.71	15.41	16.42	168.0	148.4	2.49	19.4	16.02	1.58
5	V01H1	1961.4	3.00	5.96	8.47	9.97	11.30	12.49	13.41	13.99	84.0	210.7	2.52	20.4	15.66	1.54
6	V01H2	2077.8	3.33	4.34	4.58	5.16	5.80	6.13	6.56	7.15	8.0	216.7	2.67	20.5	15.66	1.54
7	V02H1	2191.8	0.80	0.97	0.97	0.98	0.92	1.02	1.07	1.14	8.0	118.2	2.80	21.0	15.56	1.53

TABLE A-1 DETAILS OF EXPERIMENTAL DATA (Continued)

Series X
Mixture Composition: C_6H_6 = 0.259 %
Oxygen = 0.28 %
Additive = 11.5 ppm $Fe(CO)_5$
Argon = 99.740 %

RUN	EXP	T_s	SOOT YIELD * E(M) (%), AT TIME (ms)								DELAY	RATE	P_s	T_1	C_s	$[C]_s \times 10^{-17}$
NO.	NO.	(K)	0.25	0.50	0.75	1.00	1.25	1.50	1.75	2.00	(μsec)	(ms^{-1})	(atm)	(C)	(mol/m^3)	($atom/cm^3$)
1	X04H1	1584.6	0.39	0.25	0.14	0.24	0.31	0.37	0.27	0.32	2216.0	15.5	2.18	19.8	16.75	1.57
2	X03H2	1680.6	0.17	0.10	0.07	0.32	0.54	0.96	2.06	3.26	1416.0	75.8	2.31	19.5	16.73	1.57
3	X04H2	1781.7	0.26	1.16	1.96	3.86	5.90	8.29	11.36	14.14	486.0	89.6	2.44	20.0	16.72	1.57
4	X05H1	1848.9	0.48	2.27	4.64	7.59	11.05	14.05	16.03	17.62	282.0	106.4	2.53	19.9	16.67	1.57
5	X01H1	1935.1	2.55	5.99	8.96	11.11	12.93	14.02	14.89	15.73	104.0	135.7	2.65	19.3	16.67	1.57
6	X01H2	1974.8	4.46	7.28	9.07	9.95	10.70	11.61	12.15	13.15	80.0	183.5	2.66	19.4	16.45	1.54
7	X05H2	2051.1	4.20	6.35	7.20	7.91	8.54	9.24	9.74	10.22	420.0	228.3	2.79	19.6	16.58	1.56
8	X02H1	2117.2	1.99	2.30	2.54	2.66	2.96	3.13	3.41	3.62	18.0	110.9	2.88	19.2	16.56	1.55
9	X03H1	2175.4	0.94	1.05	1.12	1.14	1.14	1.12	1.32	1.23	0.0	107.1	2.90	19.4	16.25	1.53

TABLE A-1 DETAILS OF EXPERIMENTAL DATA (Continued)

Series Y
Mixture Composition: C_6H_6 = 0.295 %
Oxygen = 0.28 %
Additive = 62.5 ppm CO
Argon = 99.699 %

RUN	EXP	T_s	SOOT YIELD * E(M) (%), AT TIME (ms)								DELAY	RATE	P_s	T_1	C_s	[C], X 10^{-17}
NO.	NO.	(K)	0.25	0.50	0.75	1.00	1.25	1.50	1.75	2.00	(μsec)	(ms^{-1})	(atm)	(C)	(mol/m^3)	($atom/cm^3$)
1	Y04H1	1630.5	0.00	0.06	0.13	0.02	0.00	0.11	0.15	0.28	1738.0	6.7	2.01	17.9	15.03	1.61
2	Y03H2	1680.6	0.07	0.05	0.02	0.12	0.19	0.44	0.85	1.56	1586.0	43.2	2.03	19.0	14.74	1.58
3	Y03H1	1767.1	0.21	0.65	1.42	2.70	4.40	6.48	9.12	11.97	546.0	58.5	2.12	19.3	14.63	1.56
4	Y02H2	1906.7	1.15	3.81	6.32	9.05	11.42	13.19	14.62	15.60	142.0	103.2	2.31	19.1	14.75	1.58
5	Y05H1	1937.2	2.56	5.39	7.97	9.57	10.67	11.60	12.36	13.12	96.0	185.7	2.33	18.0	14.65	1.57
6	Y01H1	2069.4	3.70	5.39	6.03	7.04	7.59	8.08	8.76	9.63	64.0	260.0	2.47	19.0	14.58	1.56
7	Y04H2	2096.4	2.95	3.73	4.54	4.82	5.18	5.60	6.00	6.27	---	---	2.60	18.0	15.10	1.61
8	Y01H2	2141.2	2.93	3.60	4.22	4.34	4.73	5.05	5.33	5.61	48.0	256.7	2.55	19.0	14.49	1.55
9	Y02H1	2193.2	0.63	0.82	0.87	0.71	0.77	0.79	0.84	1.00	20.0	105.6	2.79	19.1	15.50	1.66

TABLE A-1 DETAILS OF EXPERIMENTAL DATA (Continued)

Series Z
Mixture Composition: C_6H_6 = 0.111 %
Oxygen = 0.12 %
Additive = 0.0
Argon = 99.889 %

RUN NO.	EXP NO.	T_s (K)	SOOT YIELD * E(M) (%), AT TIME (ms) 0.25	0.50	0.75	1.00	1.25	1.50	1.75	2.00	DELAY (μsec)	RATE (ms^{-1})	P_s (atm)	T_1 (C)	C_s (mol/m^3)	$[C]_s \times 10^{-17}$ ($atom/cm^3$)
1	Z03H2	1602.4	0.62	0.60	0.53	0.34	0.66	0.97	1.95	3.00	1670.0	69.0	4.98	26.8	37.87	1.52
2	Z03H1	1725.2	0.20	0.33	0.45	1.31	3.11	5.10	7.65	10.69	910.0	71.2	5.54	26.5	38.44	1.54
3	Z04H1	1795.6	0.63	2.04	4.99	8.63	11.73	14.72	16.80	18.17	366.0	112.9	5.69	24.0	38.65	1.55
4	Z01H1	1817.3	0.30	1.83	4.91	7.95	11.12	13.84	15.99	17.69	318.0	76.6	5.86	20.0	39.30	1.58
5	Z01H2	1902.2	2.27	5.97	8.91	11.08	12.26	13.61	14.52	15.36	86.0	126.5	6.08	20.2	38.96	1.56
6	Z02H1	1996.2	4.00	6.64	8.79	9.76	10.18	10.97	13.46	12.42	64.0	202.5	6.25	23.5	38.16	1.53
7	Z04H2	2074.7	1.68	1.86	1.84	1.70	1.82	1.97	2.14	2.12	0.0	73.8	6.53	23.5	38.38	1.54
8	Z02H2	2151.7	1.16	1.05	1.16	1.38	1.36	1.20	1.56	1.65	0.0	127.3	6.76	25.0	38.29	1.54

TABLE A-1 DETAILS OF EXPERIMENTAL DATA (Continued)

Series AA
Mixture Composition: C_6H_6 = 0.123 %
Oxygen = 0.12 %
Additive = 0.318 ppm $Fe(CO)_5$
Argon = 99.877 %

RUN NO.	EXP NO.	T_s (K)	SOOT YIELD * E(M) (%), AT TIME (ms) 0.25	0.50	0.75	1.00	1.25	1.50	1.75	2.00	DELAY (μsec)	RATE (ms^{-1})	P_s (atm)	T_1 (C)	C_s (mol/m^3)	[C], X 10^{-17} ($atom/cm^3$)
1	AA2H2	1643.7	0.09	0.06	0.17	0.30	0.43	0.41	1.02	1.60	1632.0	37.6	4.81	22.2	35.63	1.58
2	AA3H1	1737.5	0.28	0.34	0.25	0.92	2.01	3.93	6.60	9.96	1156.0	101.7	5.06	22.5	35.53	1.58
3	AA1H1	1840.2	0.82	3.17	6.42	9.72	12.95	15.22	16.85	17.97	250.0	126.5	5.36	21.2	35.48	1.58
4	AA1H2	1892.7	2.80	5.83	8.76	11.43	12.71	13.83	14.19	15.26	98.0	135.4	5.41	21.7	34.83	1.55
5	AA3H2	1945.6	4.27	8.21	10.89	12.23	13.42	14.33	15.45	16.36	50.0	173.6	5.54	22.5	34.73	1.54
6	AA2H1	2018.8	3.59	5.04	5.98	6.75	6.88	7.46	8.01	8.50	42.0	202.6	5.80	21.9	35.00	1.56
7	AA4H1	2138.8	2.40	2.50	2.48	2.67	3.28	2.91	2.91	3.23	0.0	162.5	6.13	22.3	34.91	1.55

TABLE A-1 DETAILS OF EXPERIMENTAL DATA (Continued)

Series BB
Mixture Composition: C_6H_6 = 0.119 %
Oxygen = 0.12 %
Additive = 1.59 ppm CO
Argon = 99.881 %

RUN NO.	EXP NO.	T_s (K)	SOOT YIELD * E(M) (%), AT TIME (ms) 0.25	0.50	0.75	1.00	1.25	1.50	1.75	2.00	DELAY (μsec)	RATE (ms^{-1})	P_s (atm)	T_1 (C)	C_s (mol/m³)	$[C]_s \times 10^{-17}$ (atom/cm³)
1	BB3H2	1625.6	0.11	0.27	0.23	0.56	0.39	0.50	1.02	1.48	1884.0	76.1	4.89	22.0	36.65	1.58
2	BB4H1	1717.9	0.26	0.40	1.53	3.16	5.59	8.39	12.31	15.84	738.0	100.4	5.14	22.0	36.45	1.57
3	BB1H1	1804.8	1.15	2.72	5.96	9.88	14.15	17.23	19.87	21.52	358.0	133.8	5.37	21.5	36.27	1.56
4	BB1H2	1904.8	2.84	7.71	11.74	14.59	15.99	17.43	18.17	19.55	116.0	212.1	5.64	21.7	36.11	1.55
5	BB2H1	2000.4	4.59	6.55	7.73	8.63	8.87	9.33	10.22	10.96	24.0	380.0	5.92	21.7	36.06	1.55
6	BB2H2	2067.2	2.94	3.45	4.00	4.40	4.44	4.56	4.53	4.60	0.0	187.5	6.07	21.7	35.79	1.54
7	BB3H1	2135.6	1.41	1.01	1.37	1.20	1.20	1.39	1.49	1.60	0.0	183.3	6.21	21.9	35.42	1.52

TABLE A-1 DETAILS OF EXPERIMENTAL DATA (Concluded)

Series CC
Mixture Composition: C_6H_6 = 0.293 %
Oxygen = 3.0 ppm
Additive = 0.0
Argon = 99.707 %

RUN	EXP	T_s	SOOT YIELD * E(M) (%), AT TIME (ms)								DELAY	RATE	P_s	T_1	C_s	$[C]_s \times 10^{-17}$
NO.	NO.	(K)	0.25	0.50	0.75	1.00	1.25	1.50	1.75	2.00	(usec)	(ms^{-1})	(atm)	(C)	(mol/m^3)	($atom/cm^3$)
1	CC3H2	1626.2	0.39	0.46	0.31	0.39	0.37	0.51	0.48	0.48	---	---	2.00	21.0	14.98	1.59
2	CC3H1	1713.7	0.47	0.52	0.49	0.89	1.56	2.34	4.08	6.15	1260.0	93.9	2.09	21.0	14.88	1.57
3	CC2H2	1788.0	0.26	0.56	1.63	3.41	6.65	10.99	17.47	23.61	904.0	194.1	2.16	20.8	14.74	1.56
4	CC4H2	1863.2	0.89	3.28	6.88	11.46	16.65	21.70	27.60	32.03	304.0	160.8	2.27	20.5	14.86	1.57
5	CC4H1	1905.7	1.62	5.87	11.20	16.39	21.51	26.28	30.25	32.72	162.0	183.8	2.32	20.0	14.87	1.57
6	CC1H1	1978.3	1.00	4.25	8.66	13.82	20.19	24.93	29.06	32.50	236.0	186.7	2.33	20.0	14.36	1.52
7	CC5H1	2028.6	5.76	10.12	13.24	15.71	17.42	18.87	20.84	22.33	68.0	386.1	2.43	20.5	14.58	1.54
8	CC1H2	2045.9	5.50	7.46	8.77	10.11	10.90	12.11	13.14	14.85	40.0	427.8	2.39	20.3	14.26	1.51
9	CC2H1	2239.5	2.11	2.49	2.68	3.08	3.46	3.91	4.54	4.76	0.0	182.1	2.67	20.5	14.52	1.54

(The reverse of this page is blank)